



**1,3-Dithianes as Assembling Ligands for the
Construction of Copper(I) Coordination Polymers.
Investigation of the Impact of the RC(H)S 2 C 3 H 6
Substituent and Reaction Conditions on the
Architecture of the 0D–3D Networks**

Abhinav Raghuvanshi, Michael Knorr, Lena Knauer, Carsten Strohmann,
Stephanie Boullanger, Virginie Moutarlier, Lydie Viau

► **To cite this version:**

Abhinav Raghuvanshi, Michael Knorr, Lena Knauer, Carsten Strohmann, Stephanie Boullanger, et al.. 1,3-Dithianes as Assembling Ligands for the Construction of Copper(I) Coordination Polymers. Investigation of the Impact of the RC(H)S 2 C 3 H 6 Substituent and Reaction Conditions on the Architecture of the 0D–3D Networks. *Inorganic Chemistry*, 2019, 58 (9), pp.5753-5775. 10.1021/acs.inorgchem.9b00114 . hal-02129882

HAL Id: hal-02129882

<https://hal.science/hal-02129882>

Submitted on 14 Jan 2022

HAL is a multi-disciplinary open access archive for the deposit and dissemination of scientific research documents, whether they are published or not. The documents may come from teaching and research institutions in France or abroad, or from public or private research centers.

L'archive ouverte pluridisciplinaire **HAL**, est destinée au dépôt et à la diffusion de documents scientifiques de niveau recherche, publiés ou non, émanant des établissements d'enseignement et de recherche français ou étrangers, des laboratoires publics ou privés.

1,3-Dithianes as assembling ligands for the
construction of Cu(I) coordination polymers.
Investigation of the impact of the $RC(H)S_2C_3H_6$
substituent and reaction conditions on the
architecture of the 0D-3D networks

Abhinav Raghuvanshi,[†] Michael Knorr,^{*†} Lena Knauer,[‡] Carsten Strohmann,^{*‡} Stéphanie
Boullanger,[†] Virginie Moutarlier[†] and Lydie Viau^{*†}

[†]Institut UTINAM, UMR CNRS 6213, 16 Route de Gray, Université Bourgogne Franche-
Comté, 25030 Besançon, France

[‡]Anorganische Chemie, Technische Universität Dortmund, Otto-Hahn-Straße 6, 44227
Dortmund, Germany

ABSTRACT

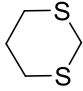
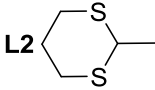
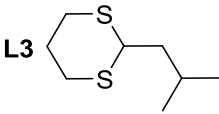
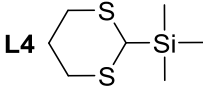
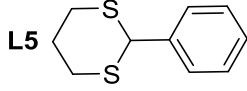

The parent compound 1,3-dithiane **L1** was reacted with CuI providing the 1D coordination polymer $[\{\text{Cu}(\mu_2\text{-I})_2\text{Cu}\}(\mu_2\text{-L1})_2]_n$ **CP1**, an isostructural compound $[\{\text{Cu}(\mu_2\text{-Br})_2\text{Cu}\}(\mu_2\text{-L1})_2]_n$ **CP2** was isolated upon treatment of CuBr with **L1**. In contrast, treatment of **L1** with CuCl results in the formation of 2D polymeric $[\{\text{Cu}(\mu_2\text{-Cl})_2\text{Cu}\}(\mu_2\text{-L1})]_n$ **CP3**, in which each sulfur atom acts as a 4-electron donor. The 1D compounds $[\{\text{Cu}(\mu_2\text{-X})_2\text{Cu}\}(\mu_2\text{-L2})_2]_n$ **CP7** (X = Br) and **CP8** (X = Cl) resulting from treatment of 2-methyl-1,3 dithiane **L2** with CuBr and CuCl are isostructural with their CuI homologue $[\{\text{Cu}(\mu_2\text{-I})_2\text{Cu}\}(\mu_2\text{-L2})_2]_n$ **CP5**, reported previously. Using CuCN, a 2D CP of composition $[\{\text{Cu}(\mu_2\text{-CN})_2\text{Cu}\}(\mu_2\text{-L2})_2]_n$ **CP9** has been isolated. Complexation of 2-isobutyl-1,3-dithiane **L3** on CuI generates a 2D material $[\{\text{Cu}_3(\mu_3\text{-I})(\mu_2\text{-I})_2(\mu_2\text{-L3})_2\}]_n$ **CP10**, incorporating usual trinuclear $\mu_3\text{-I}$ -capped Cu clusters as SBUs, whereas 2D-polymeric compounds $[\{\text{Cu}(\mu_2\text{-Br})_2\text{Cu}\}(\mu_2\text{-L3})_2]_n$ **CP11** and $[\{\text{Cu}(\mu_2\text{-Cl})_2\text{Cu}\}(\mu_2\text{-L3})_2]_n$ **CP12** were obtained with CuBr and CuCl. Treatment of 2-Me₃Si-1,3-dithiane **L4** with CuX yields the series $[\{\text{Cu}_2(\mu_4\text{-X})(\mu_2\text{-X})\}(\mu_2\text{-L4})]_n$ **CP13-CP15**. With 2-phenyl-1,3-dithiane **L5**, the outcome of the reaction with CuI depends on the reaction conditions. Reaction with CuI in MeCN provides a 1D ribbon $[\{\text{Cu}(\mu_2\text{-I})_2\text{Cu}\}(\text{MeCN})_2(\mu_2\text{-L5})_2]_n$ **CP16**, whereas treatment of CuI with **L5** in hot EtCN yields 2D-polymeric $[\{\text{Cu}_3(\mu_3\text{-I})(\mu_2\text{-I})_2(\mu_2\text{-L5})_2\}]_n$ **CP17**. A reversible phase transition from triclinic *P*-1 to monoclinic *P*2₁/*m* is observed when recording the structure of **CP16** at 5 different temperatures in the 100-300 K range. Ligand **L6** containing a ferrocenyl function at the 2-position was also probed as organometallic dithioether ligand. Reaction of **L6** with 1 equiv. of CuI produces the 0D dinuclear complex $[\{\text{Cu}(\mu_2\text{-I})_2\text{Cu}\}(\eta^1\text{-L6})_2(\text{MeCN})_2]$ (**D1**), whereas treatment with 2 equiv. of CuI affords the novel 1D CP $[\{\text{Cu}(\mu_3\text{-I})_2\text{Cu}\}(\mu\text{-L6})]_n$ **CP18**, in which both S atoms of one **L6** molecule span two copper centers of the infinite (CuI)_n ribbon. Some selected results of thermal analyses and luminescence measurements are also presented.

INTRODUCTION

Polydentate macrocyclic thiacyclic crown ethers ligands are able to coordinate a wide range of transition metal complexes both in endocyclic and exocyclic manner yielding discrete molecular complexes. They have also been used as assembling ligands to construct 1D and 2D coordination polymers and 3D MOFs.¹⁻¹⁰ The less flexible six-membered dithiaheterocycle 1,3-dithiane **L1** (also named 1,3-dithiacyclohexane) has also been used in the past as mono- and bidentate ligand to coordinate to a series of early and late transition metal complexes. Crystallographically characterized examples include mono- and dinuclear compounds $[(C_6H_6)Cr(CO)_2(\kappa^1-L1)]$,¹¹ $[Fe(CO)_4((\kappa^1-L1))]$,¹² $[(C_5H_5)Ru(PPh_3)_2((\kappa^1-L1))][CF_3SO_3]$,¹³ $[(C_5Me_5)IrCl_2((\kappa^1-L1))]$ and $[{(C_5Me_5)IrCl_2}_2(\mu_2-L1)]$,¹⁴ as well as polynuclear clusters such as $[(\mu_2-H)_2Ru_3(CO)_8Cl(\mu_3-\eta^3-L1)]$ and $[H_4Ru_4(CO)_{10}(\mu_2-L1)]$.¹⁵ ¹⁶ The propensity of 1,3-dithiane to act even as a μ_2-S,S 4-electron donor has been evidenced for $[Os_6CO_{16}(\mu_2-L1)]$, where **L1** is bridging across an Os–Os edge via one of the sulfur atoms.¹⁷ The use of 1,3-dithiane as assembling ligand for the construction of coordination polymers (CPs) has been first demonstrated by the crystallographic characterization of 1D polymeric 1,3-dithiane-dimercury(I) dinitrate.¹⁸ Several CPs have been built up by treatment of 1,3-dithiane with $AgNO_3$, $AgBF_4$ and $AgPF_6$, respectively.¹⁹ More recently, Keller and Knaust reacted $[Cu(MeCN)_4]BF_4$ with **L1** and obtained four coordination networks depending on metal-to-ligand ratio and solvent conditions used.²⁰ We have previously shown that the isomeric 1,2-dithiane heterocycle is formed upon treatment of 1,4-butanedithiol in the presence of CuI yielding the luminescent 1D material $[{Cu}(\mu_2-I)_2Cu\{(1,2-dithiane)_2\}_n]$ featuring rhomboid $Cu(\mu_2-I)_2Cu$ clusters, which are linked through the S-atoms of six-membered 1,2-dithiane heterocycles.²¹ In contrast to $[Cu(MeCN)_4]^+$ salts, CuI and CuBr form upon complexation with thioethers readily halide-bridged polynuclear aggregates, whose nuclearities and geometries are almost unpredictable.^{5, 22-30} We and other research groups encountered after ligation of aliphatic and aromatic dithioethers $RS(CH_2)_nSR$ ($n = 1-8$) and $RSCH_2C\equiv CCH_2SR$ a panoply of discrete molecular compounds, CPs and MOFs of varying dimensionality incorporating as connecting nodes the $Cu(\mu_2-X)_2Cu$ rhomboid, the tetranuclear closed-cubane Cu_4I_4 cluster, the prismane-shaped Cu_6I_6 cluster and the fused octanuclear Cu_8I_8 cluster.³¹⁻⁴⁵ Apart from the fascinating structural richness of these compounds, their photophysical properties, often associated with intense photoluminescence and luminescence thermochromism,^{30, 46, 47} intrigued us to investigate in

details the coordination chemistry of 1,3-dithiane **L1** and 2-substituted derivatives such as 2-methyl-1,3-dithiane **L2**, 2-isobutyl-1,3-dithiane **L3**, 2-Me₃Si-1,3-dithiane **L4**, 2-phenyl-1,3-dithiane **L5** and 2-ferrocenyl-1,3-dithiane **L6** *vis-à-vis* CuI, CuBr and CuCl. This study completes our recent investigation on the coordination of 2-methyl-1,3-dithiane **L2** on CuI where, depending on the reaction conditions, both topological isomers of composition [$\{\text{Cu}(\mu_2\text{-I})_2\text{Cu}\}(\mu_2\text{-L2})_2]_n$ or the luminescent 3D material [$\{\text{Cu}_8(\mu_3\text{-I})_8\}(\mu_2\text{-L2})_4]_n$, exhibiting an unprecedented octanuclear Cu₈I₈S₈ SBU, have been prepared and structurally characterized.⁴⁸ The chemical structures of the investigated ligands with the dimensionalities and nuclearities of the secondary building units of the resulting CPs are shown in Chart 1.

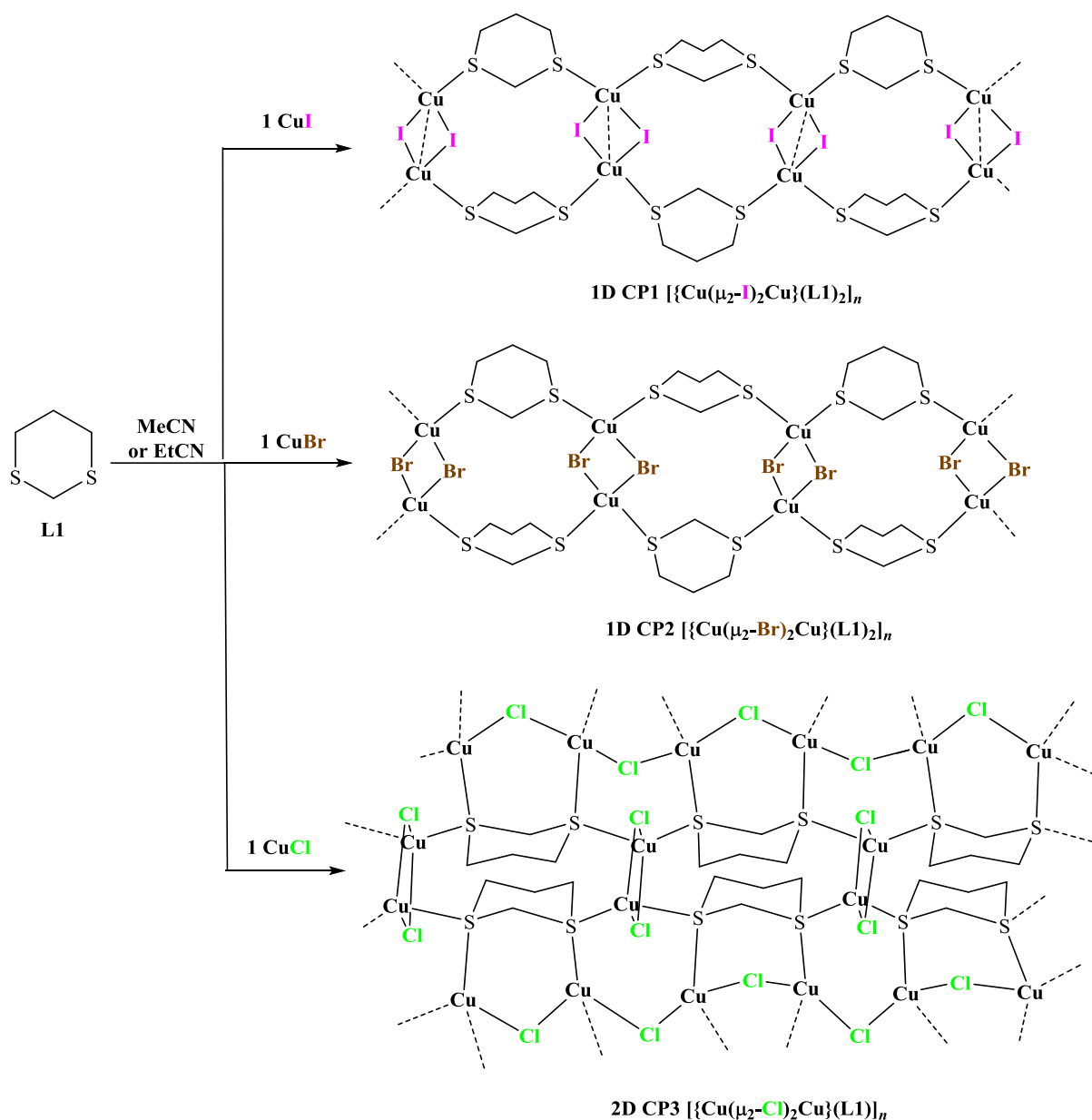
Chart 1. Ligands and coordination polymers investigated

| Ligand | CuX, X= | CPs | SBU | Dimensionality |
|-----------------------------------------------------------------------------------------------|---------|-------------|-----------------------------------------------------------------------|----------------|
| L1  | I | CP1 | Cu ₂ (μ ₂ -I) ₂ | 1D |
| | Br | CP2 | Cu ₂ (μ ₂ -Br) ₂ | 1D |
| | Cl | CP3 | Cu ₂ (μ ₂ -Cl) ₂ | 2D |
| L2  | | CP4 | Cu ₂ (μ ₂ -I) ₂ | 2D |
| | I | CP5 | Cu ₂ (μ ₂ -I) ₂ | 1D |
| | | CP6 | Cu ₈ (μ ₃ -I) ₈ | 3D |
| | Br | CP7 | Cu ₂ (μ ₂ -Br) ₂ | 1D |
| | Cl | CP8 | Cu ₂ (μ ₂ -Cl) ₂ | 1D |
| L3  | CN | CP9 | Cu(μ ₂ -CN) | 2D |
| | I | CP10 | Cu ₃ (μ ₃ -I)(μ ₂ -I) ₂ | 2D |
| | Br | CP11 | Cu ₂ (μ ₂ -Br) ₂ | 2D |
| L4  | Cl | CP12 | Cu ₂ (μ ₂ -Cl) ₂ | 2D |
| | I | CP13 | Cu ₂ (μ ₄ -I)(μ ₂ -I) | 1D |
| | Br | CP14 | Cu ₂ (μ ₄ -Br)(μ ₂ -Br) | 1D |
| L5  | Cl | CP15 | Cu ₂ (μ ₄ -Cl)(μ ₂ -Cl) | 1D |
| | I | CP16 | Cu ₂ (μ ₂ -I) ₂ | 1D |
| | | CP17 | Cu ₃ (μ ₃ -I)(μ ₂ -I) ₂ | 2D |
| L6  | Br | CP18 | Cu ₃ (μ ₃ -Br)(μ ₂ -Br) ₂ | 2D |
| | I | D1 | Cu ₂ (μ ₂ -I) ₂ | 0D |

RESULTS AND DISCUSSION

Synthesis and X-Ray diffraction characterization

*Treatment of 1,3-dithiane **L1** with CuX (X=I, Br, Cl).* In continuation of our previous work on the coordination chemistry of cyclic⁴⁹ and acyclic dithioether ligands on CuX salts and to complete the series of ionic Cu(I) networks obtained by Keller and Knaust²⁰ by treatment of $[\text{Cu}(\text{MeCN})_4]\text{BF}_4$ with 1,3-dithiane **L1**, we reacted this heterocycle with CuI in a 1:1 ratio. After heating in EtCN, a colorless crystalline material of composition $[\{\text{Cu}(\mu_2\text{-I})_2\text{Cu}\}(\mu_2\text{-L1})_2]_n$ was obtained in over 90% yield (Scheme 1).



Scheme 1. Synthesis of the 1D CPs $[\{\text{Cu}(\mu_2\text{-X})_2\text{Cu}\}(\mu_2\text{-L1})_2]$ **CP1** ($\text{X} = \text{I}$) and **CP2** ($\text{X} = \text{Br}$) and the 2D CP $[\{\text{Cu}(\mu_2\text{-Cl})_2\text{Cu}\}(\mu_2\text{-L1})]$ **CP3**.

An X-ray diffraction study revealed formation of ribbon-like 1D coordination polymer, in which rhomboid $\text{Cu}(\mu_2\text{-I})_2\text{Cu}$ units are linked through bridging dithiane cycles using both S atom as donor sites (Figures 1 and S1). Let us first compare the structural features of $[\{\text{Cu}(\mu_2\text{-I})_2\text{Cu}\}(\mu_2\text{-L1})_2]$ with those of its 1D isomer $[\{\text{Cu}(\mu_2\text{-I})_2\text{Cu}\}(1,2\text{-dithiane})_2]_n$.²¹ This latter is assembled by rhomboid $\text{Cu}(\mu_2\text{-I})_2\text{Cu}$ clusters, which are linked through the S-atoms of six-membered 1,2-dithiane heterocycles, thus generating an infinite ribbon. But in contrast to

$[\{\text{Cu}(\mu_2\text{-I})_2\text{Cu}\}(\mu_2\text{-L1})_2]_n$, where the centrosymmetric $\text{Cu}(\mu_2\text{-I})_2\text{Cu}$ units are arranged roughly perpendicular with respect to the 1,3-dithiane cycles, those of $[\{\text{Cu}(\mu_2\text{-I})_2\text{Cu}\}(1,2\text{-dithiane})_2]_n$ are approximately coplanar. Another striking difference concerns the $\text{Cu}\cdots\text{Cu}$ distances within the $\text{Cu}(\mu_2\text{-I})_2\text{Cu}$ rhomboids, which are far longer in the 1,3-dithiane isomer than in 1,2-dithiane one (2.8904(6) vs. 2.6843(18) Å).

The coordination mode of $[\{\text{Cu}(\mu_2\text{-I})_2\text{Cu}\}(\mu_2\text{-L1})_2]_n$ is more reminiscent to that encountered in 1D CP $[\{\text{Cu}(\mu_2\text{-I})_2\text{Cu}\}_2\{\mu\text{-PhS}(\text{CH}_2)_2\text{SPh}\}_2]_n$, displaying a $\text{Cu}\cdots\text{Cu}$ separation of 2.8058(11) Å.³² Other complexes exhibiting a rhomboidal Cu_2I_2 unit and weak $\text{Cu}\cdots\text{Cu}$ interactions close to the values of $[\{\text{Cu}(\mu_2\text{-I})_2\text{Cu}\}\{\mu\text{-PhS}(\text{CH}_2)_m\text{SPh}\}_2]_n$ ($m = 2,3,5$) have been reported for the 3D CP $[\text{Cu}_2\text{I}_2[16]\text{aneS}_4]_n$ ($[16]\text{aneS}_4 = 1,5,9,13\text{-tetrathiacyclohexadecane}$) (2.8079(12) Å and dinuclear $[\{\text{MeSi}(\text{CH}_2\text{SMe})_3\}\text{CuI}]_2$ (2.862(2) Å).^{5, 19, 50, 51}

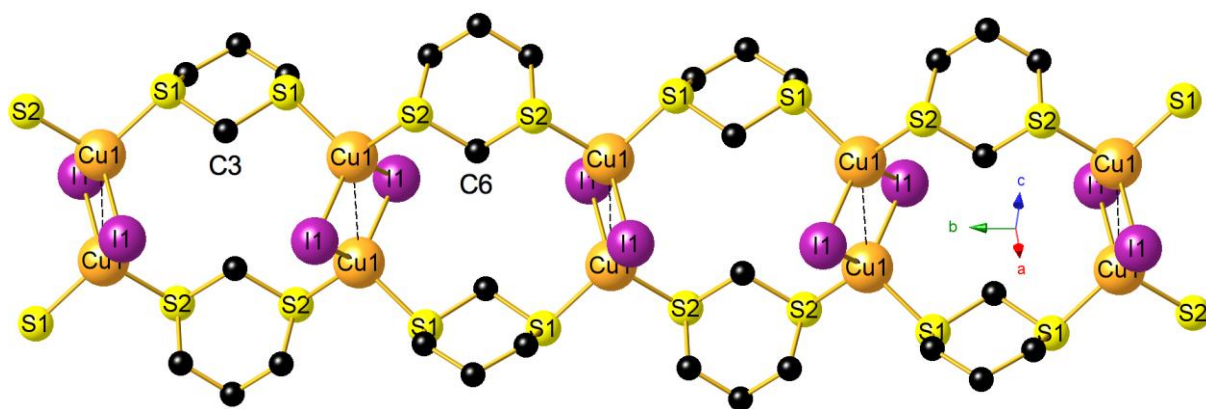


Figure 1. View of the 1D ribbon of $[\{\text{Cu}(\mu_2\text{-I})_2\text{Cu}\}(\text{L1})_2]_n$ **CP1** running along b axis. Selected bond lengths (Å) and angles (°): $\text{Cu}\cdots\text{Cu}\#$ 2.8904(6), Cu-I 2.5989(4), $\text{Cu-I}\#$ 2.6492(3), Cu-S1 2.3312(7), Cu-S2 2.3262(6); $\text{Cu-I-Cu}\#$ 66.829(11), S1-Cu-S2 103.93(2), S1-Cu-I 111.443(3), $\text{S1-Cu-I}\#$ 109.053(18), S2-Cu-I 110.461(18), $\text{S2-Cu-I}\#$ 108.333(18).

The homogeneity of the phase was ascertained by recording the PXRD spectrum (Figure S17). Previous studies from our group have shown that the CuI -to-ligand ratio may have a crucial impact on the architecture as well as on nuclearity within the $(\text{CuI})_n$ clusters of the resulting network.⁴⁸ For example, mixing CuI and $\text{PhS}(\text{CH}_2)_5\text{SPh}$ in a 2:1 ratio results in formation of $[\text{Cu}_4\text{I}_4\{\mu\text{-PhS}(\text{CH}_2)_5\text{Ph}\}_2]_n$ in which cubane-like $\text{Cu}_4(\mu_3\text{-I})_4$ cluster are linked by the bridging dithioether ligand giving rise to a 1D necklace structure.³⁷ However, a 1D-chain with composition $[\{\text{Cu}(\mu_2\text{-I})_2\text{Cu}\}\{\mu\text{-PhS}(\text{CH}_2)_5\text{SPh}\}_2]_n$, incorporating rhomboid Cu_2I_2 units,

is produced upon treatment of CuI with 1,5-bis(phenylthio)pentane in a 1:1 ratio. Therefore, we reacted 1,3-dithiane also with two equivalents of CuI in MeCN solution. However, a comparison of the PXRD spectra (Figure S17) revealed that no other species is present in the precipitated colorless bulk material. Note also, that in this case and in contrast to **L2** (see below),⁴⁸ the order of addition of the reactants does not affect the outcome of the reaction.

We reacted under analogous condition **L1** also with CuBr. Again a colorless, sparingly soluble material of composition $[\{\text{Cu}(\mu_2\text{-Br})_2\text{Cu}\}(\mu_2\text{-L1})_2]_n$ **CP2** was formed (Figure 2 and Figure S2), crystallizing like $[\{\text{Cu}(\mu_2\text{-I})_2\text{Cu}\}(\mu_2\text{-L1})_2]_n$ in the orthorhombic space group *Pnma*. Compared with the latter, the Cu···Cu contact of 2.9143(3) Å is looser and matches well with that of 1D CP $[\{\text{Cu}(\mu_2\text{-Br})_2\text{Cu}\}(\mu_2\text{-PhSCH}_2\text{SPh})_2]_n$ (2.9192(8) Å).⁴⁰

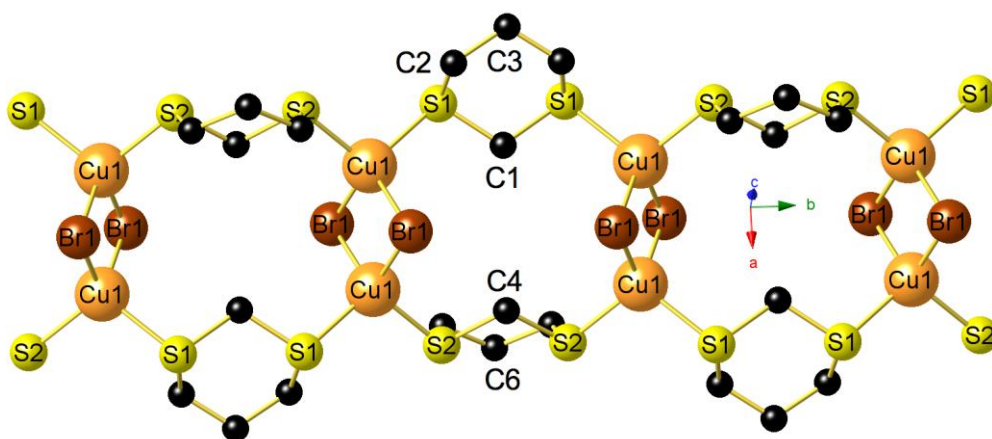
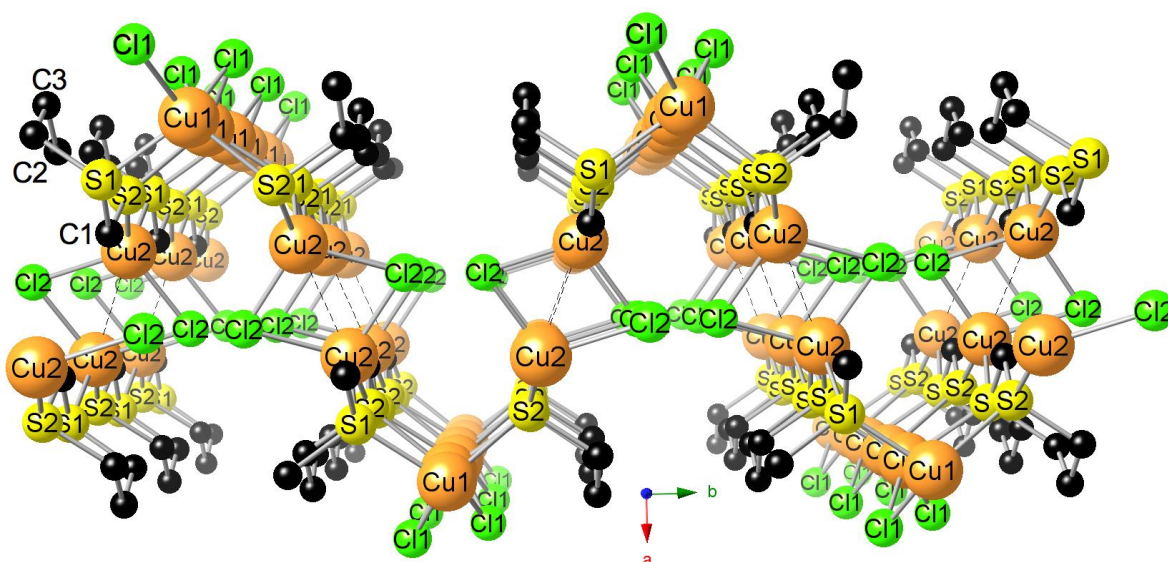


Figure 2. View of the 1D ribbon of $[\{\text{Cu}(\mu_2\text{-Br})_2\text{Cu}\}(\mu_2\text{-L1})_2]_n$ **CP2**. Selected bond lengths (Å) and angles (°): Cu···Cu# 2.9143(3), Cu–Br 2.4478(2), Cu–Br# 2.5088(2), Cu–S1 2.2989(3); Cu–S2 2.3009(3), Cu–Br–Cu# 72.011(6), S1–Cu–S2 105.170(11), S1–Cu–Br 112.192(9), S1–Cu–Br# 109.151(9), S2–Cu–Br 113.089(8), S2–Cu–Br# 109.169(9).

Tan and Ang reported that **L1** reacts readily with CuCl₂ to form a paramagnetic species [CuCl₂**L1**] undergoing spontaneously reduction to give finally [Cu₂Cl₂**L1**] according to elemental analysis and magnetic measurements.⁵² We repeated this experience using CuCl₂·2H₂O as starting material and noticed also progressive discoloration of the initially green solution to yellowish with precipitation of a colorless powder, which was analyzed to have indeed a composition [Cu₂Cl₂**L1**]. **Note that other examples of the reduction of CuCl₂ in the presence of thioethers have been reported previously.**^{53, 54} In an alternative approach, we added a twofold amount of CuCl to a MeCN solution of **L1**, causing rapid precipitation of a microcrystalline solid in over 85% yield (Scheme 1). This latter was analyzed to have also a

2:1 Cu:**L1** composition, different from the 1:1 Cu:**L1** composition found for **CP1** and **CP2**. By recrystallization of a sample from hot EtCN, small single-crystals crystallizing in the monoclinic space group $P2(1)/c$ could be grown. Examination of the X-ray data of $[\{\text{Cu}(\mu_2\text{-Cl})_2\text{Cu}\}(\mu_2\text{-L1})]_n$ **CP3** (Figure 3) reveals that the dimensionality of the network has changed to 2D. Like in **CP1** and **CP2**, rhomboid $\text{Cu}(\mu_2\text{-X})_2\text{Cu}$ SBUs are present, but they are composed of two crystallographically distinct Cu atoms with Cu1····Cu2 separation of 2.809(2) Å. Apart from the dimensionality, the second salient feature concerns the bonding mode of the S atoms. Whereas in **CP1** and **CP2** all S-atoms act as 2-electron donors, in **CP3** both lone pairs of the S-donors are engaged in bonding as schematically shown in Scheme 1. The propensity of 1,3-dithiane to act as a μ_2 -S,S 4-electron donor has been previously evidenced for the cluster $[\text{Os}_6\text{CO}_{16}(\mu_2\text{-L1})]$, where **L1** is bridging across an Os–Os edge via one of the sulfur atoms.¹⁷



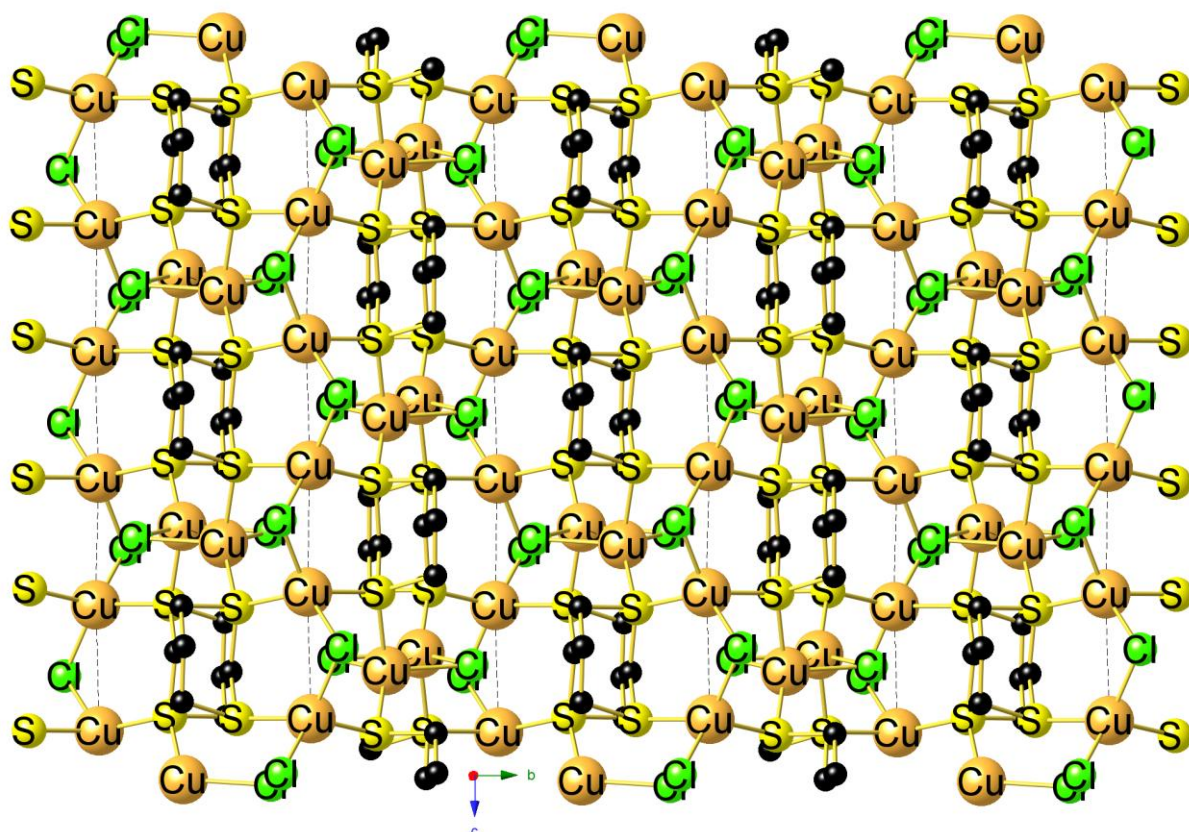


Figure 3. (top) Perspective view down the c axis on the a,b plane of the 2D network of $[\{\text{Cu}(\mu_2\text{-Cl})_2\text{Cu}\}(\mu_2\text{-L1})]_n$ **CP3**. (bottom) View on the b,c plane of the 2D network of **CP3**. Selected bond lengths (Å) and angles (°): Cu1 \cdots Cu2 2.809(2), Cu1–Cl1 2.302(2), Cu1–Cl2 2.339(2), Cu1–S1 2.294(2), Cu1–S2 2.317(4); Cu2–S2 2.263(2); Cu1–Cl1–Cu2 92.68(7), Cu1–Cl2–Cu2 73.33(7), S1–Cu1–S2 106.97(8), S1–Cu–S2 108.21(8), S1–Cu1–Cl1 123.18(8), S2–Cu2–Cl2 124.64(8). Symmetry transformations used to generate equivalent atoms: $^11-X, 1-Y, -Z$; $^2+X, +Y, -1+Z$; $^3+X, 3/2-Y, 1/2+Z$; $^4+X, 3/2-Y, -1/2+Z$; $^5+X, +Y, 1+Z$.

The comparison of the PXRD pattern of the material obtained by reduction of CuCl_2 and direct complexation of **L1** confirms that (i) both compounds have the identical composition and (ii) the experimental diffractogram of **CP3** matches with the calculated one (Figure 4).

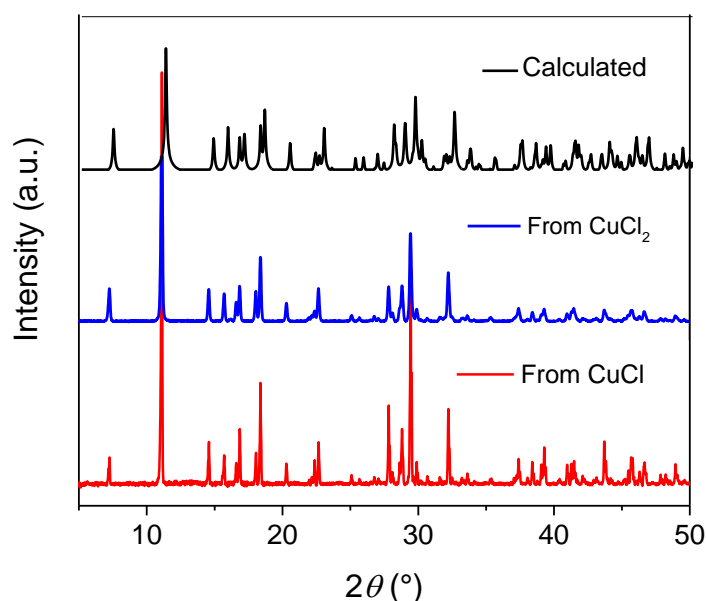
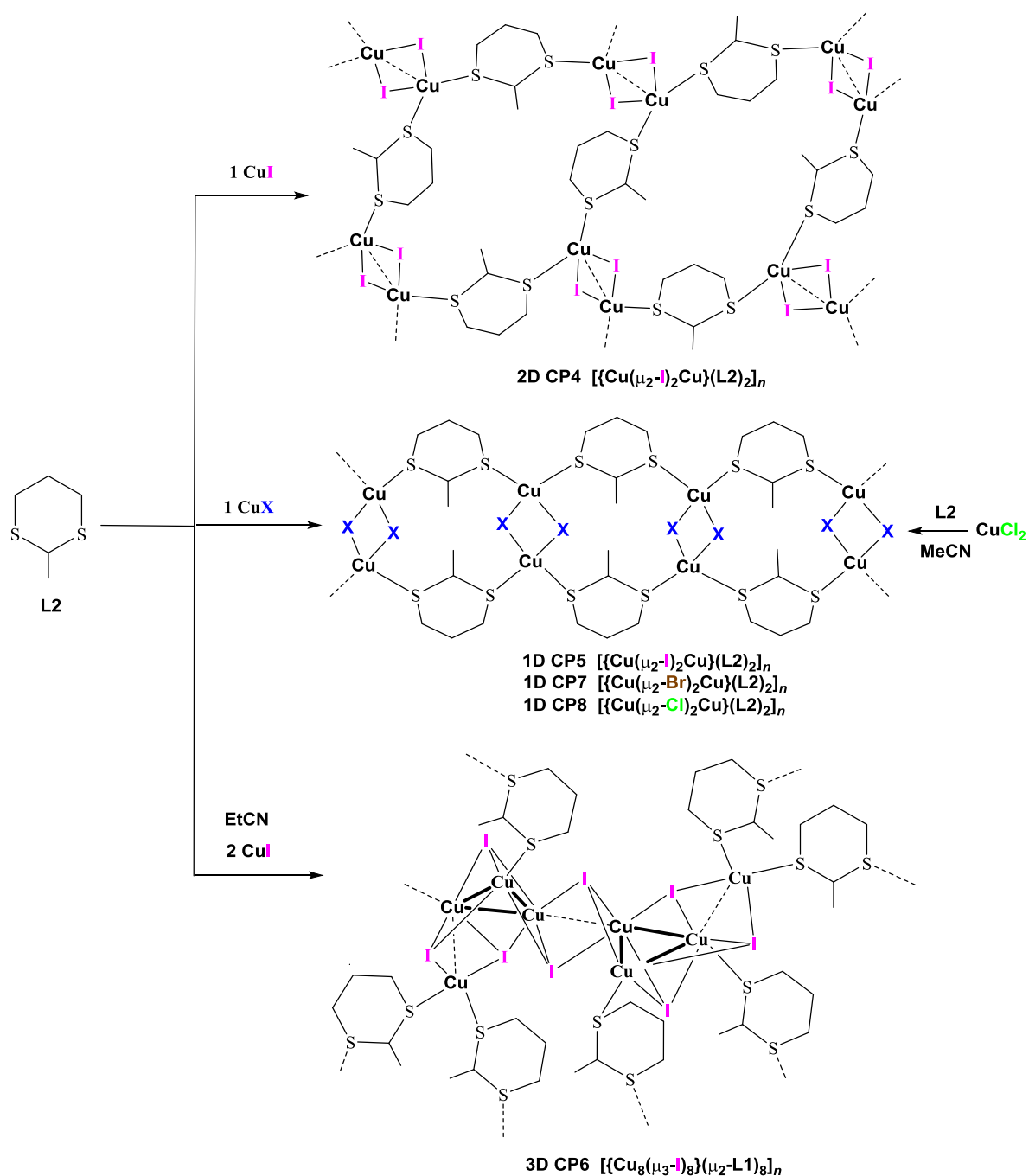


Figure 4. Comparison of the PXRD patterns of the products obtained by treatment of CuCl_2 and CuCl with **L1** and comparison of the experimental PXRD of **CP3** with the simulated pattern.

*Treatment of 2-methyl-1,3-dithiane **L2** with CuX ($X=\text{I}, \text{Br}, \text{Cl}$) and CuCN .* In contrast to **L1**, its derivative 2-methyl-1,3-dithiane **L2** bearing a sterically more crowded substituent at the 2-position of the dithiane cycle, has been very scarcely probed as ligand in coordination chemistry. The few representatives, whose fluxional behavior has been investigated by NMR techniques in solution, are $[\text{M}(\text{CO})_5\text{L2}]$ and $[\text{Fe}(\text{CO})_4\text{L2}]$.^{55, 56} According to a survey of the CSD data base, there are no examples of crystallographically characterized coordination compounds ligated with alkyl- or aryl-substituted dithianes. Recently, we investigated in depth the reactivity of **L2** toward CuI . When **L2** and CuI were reacted in a 1:1 ratio, we evidenced the formation of two topological 1D (**CP5**) and 2D (**CP4**) isomers of formula $[\{\text{Cu}_2\text{I}_2\}(\text{L2})_2]_n$ featuring dinuclear $\{\text{Cu}_2(\mu_2\text{-I})_2\}$ rhomboids.⁴⁸ We also demonstrated that the network dimensionality can be controlled by the order of reactants addition. More interestingly, when 2 eq. of **L2** were used, a strongly luminescent non-porous 3D coordination polymer $[\{\text{Cu}_8(\mu_3\text{-I})_8\}(\mu_2\text{-L2})_4]_n$ **CP6**, incorporating unprecedented $\text{Cu}_8\text{I}_8\text{S}_8$ clusters (built upon two side-fused open cubanes) was obtained (Scheme 2). We have furthermore shown that **CP4** and **CP5** can be converted in hot butyronitrile to strongly luminescent **CP6**. For comparison, we extended our study on the coordination chemistry of **L2** toward CuBr and CuCl vs CuI .



Scheme 2. Synthesis of 2-methyl-1,3-dithiane-linked CPs **CP4-CP8**.⁴⁸

Addition of a slight excess of **L2** to MeCN solutions of CuBr and CuCl resulted in fast deposition of large amounts of microcrystalline solids. X-ray suitable single crystals crystallizing in both cases in the monoclinic space group $C2/m$ were obtained from dissolution of solid samples in hot EtCN or by slow partial evaporation of MeCN solutions. The crystal structures of the resulting 1D CPs $[\{\text{Cu}(\mu_2\text{-Br})_2\text{Cu}\}(\mu_2\text{-L2})_2]_n$ **CP7** and $[\{\text{Cu}(\mu_2\text{-Cl})_2\text{Cu}\}(\mu_2\text{-L2})_2]_n$ **CP8** were determined by single-crystal X-ray diffraction.

$\text{Cl})_2\text{Cu}\{\mu_2\text{-L2}\}_n$ **CP8** shown in Figures 5 and 6 (Figures S3 and S4) are isostructural with their iodo analogue $[\{\text{Cu}(\mu_2\text{-I})_2\text{Cu}\}\{\mu_2\text{-L2}\}_n]$ **CP5**, constituting thus a unique case allowing a comparative description. The non-bonding $\text{Cu}\cdots\text{Cu}\#$ contacts of the centrosymmetric $[\{\text{Cu}(\mu_2\text{-X})_2\text{Cu}\}]$ rhomboids shorten systematically from 3.367 to 3.176 Å going from I to Br and reach 3.0517(8) Å for $\text{X} = \text{Cl}$. The Cu-X-Cu angles are not much affected by this shrinking of the $\text{Cu}\cdots\text{Cu}\#$ contacts and evolve from $79.042(10)^\circ$ ($\text{X} = \text{I}$), $79.165(16)^\circ$ ($\text{X} = \text{Br}$) to $79.851(16)^\circ$ ($\text{X} = \text{Cl}$). Within this series, the Cu-S bond length falls with increasing electronegativity of the bridging halide from 2.3316(4), 2.3097(6), to 2.3060(4) Å. We are not aware of other complete literature-known $[\{\text{S}_2\text{Cu}(\mu_2\text{-X})_2\text{Cu}\}\text{S}_2]$ series. Note that an opposite evolution of the $\text{Cu}\cdots\text{Cu}$ separation is noticed in the case of the **L1**-ligated compound $[\{\text{Cu}(\mu_2\text{-X})_2\text{Cu}\}\{\mu_2\text{-L1}\}_n]$ **CP1** and **CP2** ($\text{X} = \text{I}, \text{Br}$; see above). The same tendency has been reported for the isomorphous molecular compounds $[\{\text{Cu}(\mu_2\text{-X})_2\text{Cu}\}(\mu\text{-PhCH}_2\text{SCH}_2\text{C}\equiv\text{CCH}_2\text{SCH}_2\text{Ph})_2]$, where in the case of $\text{X} = \text{I}$ the $\text{Cu}\cdots\text{Cu}$ distance is shorter than for $\text{X} = \text{Br}$ [2.9279(5) vs. 3.0075(5) Å].⁵⁷ The opposite trend has been noticed by Bowmaker *et al.* for 1:1:1 adducts of copper(I) halides with phosphine and amine donor ligands, $[\{\text{CuX}[\text{PPh}_2(\text{C}_6\text{H}_4\text{Me-o})](\text{cpy})\}_2]$ ($\text{cpy} = 4\text{-cyanopyridine}$; $\text{X} = \text{Cl}, \text{Br}$ or I). In this latter series, the $\text{Cu}\cdots\text{Cu}$ distances increase from 3.119(3) to 3.201(2) to 3.304(2) Å.⁵⁸ Currently, we have no explanation to rationalize these findings.

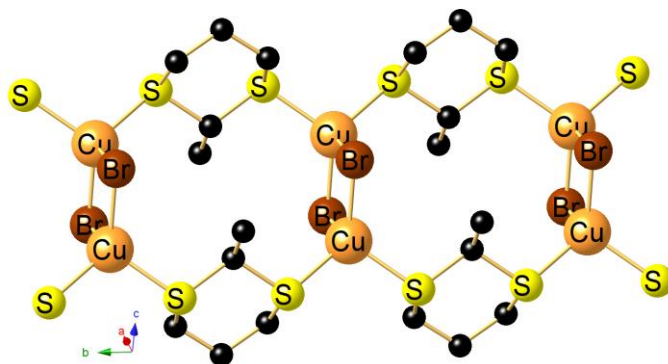


Figure 5. View of a segment of the 1D ribbon of $[\{\text{Cu}(\mu_2\text{-Br})_2\text{Cu}\}\{\mu_2\text{-L2}\}_n]$ **CP7**. Selected bond lengths (Å) and angles ($^\circ$): $\text{Cu}\cdots\text{Cu}\#$ 3.176, Cu-Br 2.4393(6), $\text{Cu-Br}\#$ 2.5428(5), Cu-S 2.3097(6), $\text{Cu-S}\#$ 2.3098(6), $\text{Cu-Br-Cu}\#$ $79.165(16)$, $\text{Br-Cu-Br}\#$ $100.835(16)$, S-Cu-Br $118.096(18)$, $\text{S-Cu-Br}\#$ $107.533(18)$, $\text{S}\#-\text{Cu-Br}$ $118.096(18)$, $\text{S-Cu-S}\#$ $103.97(3)$.

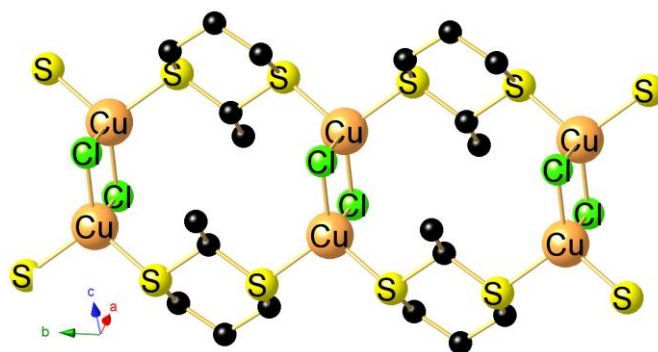
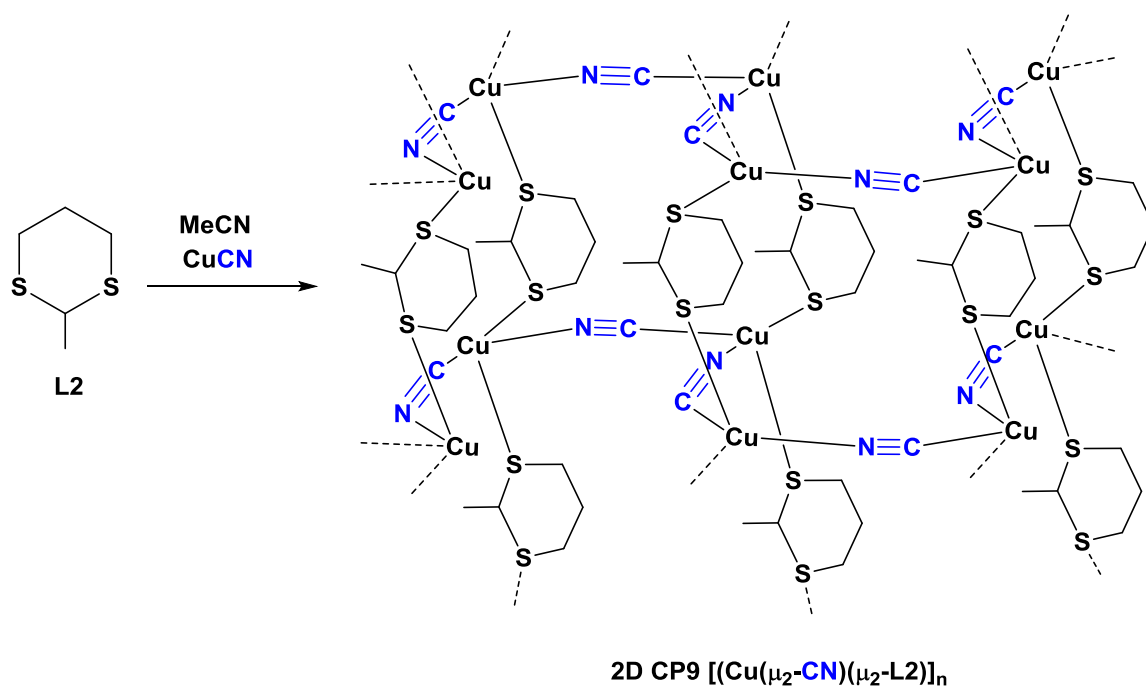


Figure 6. View of a segment of the 1D ribbon of $[\{\text{Cu}(\mu_2\text{-Cl})_2\text{Cu}\}(\mu_2\text{-L2})_2]_n$ **CP8**. Selected bond lengths (Å) and angles (°): Cu····Cu# 3.0517(8), Cu–Cl 2.3133(7), Cu–Cl# 2.4393(7), Cu–S 2.3060(4), Cu–Cl–Cu# 79.851(16), Cl–Cu–Cl# 100.148(15), S–Cu–Cu# 126.738(10), S–Cu–S# 104.13(2), S#–Cu–Cl 118.741(11), S–Cu–Cl# 106.997(13).

Although less common than CuX thioether adducts, the pseudohalide salt CuCN is also known to form both discrete molecular complexes and coordination polymers with varying dimensionalities upon treatment with thioether ligands. Examples are the dinuclear species $[(9\text{S}3)\text{Cu}(\mu_2\text{-CN})(9\text{S}3)]\text{BF}_4$ (9S3 = 1,4,7-trithiacyclononane) or an 3D network of formula $[(\text{Cu}(\mu_2\text{-CN})(\mu_2\text{-SMe}_2))]_n$.^{59, 60} Another example of a 3D network assembled by tetrahydrothiophene ligands is $[(\text{Cu}(\mu_2\text{-CN})(\mu_2\text{-THT}))]_n$.⁶⁰ When adding a slight excess of **L2** to hot suspension of CuCN in MeCN a greyish microcrystalline solid precipitated rapidly. We failed to obtain acceptable elemental analysis or PXRD data for this compound, which seems to lose progressively the somewhat volatile **L2** ligand upon drying. The facile release of CuCN-bound ligands yielding CuCN has been evidenced by means of thermal analysis elsewhere.⁶⁰



Scheme 3. Synthesis of $[(\text{Cu}(\mu_2\text{-CN})(\mu_2\text{-L2}))_n]$ **CP9**.

Characteristic in the ATR-IR spectrum of **CP9** is the presence of an intense $\nu(\text{C}\equiv\text{N})$ vibration occurring at 2121 cm^{-1} indicative for a covalently bound cyanide ligand (Fig S33 ESI). As in other CuCN CPs ligated by donor ligands, the $\nu(\text{C}\equiv\text{N})$ stretch is markedly red-shifted compared to that of uncoordinated CuCN (2170 cm^{-1}).⁶¹ Due to its poor solubility, a small amount was re-dissolved in hot benzyl cyanide at $180\text{ }^\circ\text{C}$ in the presence of **L2** and then allowed to reach ambient temperature forming a product crystallizing in the orthorhombic space group $Cmc2_1$. A view of the corrugated 2D sheets of $[(\text{Cu}(\mu_2\text{-CN})(\mu_2\text{-L2}))_n]$ **CP9** is shown in Figure 7. The layers are constructed by two crystallographically different tetrahedral Cu1 and Cu2 centers, each one ligated by one C-bound cyanide, one N-bound cyanide from a neighbored Cu atom and the S atoms of two **L2** ligands. A view down the *b* axis on a 2D sheet of **CP9** is given in Figure S5.

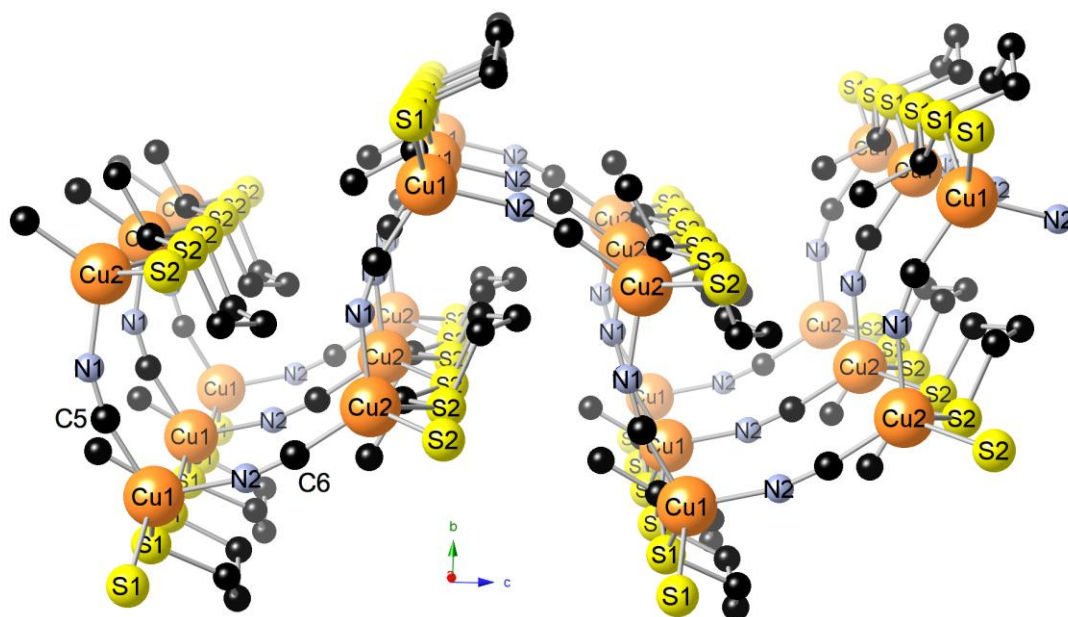
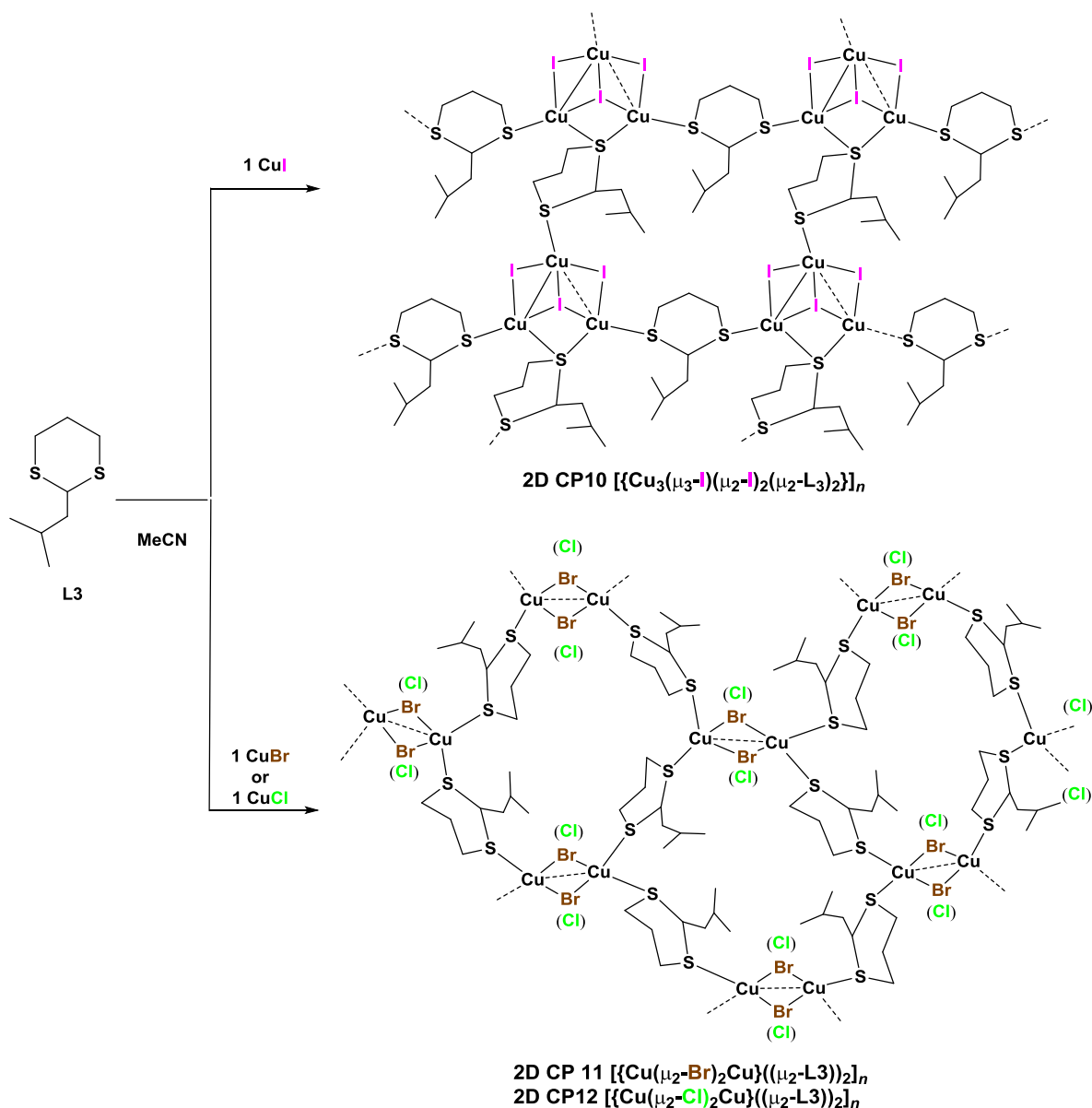


Figure 7. View down the *a* axis of the 2D layer of $[\{Cu(\mu_2-CN)_2Cu\}(\mu_2-L2)_2]_n$ **CP9**. Selected bond lengths (Å) and angles (°): Cu1–C5 1.935(3), Cu2–C6 1.920(3), Cu1–S1 2.3469(6), Cu2–S2 2.4032(6), Cu1–N2 2.006(6), Cu2–N1 2.015(3), C5–N1 1.142(4), C6–N2 1.153(4); S1–Cu1–S1 99.39(3), S2–Cu2–S2 95.64(3), S1–Cu1–S1 104.92(5), N1–Cu2–S2 102.35(6).

Treatment of 2-isobutyl-1,3-dithiane L3 with CuX (X = I, Br, Cl). Intrigued by the striking differences concerning the dimensionalities and nuclearities of the polymeric materials obtained from reaction of CuX with **L1** and **L2**, we investigated also in detail the effect of the substitution at the 2-position by a bulkier isobutyl group. We therefore reacted first CuI with 2-isobutyl-1,3-dithiane **L3** in a 1:1 ratio (Scheme 4). A white precipitate immediately formed at room temperature. Dissolution of a small amount of this powder into hot acetonitrile led to the formation of the 2D **CP10** of composition $[\{Cu_3(\mu_3-I)(\mu_2-I)_2(\mu_2-L3)_2\}]_n$ which crystallizes in the triclinic space group *P*-1. Here, again, addition of an excess of **L3** (ratio 1:2) led also to **CP10** as proven by PXRD (Figure S21). The most salient feature in the crystal structure is the occurrence of triangular Cu_3I_3 SBUs, capped by a μ_3 -iodo ligand and two μ_2 -bond I atom spanning two edges (Figures 8 and S6). All Cu···Cu contacts are quite different ranging between weakly bonding (Cu2–Cu3 2.7625(3)), to clearly non-bonding Cu1···Cu3 2.9554(3) and Cu1···Cu2 3.336 Å. The structure presents four non-equivalent sulfur atoms. The particularity is that the S3 atom acts as 4-electron donor while the others are only two electrons donors. Thus, one isobutyl-1,3 dithiane ligand acts solely as a κ_1S - κ_1S ligand while

the second one acts as a $\kappa_1\text{S}-\mu_2\text{S}$ ligand. The first dimension is maintained through the coordination of one ligand to two Cu_3I_3 SBUs thus forming Cu1-S1-S2-Cu2 ribbons. The coordination of S3 to Cu1 and Cu2 and of S4 to Cu3 led to the second dimension, thus generating 19-membered macrocycles.



Scheme 4. Synthesis of the 2D CPs **CP10**, **CP11** and **CP12** obtained by treatment of CuX with **L3**.

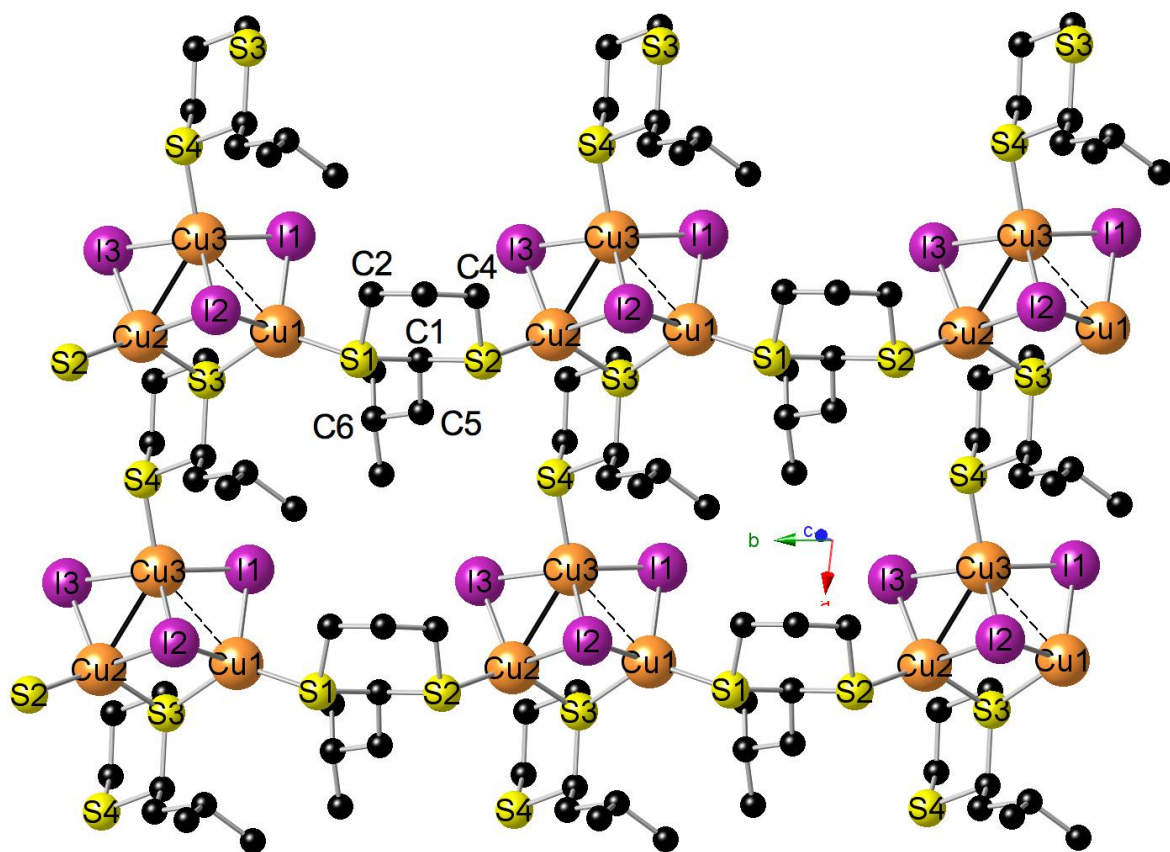


Figure 8. View down the c axis of the 2D network of $[\{Cu_3(\mu_3-I)(\mu_2-I)_2(\mu_2-L_3)_2\}]_n$ CP10. Selected bond lengths (Å) and angles (°): Cu1····Cu3 2.9554(3), Cu2–Cu3 2.7625(3), Cu1····Cu2 3.336 Cu1–I1 2.5910(2), Cu3–I1 2.6643(2), Cu1–I2 2.8034(2), Cu2–I2 2.8340(2), Cu3–I2 2.6486(2), Cu2–I3 2.5875(2), Cu3–I3 2.6481(2), Cu1–S1 2.3132(3), Cu1–S3 2.3179(3), Cu2–S3 2.2791(3), Cu2–S2 2.2976(3), Cu1–I1–Cu3 68.423(6), Cu1–I2–Cu2 72.560(6), Cu1–I2–Cu3 65.578(6), Cu2–I2–Cu3 60.400(6), Cu2–I3–Cu3 63.681(7), Cu1–S3–Cu2 93.047(12), S1–Cu1–S3 132.568(13), S2–Cu2–S3 136.460 (13).

Several other examples of CPs incorporating trinuclear $Cu_3I_xS_3$ ($X = 3,4$) motifs such as catena-[tris(μ_3 -I)-(μ₂-I)-(ethyl-(*N*-ethyl-4-pyridinio)sulfido)-tricopper(I)] (EtS-4-C₅H₄NEt)[Cu₃I₄], constructed of Cu₃I₄[−] and EtS-C₅H₄N⁺Et components, are literature-known.⁶² The assembly of a 3D CP [(Cu₃I₃)(thiacrown) • (MeCN) • (CH₂Cl₂) • (2H₂O)]_n by mixing calix[4]-bis-thiacrown with CuI in CH₂Cl₂ and MeCN has been reported by Lee *et al.* Upon removal of the coordinated solvent molecules by heating, the initial solvent-coordinated CP undergoes a single-crystal-to-single-crystal transformation to the desolvated polymer [(Cu₃I₃)(thiacrown) • (0.5H₂O)]_n.^{7, 63} For other Cu₃I₃ containing compounds, see also:^{64, 65} There is also a report on the molecular compound [Cu₃I₄(dodecylMeS)₃](dodecylMe₂S)

Å and a dodecyldimethylsulphonium cation as counterion.⁶⁶ However, the structural features of **CP10** differ considerably from those examples. Although the iodocuprates $[\text{Cu}_3\text{I}_4(\text{dodecylMeS})_3][\text{dodecylMe}_2\text{S}]$ and $(\text{EtS-4-C}_5\text{H}_4\text{NEt})[\text{Cu}_3\text{I}_4]$ incorporate like **CP10** triangular Cu clusters, those triangles are far more symmetric with mean Cu–Cu distances below 2.8 Å.^{62, 66} The SBUs of $[(\text{Cu}_3\text{I}_3)(\text{thiacrown}) \cdot (\text{MeCN}) \cdot (\text{CH}_2\text{Cl}_2) \cdot (2\text{H}_2\text{O})]_n$ do not form triangles, but are described as three-runged ladder type Cu_3I_3 units bearing exclusively μ_2 -bound iodo ligands.⁷ Although the two latter materials own also a $\text{Cu}_3\text{I}_3\text{S}_4$ composition like **CP10**, there is one CuI unit without any Cu–S bond and two CuI units connected each to two S-donor sites.

The treatment of **L3** with CuBr under analogous reaction conditions gives also rise to a 2D network but, in contrast to that of **CP10**, the topology of this colorless material crystallizing in the monoclinic space group $P2_1/c$ is rather trivial (Scheme 4). Figures 9 and S7 show that the 2D layers of $[\{\text{Cu}(\mu_2\text{-Br})_2\text{Cu}\}(\mu_2\text{-L3})_2]_n$ **CP11** are composed of rhomboid $\text{Cu}(\mu_2\text{-Br})_2\text{Cu}$ SBUs, whose Cu–Cu distance matches with that of **CP2** (2.9057(2) vs 2.9143(3) Å). Unlike the $\text{Cu}(\mu_2\text{-Br})_2\text{Cu}$ SBUs of **CP2** and **CP7**, the two Cu atoms of **CP11** are crystallographically different.

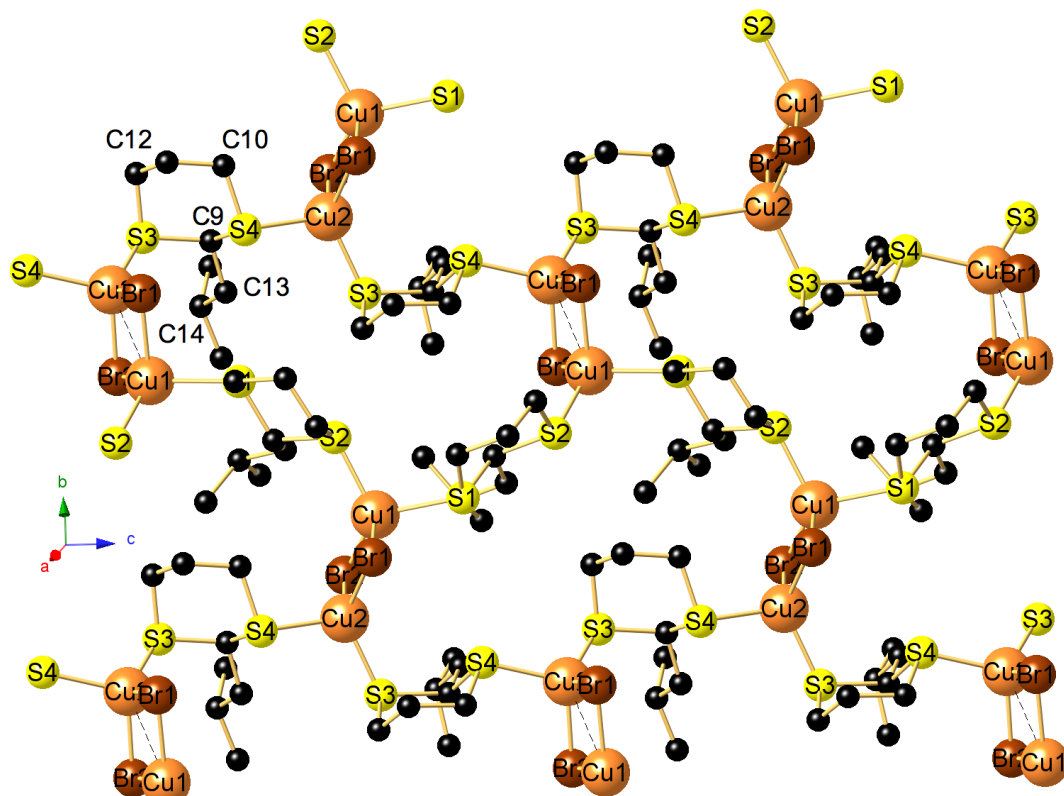


Figure 9 View on the b,c plane of the 2D network of $[\{\text{Cu}(\mu_2\text{-Br})_2\text{Cu}\}(\mu_2\text{-L3})_2]_n$ **CP11**. Selected bond lengths (Å) and angles (°): Cu1–Cu2 2.9057(2), Cu1–Br1 2.5636(2), Cu1–Br2 2.4136(2), Cu2–Br1 2.4834(2), Cu2–Br2 2.4872(2), Cu1–S1 2.3882(3), Cu1–S2 2.3161(3), Cu2–S3 2.2724(3), Cu2–S4 2.3249(3); Cu1–Br1–Cu2 70.279(6), Cu1–Br2–Cu2 72.710(7), Br1–Cu1–Br2 108.328(7), Br1–Cu2–Br2 108.578(7), S1–Cu1–S2 105.945(11), S3–Cu2–S4 108.523(12).

The isostructural 2D CP $[\{\text{Cu}(\mu_2\text{-Cl})_2\text{Cu}\}(\mu_2\text{-L3})_2]_n$ **CP12** shown in Figures 10 and S8 results from treatment of a solution of CuCl in MeCN with **L3**. Compared with the Cu1····Cu2 distance of the $\text{Cu}(\mu_2\text{-X})_2\text{Cu}$ rhomboid of its bromo analogue **CP11**, that of **CP12** shrinks somewhat (2.9057(2) vs. 2.8715(9) Å), in line with the trend noticed for **CP7** and **CP8** within the $[\{\text{Cu}(\mu_2\text{-X})_2\text{Cu}\}(\mu_2\text{-L2})_2]_n$ series (see above).

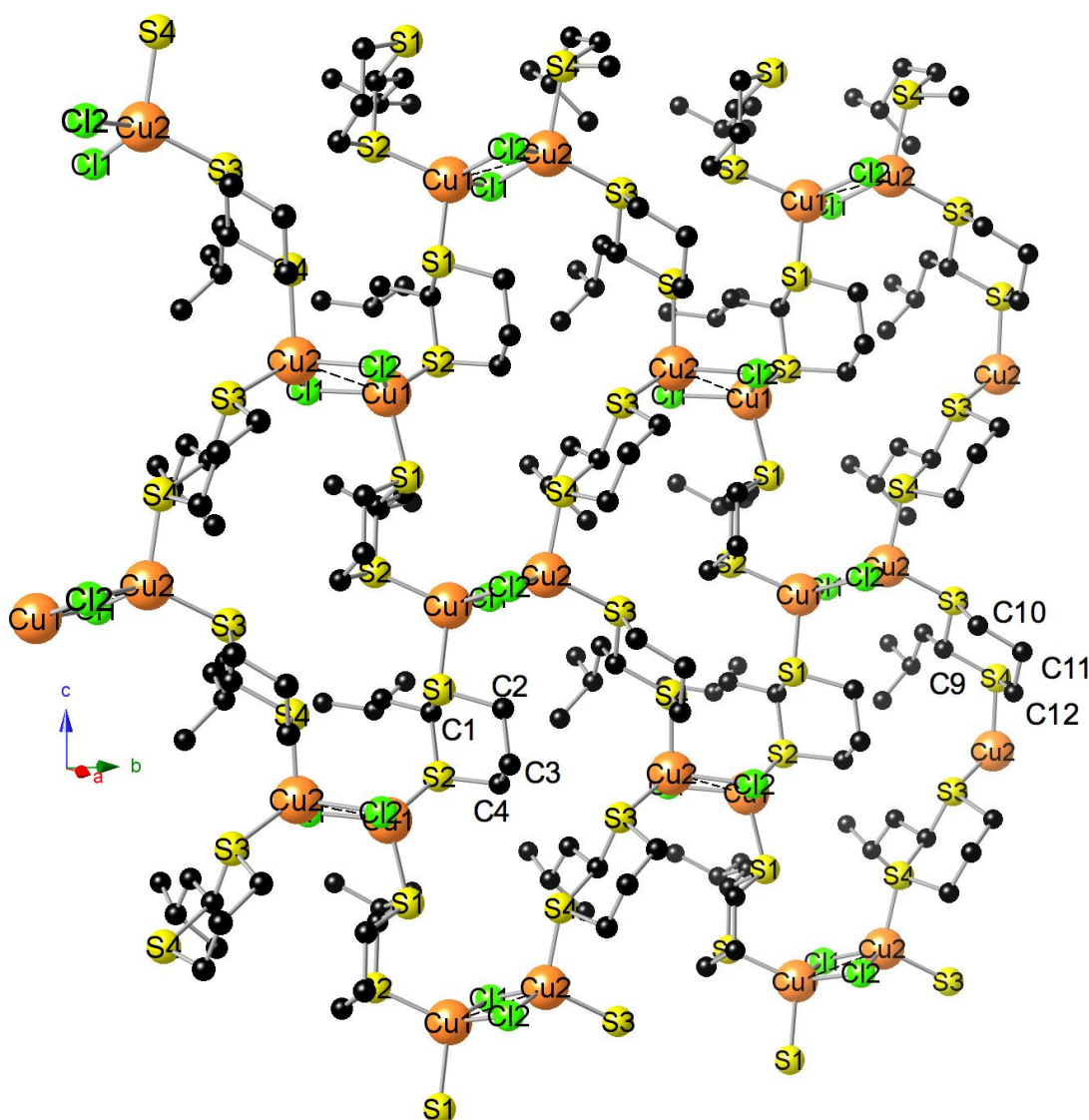
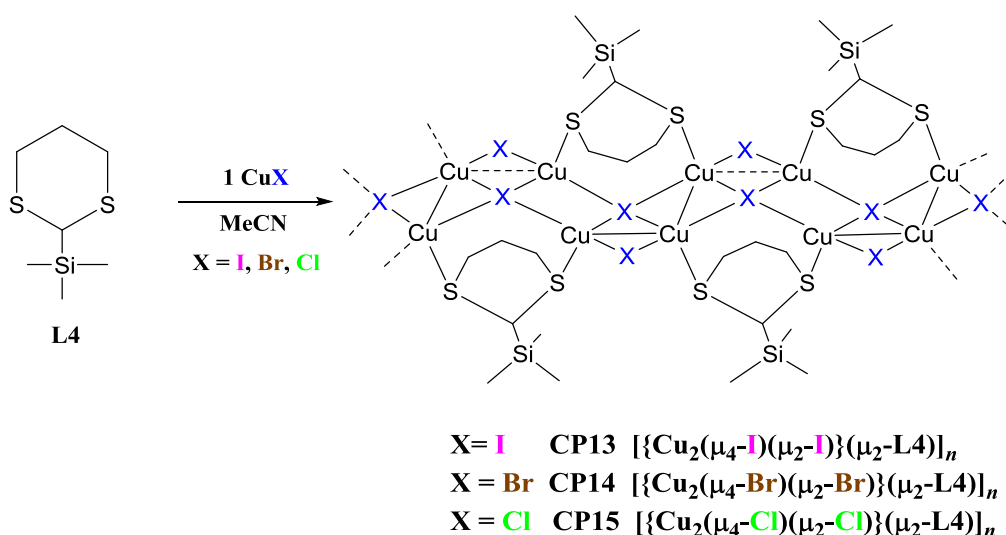


Figure 10. View down the *a* axis on the *bc* plane of the 2D network of $[\{\text{Cu}(\mu_2\text{-Cl})_2\text{Cu}\}(\mu_2\text{-L3})_2]_n$ **CP12**. Selected bond lengths (Å) and angles (°): Cu1–Cu2 2.8715(9), Cu1–Cl1 2.3813(13), Cu1–Cl2 2.38106(13), Cu2–Cl1 2.2890(13), Cu2–Cl2 2.4413(13), Cu1–S1 2.33231(13), Cu1–S2 2.2624(13), Cu2–S3 2.2992(13), Cu2–S4 2.3829(12); Cu1–Cl1–Cu2 75.85(4), Cu1–Cl2–Cu2 73.08(4), Cl1–Cu1–Cl2 104.968(5), Cl1–Cu2–Cl2 105.94(5), S1–Cu1–S2 108.70(5), S3–Cu2–S4 106.81(15).

Treatment of 2-Trimethylsilyl-1,3-dithiane L4 with CuX (X = I, Br, Cl). In order to evaluate the impact of a heteroelement at the 2-position of the dithiane cycle, we extended our systematic investigation on 2-trimethylsilyl-1,3-dithiane bearing a bulky SiMe₃ group. A survey of the CSD data base revealed that apart from the dinuclear complex $[\text{Ag}(\text{Me}_3\text{Si-dithiane})_2(\text{CF}_3\text{SO}_3)_2]$ obtained by complexation of 2-trimethylsilyl-1,3-dithiane on silver triflate,⁶⁷ no other examples of crystallographically characterized coordination compounds ligated with **L4** have been reported so far.

Addition of a stoichiometric amount of **L4** to a MeCN solution of CuI caused fast precipitation of colorless solid, which, surprisingly had composition $[(\text{Cu}_2\text{I}_2)(\text{L4})]$ indicating a 2:1 metal-to-ligand ratio (Scheme 5). Indeed, recrystallization of a sample of the collected material from hot MeCN afforded fine needle-shaped crystals whose crystallographic characterization confirmed this $[(\text{Cu}_2\text{I}_2)(\text{L4})]$ composition. Note that this compound $[\{\text{Cu}_2(\mu_4\text{-I})(\mu_2\text{-I})\}(\mu_2\text{-L4})]_n$ **CP13** is markedly more soluble than **CP1**, **CP4** and **CP5**, probably due the presence of the SiMe₃ substituent.



Scheme 5. Synthesis of the 1D CPs $[\{\text{Cu}_2(\mu_4\text{-X})(\mu_2\text{-X})\}(\mu_2\text{-L4})]_n$ **CP13**, **CP14** and **CP15**

The crystal structure of the resulting 1D ribbon is shown in Figures 11 and S9 and diverges much from the $\text{Cu}(\mu_2\text{-I})_2\text{Cu}$ rhomboid containing 1D architectures of **CP1** and **CP5**. The array of the crystallographically non-equivalent Cu1 and Cu2 atoms may be considered as meander-shaped (when neglecting the long $\text{Cu2}\cdots\text{Cu2}$ separation of 3.362 Å), with Cu1–Cu1 and Cu1–Cu2 distances of 2.8203(12) and 2.9838(9) Å, respectively. Each Cu1–Cu2 bond is quite symmetrically bridged by a μ_2 -type I2 atom with Cu1–I2 and Cu2–I2 distances of 2.6139(7) and 2.5930(7) Å, respectively. Particularly noteworthy is the capping of each Cu1–Cu2–Cu2 segment by a μ_4 -type I1 ligand, with Cu–I distances ranging from 2.6139(7) to 2.7005(7) Å. The two sulfur atoms of **L4** span additionally two remote Cu1 and Cu2 atoms with Cu1–S1 and Cu2–S2 bond lengths of 2.3053(11) and 2.3131(11) Å, respectively. Figure 11 shows also the alignment of the **L4** ligands adopting a chair conformation with the SiMe_3 groups pointing away from the inorganic $[\{\text{Cu}_2(\mu_4\text{-I})(\mu_2\text{-I})\}]_n$ ribbon.

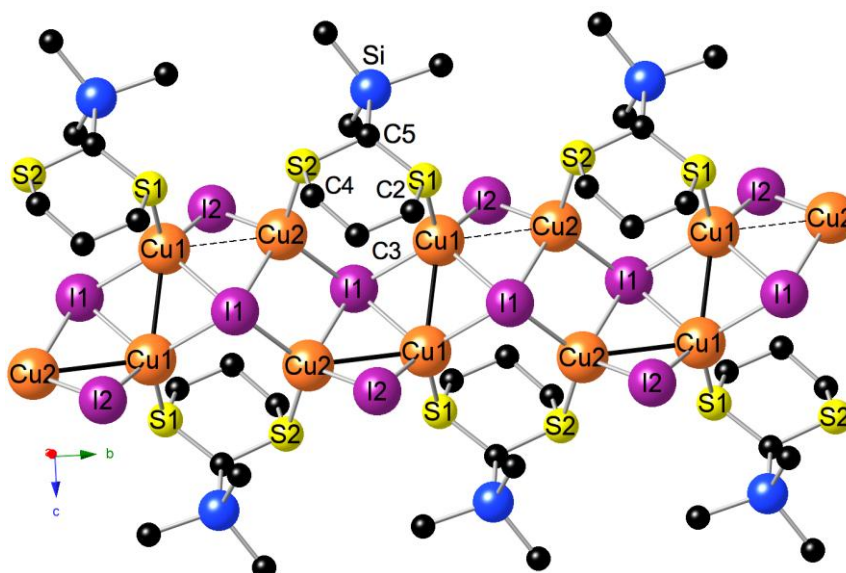


Figure 11. View of a segment of the 1D ribbon of $[\{\text{Cu}_2(\mu_4\text{-I})(\mu_2\text{-I})\}(\mu_2\text{-L4})]_n$ **CP13** running along the *b* axis. Selected bond lengths (Å) and angles (°): Cu1–Cu1# 2.8203(12), Cu1–Cu2# 2.9838(9), Cu2 \cdots Cu2# 3.362, Cu1 \cdots Cu2 3.975, Cu1–I1 2.6345(7), Cu1–I1# 2.7005(7), Cu1–I2 2.6139(7), Cu2–I2 2.5930(7), Cu2–I1 2.6594(7), Cu2–I1# 2.6594(7), Cu1–S1 2.2922(13), Cu2–S2 2.2939(14); Cu1–Cu1#–Cu2 104.49(2), Cu1–I1–Cu1# 63.81(2), Cu1–I2–Cu2 69.92(2), Cu2–I1–Cu2# 76.89(2), I1–Cu1–I2 104.49(2), I1–Cu2–I2 103.61(2), S1–Cu1–I1 116.83(4), S1–Cu1–I1# 97.76(4), S1–Cu1–I2 114.06(4), S2–Cu2–I2 113.89(42).

With CuBr and **L4**, invariantly of the metal-to-ligand ratio, formation of $[\{\text{Cu}_2(\mu_4\text{-Br})(\mu_2\text{-Br})\}(\mu_2\text{-L4})]_n$ **CP14** occurred, crystallizing like its CuI homologue **CP13** as transparent

needles in the monoclinic space group $P2_1/n$ (Scheme 5). At first glance, the overall topology is very reminiscent to that of **CP13** consisting of a 1D ribbon featuring both μ_4 -type and μ_2 -type halide ligands. However, a closer inspection of the structure shown in Figure 12 reveals that the symmetry is lowered since now 4 crystallographically different Cu atoms as well as 4 different S donor sites are present. The averaged Cu \cdots Cu distances are now somewhat longer than those of **CP13** (3.063 vs. 3.055 Å), ranging from bonding (Cu2–Cu3 2.8159(3) Å) up to clearly non-bonding (Cu1 \cdots Cu4 3.409 Å). A perspective view of the packing down the c axis is presented in Figure S10.

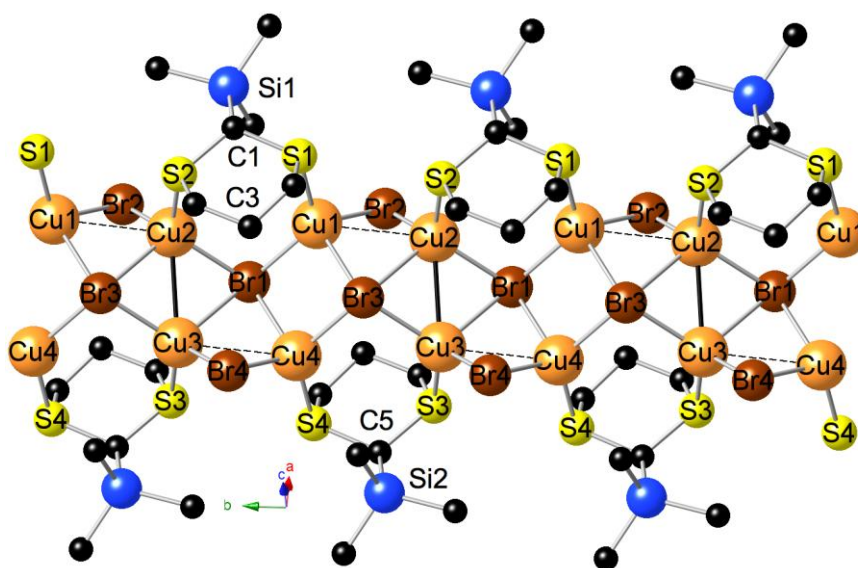


Figure 12. View of the 1D ribbon of $[\{\text{Cu}_2(\mu_4\text{-Br})(\mu_2\text{-Br})\}(\mu_2\text{-L4})]_n$ **CP14** running along the b axis. Selected bond lengths (Å) and angles (°): Cu1 \cdots Cu2 3.0074(3), Cu2–Cu3 2.8159(3), Cu3 \cdots Cu4 3.0199(3), Cu1–Br1 2.5007(3), Cu1–Br3 2.6941(3), Cu1–Br2 2.4297(3), Cu2–Br1 2.4704(3), Cu2–Br2 2.4331(3), Cu2–Br3 2.6634(3), Cu3–Br1 2.6765(3), Cu3–Br3 2.4583(3), Cu3–Br4 2.4311(3), Cu4–Br1 2.6748(3), Cu4–Br3 2.5018(3), Cu4–Br4 2.4364(2), Cu1–S1 2.2597(4), Cu2–S2 2.2570(4), Cu3–S3 2.2533(4), Cu4–S4 2.2623(4), Cu1–Br1–Cu3 126.680(8), Cu2–Br1–Cu1 95.756(9), Cu2–Br1–Cu3 66.196(8), Cu3–Br3–Cu2 66.565(8), Cu3–Br3–Cu4 95.509(9), Cu4–Br3–Cu2 126.140(8), Br1–Cu2–Br3 113.643(9), Br1–Cu2–Cu3 60.418(7), Br2–Cu2–Br1 106.680(9), Br2–Cu2–Br3 101.557(9), Br2–Cu2–Cu3 116.231(10), Br3–Cu2–Cu3 53.225(7), Br1–Cu3–Cu2 53.386(7), Br3–Cu3–Br1 113.595(9), Br3–Cu3–Cu2 60.209(7), Br4–Cu3–Br1 100.806(9), Br4–Cu3–Br3 107.349(9), Br4–Cu3–Cu2 115.971(10).

A structural quite similar 1D ribbon [$\{\text{Cu}_2(\mu_4\text{-Cl})(\mu_2\text{-Cl})\}(\mu_2\text{-L4})\}_n$ **CP15** crystallizing in the triclinic space group $P\bar{1}$ was also isolated upon stoichiometric treatment of CuCl with **L4** in MeCN solution. Whereas the Cu1–Cu1 distance of 2.883(3) Å is only slightly superior to that of **CP12**, both the Cu1···Cu2 and Cu2···Cu2 separations of 3.105 and 3.341 Å do no longer allow describing the connectivity between the Cu atoms as meander-shaped. A description as discreet Cu1–Cu1 pairs, which are connected to isolated Cu2 atoms through μ_2 -bound Cl2 atoms and capping μ_4 -bound Cl2 atoms, appears more appropriate. The metric parameters are presented in the caption of Figure 13 and a perspective view is shown in Figure S11.

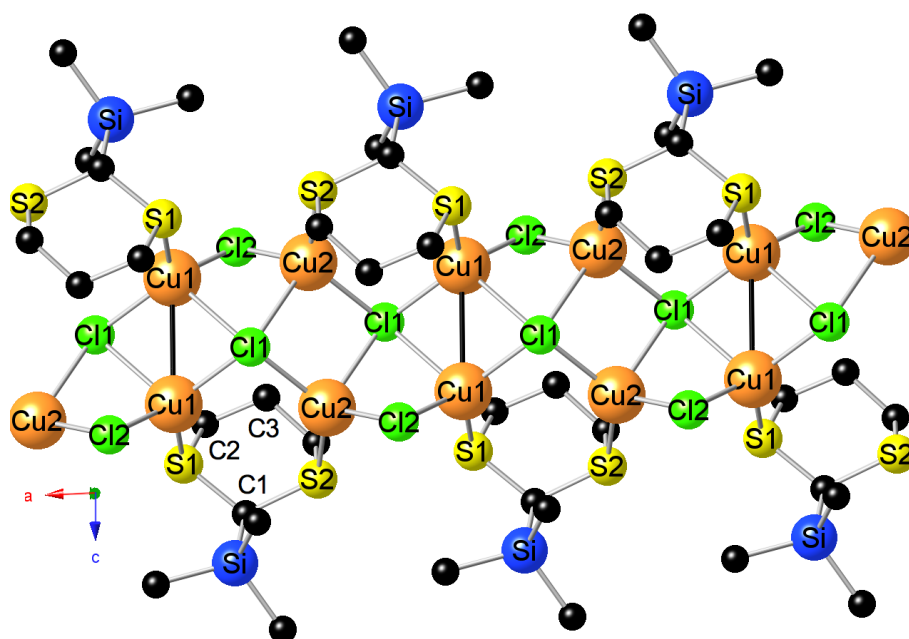
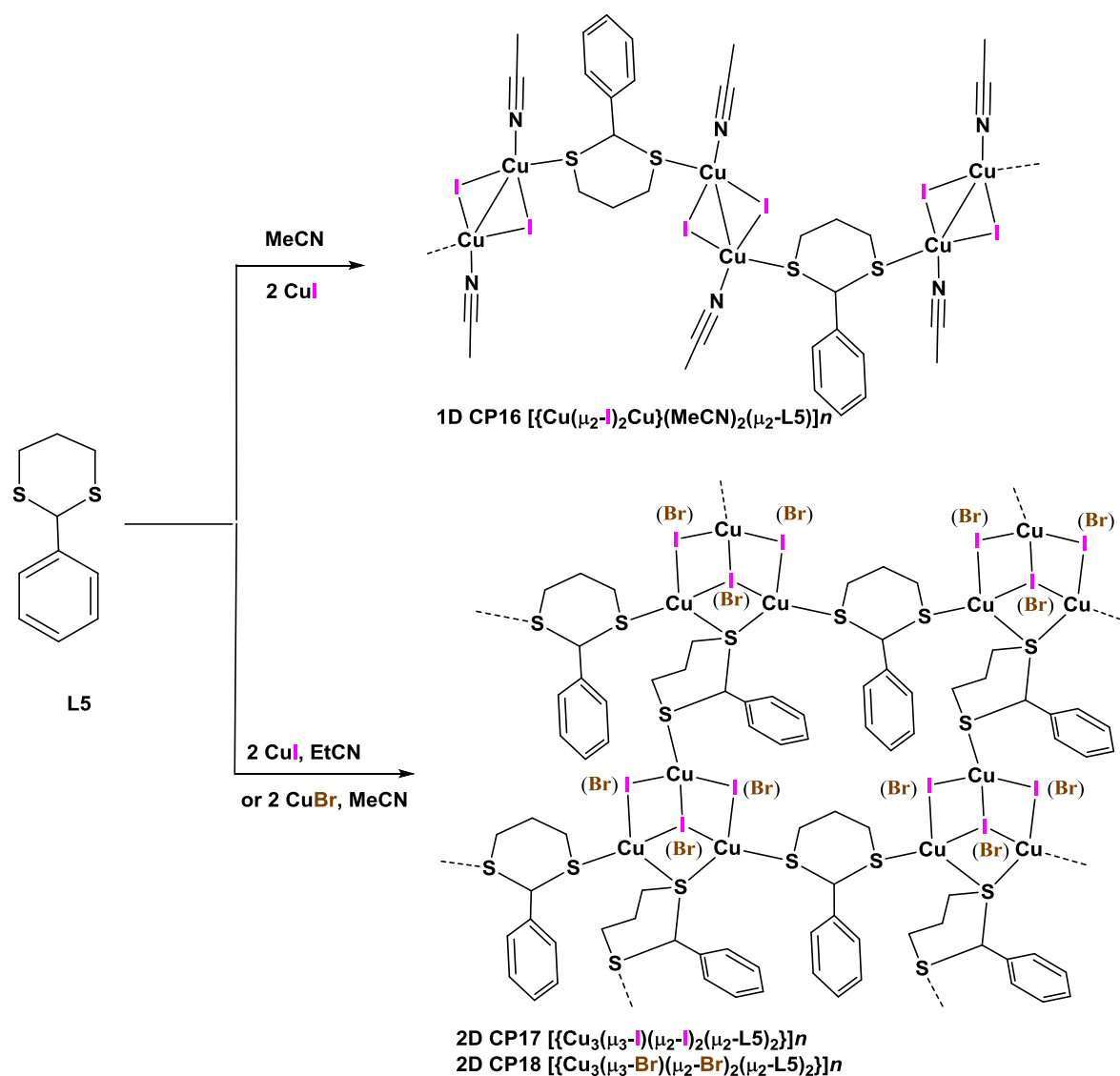


Figure 13. View of the 1D ribbon of [$\{\text{Cu}_2(\mu_4\text{-Cl})(\mu_2\text{-Cl})\}(\mu_2\text{-L4})\}_n$ **CP15** running along the a axis. Selected bond lengths (Å) and angles (°): Cu1–Cu1# 2.883(3), Cu1–Cl1 2.325(2), Cu1–Cl1# 2.681(2), Cu1–Cl2 2.294(2), Cu2–Cl2 2.306(2), Cu2–Cl1 2.342(2), Cu2–Cl1# 2.671(2), Cu1–S1 2.239(2), Cu2–S2 2.249(2); Cu1–Cl1–Cu1# 69.62(7), Cu1–Cl2–Cu2 84.91(7), Cu2–Cu1–Cu2# 83.30(7), Cl1–Cu1–Cl2 112.42(8), Cl1–Cu2–Cl2 111.20(7), S1–Cu1–Cl1 122.91(8), S1–Cu1–Cl1# 92.70(7), S1–Cu1–Cl2 116.62(8), S2–Cu2–Cl2 115.64(8).

Treatment of 2-phenyl-1,3-dithiane L5 with CuX (X = I, Br, Cl). We then investigated the effect of a bulkier and rigid phenyl substituent at the 2-position of the dithiane cycle on the structural features of the anticipated CP. For this, we treated first CuI with 2-phenyldithiane **L5** in MeCN solution using a 1:1 metal-to-ligand ratio (Scheme 6).



Scheme 6. Synthesis of 1D $[\{\text{Cu}(\mu_2\text{-I})_2\text{Cu}\}(\text{MeCN})_2(\mu_2\text{-L5})]_n$ **CP16** and 2D $[\{\text{Cu}_3(\mu_3\text{-I})(\mu_2\text{-I})_2(\mu_2\text{-L5})_2\}]_n$ **CP17** and **CP18**.

After mixing the two reactants, the resulting colorless poorly soluble precipitate was heated shortly till complete dissolution by further addition of MeCN. Upon cooling, the onset of a crystal growth on the wall was noticed. Surprisingly, elemental analysis of the resulting needle-shaped material indicated a 2:1 CuI-to-L5 composition as well as the presence of MeCN molecules. Indeed, employing a 2:1 metal-to-ligand ratio allowed to improve the yield up to 90%. An X-ray analysis of a single-crystal confirmed this composition revealing also the existence of Cu-coordinated MeCN molecules. Figure 14 shows that an undulated 1D ribbon $[\{\text{Cu}(\mu_2\text{-I})_2\text{Cu}\}(\text{MeCN})_2(\mu_2\text{-L5})]_n$ **CP16** has been formed consisting of rhomboid-shaped Cu_2I_2 SBUs linked by a **L5** heterocycle via the S1 and S2 atoms. Noteworthy is the

alternating occurrence of two different types of centrosymmetric rhomboids featuring slightly different metric parameters. In the Cu1–Cu1 SBU the metal-metal bond 2.6555(10) Å is particularly short, whereas within the Cu2–Cu2 SBU the bond distance reaches 2.7014(10) Å. Two μ_2 -spanning iodo ligands and a datively bound MeCN ligand with Cu–N distances of 1.967(4) and 1.982(4) Å complete the coordination of each copper center, respectively. A perspective view down the *c* axis is shown in Figure S12 (ESI).

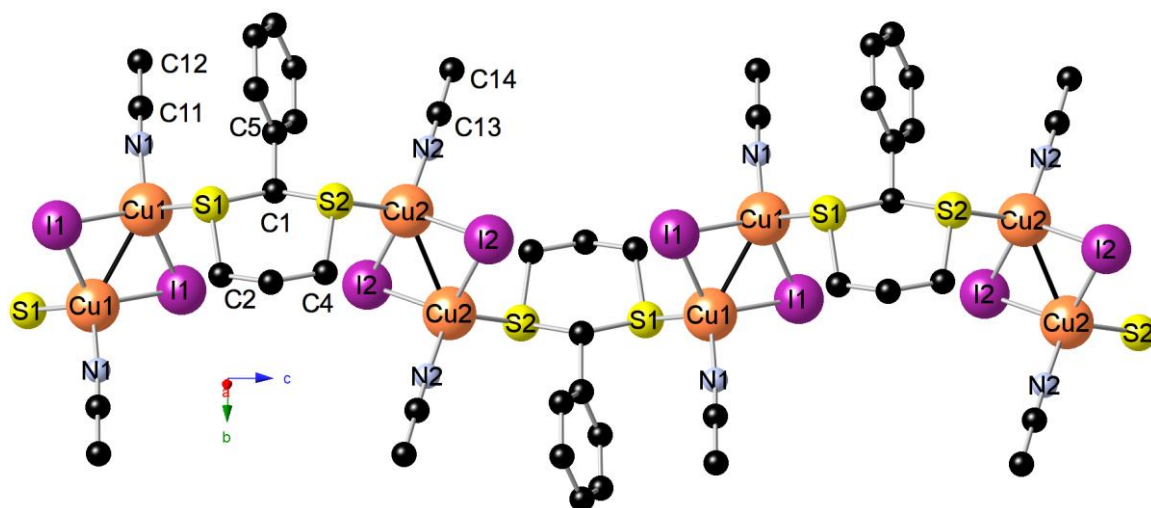


Figure 14. View of the 1D ribbon of $[\{\text{Cu}(\mu_2\text{-I})_2\text{Cu}\}(\text{MeCN})_2(\mu_2\text{-L5})]_n$ **CP16** running along the *c* axis. Selected bond lengths (Å) and angles (°) at 100 K: Cu1–Cu1# 2.6588(3), Cu2–Cu2# 2.7086(3), Cu1–I1 2.6339(2), Cu1#–I1 2.6764(2), Cu2–I2 2.6187(2), Cu2#–I2 2.6897(2), Cu1–S1 2.3193(3), Cu1–N1 1.9716(10), Cu2–S2 2.3324(3), Cu2–N2 1.9775(10); Cu1–I1–Cu1# 60.085(6), Cu2–I2–Cu2# 61.343(6), S1–Cu1–I1 98.984(11), S2–Cu2–I2 102.224(10).

Examples of CPs incorporating two different types of $\text{Cu}(\mu_2\text{-X})_2\text{Cu}$ rhomboids within the same array are quite rare. We have encountered such a case in 1D CP $[\{\text{Cu}(\mu_2\text{-Br})_2\text{Cu}\}(\mu\text{-}p\text{-MeC}_6\text{H}_4\text{SCH}_2\text{C}\equiv\text{CCH}_2\text{SC}_6\text{H}_4\text{Me-}p)_2]_n$, showing a regular alternation of $\text{Cu}(\mu_2\text{-Br})_2\text{Cu}$ SBUs (2.9662(14) Å) with a second type featuring somewhat shorter contacts (2.9306(14) Å).⁵⁷ However, the difference in the Cu–Cu distance in **CP16** is clearly more significant with $\Delta(\text{Cu–Cu } 0.0489 \text{ Å})$. We therefore subjected a single-crystal stemming from another probe to a structural analysis at 5 different temperatures in a 100–300 K range. Whereas the metric parameters at 100 K are almost identical with those presented in the caption of Figure 14, raising the temperature to 200 K causes a moderate lengthening of Cu1–Cu1 to 2.6731(7) Å and that of Cu2–Cu2 to 2.7114(7) Å. A phase transition (PT) occurs upon further heating to

250 K, resulting in a change of the space group from triclinic *P*-1 to monoclinic *P*2₁/*m*. This change impacts the symmetry of the (MeCN)SCu(μ₂-I)₂CuS(CNMe) units, which are now all crystallographically identical with Cu–Cu distance of 2.6965(5) Å. Finally, an elongation of the latter bond distance to 2.7003(6) Å was observed when recording the structure at 300 K. The reversibility of this PT was evidence by a fast scan recording at 100 K confirming reestablishment of the triclinic space group *P*-1. Some relevant metric parameters are gathered in Table 1, illustrations of the ribbons of **CP16** at 100 and 300 K are shown as Figure S13 in the ESI. Although we have already observed a PT for the 1D CP [$\{\text{Cu}_4(\mu_3\text{-I})_4\}\{\mu\text{-PhSCH}_2\text{SPh}\}_2\}_n$ from *C*2/*c* to *P*2₁/*c* upon heating,⁴⁰ the PT in the case of **CP16** accompanied by an harmonization of the metric parameters is to the best of our knowledge unique. To confirm the occurrence of the PT, DSC analysis were performed from 20°C to -80°C (Figure S36). Upon cooling/heating, a pair of exothermic/endothermic peaks was observed at -52/-58°C, indicating a reversible phase transition, in line with the PT observed by variable-temperature X-Ray diffraction analysis in the 200-250 K range.

Table 1. Evolution of bond distances and angles with temperature for **CP16**.

| | 100 K | 150 K | 200 K | 250 K | 300 K |
|-------------|-----------|-----------|------------|------------|------------|
| Cu1–Cu1# | 2.6588(3) | 2.6642(4) | 2.6731(7) | 2.6965(5) | 2.7003(6) |
| Cu2–Cu2# | 2.7086(3) | 2.7105(4) | 2.7114(7) | - | - |
| Cu1–I1 | 2.6339(2) | 2.6317(2) | 2.6317(4) | 2.6230 | 2.6191(4) |
| Cu1#–I1 | 2.6764(2) | 2.6762(3) | 2.6793(4) | 2.6948(3) | 2.6942(4) |
| Cu2–I2 | 2.6187(2) | 2.6167(2) | 2.6175(4) | - | - |
| Cu2#–I2 | 2.6897(2) | 2.6910(3) | 2.6954(4) | - | - |
| Cu1–S1 | 2.3193(3) | 2.3205(4) | 2.3250(7) | 2.3330(5) | 2.3344(6) |
| Cu2–S2 | 2.3324(3) | 2.3322(4) | 2.3347(8) | - | - |
| Cu1–I1–Cu1# | 60.085(6) | 60.249(8) | 60.431(13) | 60.920(10) | 61.071(12) |
| Cu2–I2–Cu2# | 61.343(6) | 61.399(8) | 61.353(13) | - | - |

Intrigued by both the phase transition and the preference to ligate a labile MeCN donor in **CP16** instead of coordination of a second **L5** ligand, we repeated this reaction under more forcing conditions in hot EtCN employing a 2:1 stoichiometry. After reflux for two hours, a

homogeneous material crystallizing like **CP16** in the triclinic space group *P*-1 was isolated in over 90% yield. In contrast to **CP16** exhibiting in the IR spectrum two weak peaks at 2309 and 2275 cm⁻¹ due to the $\nu(\text{C}\equiv\text{N})$ vibration,^{68,69} the IR spectrum of this compound was silent in this region. In line with this finding the crystal structure of this air-stable polymeric material shown in Figure 15 revealed formation of 2D network of composition $[\{\text{Cu}_3(\mu_3\text{-I})(\mu_2\text{-I})_2(\mu_2\text{-L5})_2\}]_n$ **CP17**, which is very reminiscent to **CP10**. Again, triangular Cu_3I_3 clusters capped by a μ_3 -iodo ligand and two μ_2 -bond I atom spanning two edges constitute the SBUs. But in contrast to **CP10**, all Cu···Cu distances are now above the sum of the Van der Waals radii of two Cu atoms and range from weakly bonding (Cu1–Cu3 2.8302(4), Cu2–Cu3 2.8948(4) Å) to clearly non-bonding (Cu1···Cu2 3.297 Å). Thus, the mean Cu_3I_3 triangle shortens from 3.0178 in **CP10** to 3.007 Å in **CP17**. A view of the unit cell showing the stacking of the layers is presented in the **ESI** as Figure S14.

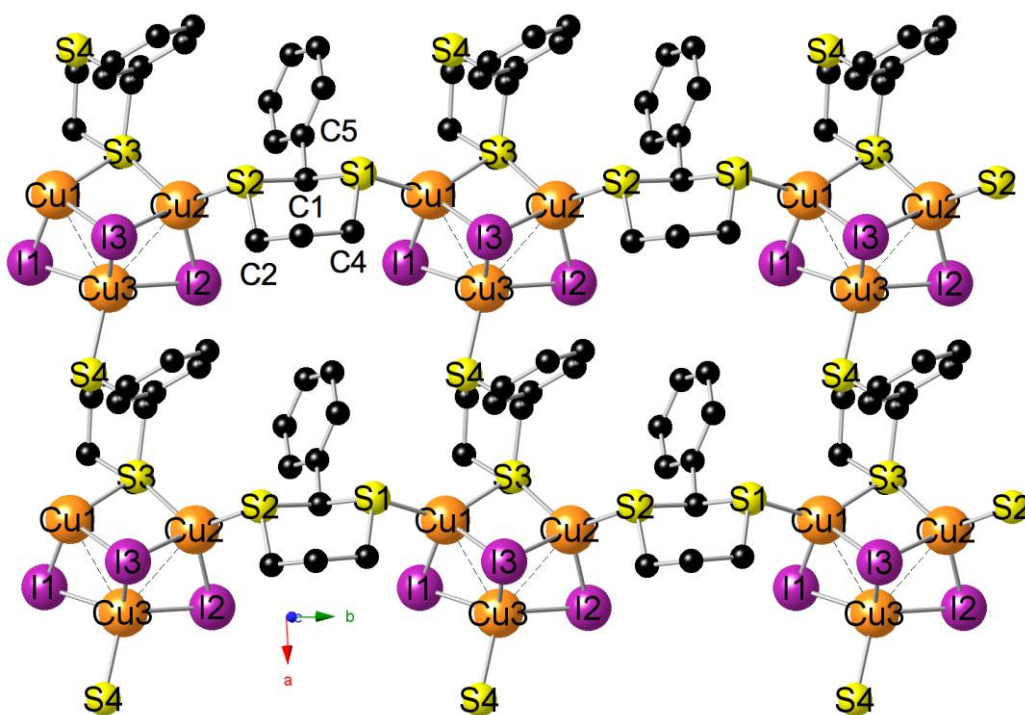


Figure 15. View on the *a, b* plane of the 2D network of $[\{\text{Cu}_3(\mu_3\text{-I})(\mu_2\text{-I})_2(\mu_2\text{-L5})_2\}]_n$ **CP17**. Selected bond lengths (Å) and angles (°): Cu1–Cu3 2.8302(4), Cu2–Cu3 2.8948(3), Cu1···Cu2 3.297, Cu1–I1 2.5905(3), Cu3–I1 2.6591(3), Cu1–I3 2.7817(3), Cu2–I3 2.7803(3), Cu3–I3 2.6483(3), Cu2–I2 2.5842(3), Cu3–I2 2.6621(3), Cu1–S1 2.3050(3), Cu1–S3 2.3122(3), Cu2–S2 2.2876(5), Cu2–S3 2.2917(5), Cu3–S4 2.3393(5); Cu1–I1–Cu3 65.235(8), Cu2–I2–Cu3 66.961(8), Cu1–I3–Cu2 72.702(8), Cu1–I3–Cu3 62.771(8), Cu2–I3–Cu3 64.397(8), Cu1–S3–Cu2 91.461(16).

An isomorphous 2D network with that of **CP17** (triclinic, *P*-1) results also from addition of **L5** to a MeCN solution of CuBr (Figures 16 and **S15**). Again, each trinuclear Cu cluster is linked to 4 adjacent Cu₃Br₃ SBUs through the S1 and S2 atoms of one **L5** molecule acting as κ_1 S- κ_1 S ligand and the S3 and S4 atoms of a second **L5** heterocycle linking in a κ_1 S- μ_2 S bonding mode, thus securing the 2-dimensional character of each layer featuring 20-membered macrocycles. Compared to **CP17**, the mean Cu····Cu distance of the Cu₃X₃ triangle shrinks only insignificantly (3.007 vs. 2.989 Å). A survey of the CSD database reveals another rare example of a Cu₃Br₃ cluster ligated by a thioether catena-(bis(μ_3 -Br)-bis(μ_3 -diallylsulfido)-tris(μ_2 -Br)-pentacopper(I), whose structure consists of infinite (Cu₂Br₂)_n ribbons and Cu₃Br₃(diallylsulfide)₂ fragments that are linked to them through Cu-S and π -olefinic C=C bonds.⁷⁰

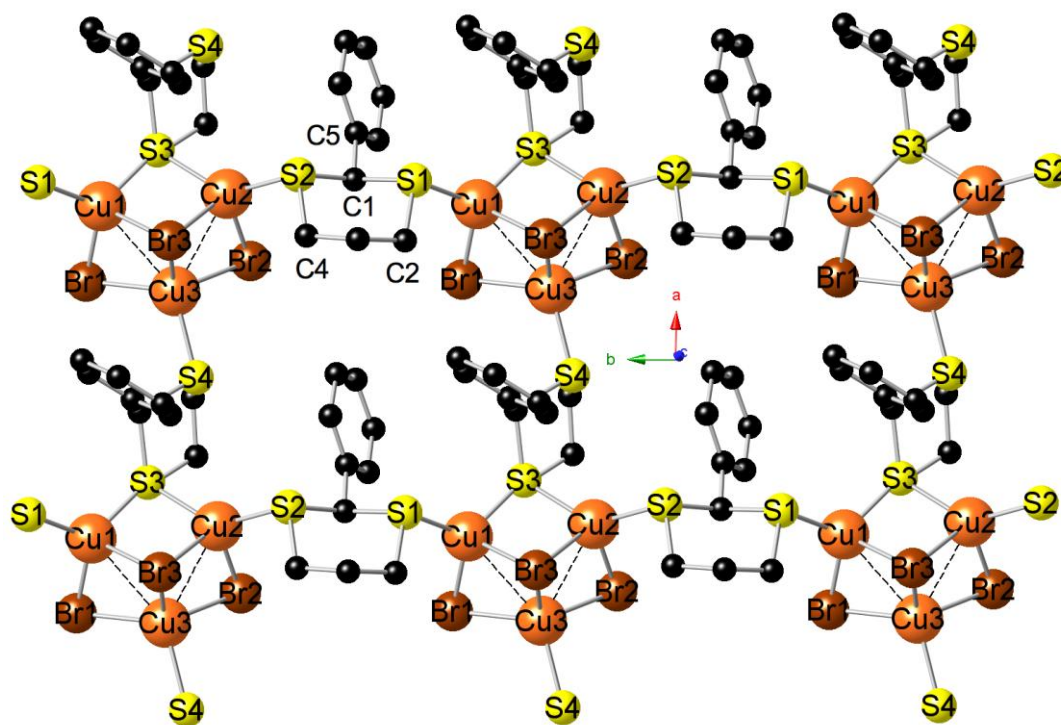


Figure 16. View on the *a,b* plane of the 2D network of [$\{Cu_3(\mu_3\text{-Br})(\mu_2\text{-Br})_2(\mu_2\text{-L5})_2\}_n$ **CP18**. Selected bond lengths (Å) and angles (°): Cu1–Cu3 2.8980(15), Cu2–Cu3 2.8194(14), Cu1····Cu2 3.249, Cu1–Br1 2.4199(13), Cu3–Br1 2.5173(14), Cu1–Br3 2.6135(13), Cu2–Br3 2.6862(13), Cu3–Br3 2.4744(14), Cu2–Br2 2.4225(13), Cu3–Br2 2.5064(13), Cu1–S1 2.266(2), Cu1–S3 2.263(2), Cu2–S2 2.270(2), Cu2–S3 2.270(2), Cu3–S4 2.293(2); Cu1–Br1–Cu3 71.85(4), Cu2–Br2–Cu3 69.76(4), Cu1–Br3–Cu2 75.61(4), Cu1–Br3–Cu3 69.38(4), Cu2–Br3–Cu3 66.08(4), Cu1–S3–Cu2 91.57(7).

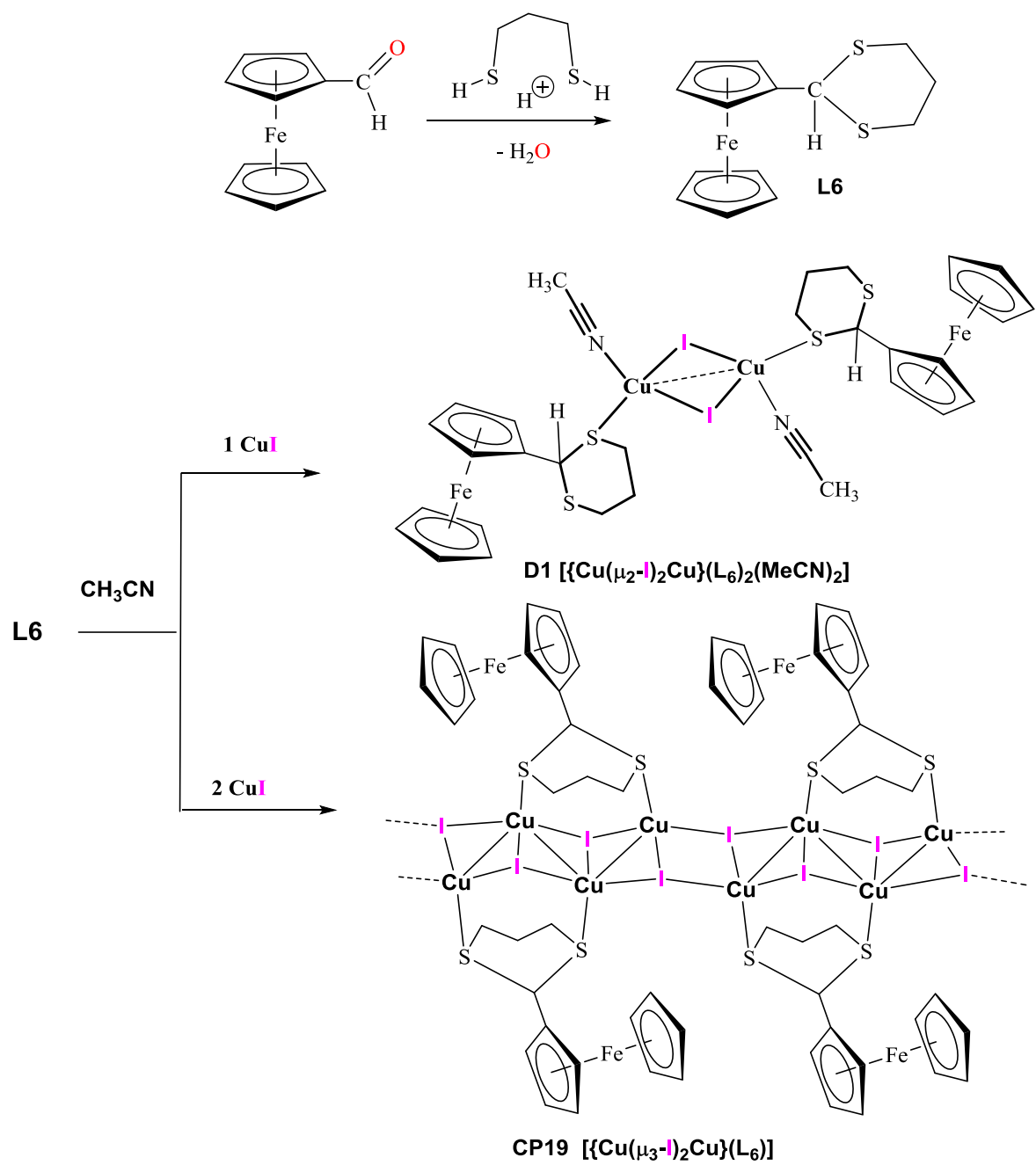
When attempting to complete the series by complexation of **L5** on CuCl at room temperature, elemental analysis on the crude compound obtained indicates a 1:1 Cu: **L5** ratio, different from the 3:2 Cu ratio expected for a compound related to **CP17** and **CP18**. The crude product was further heated in hot MECN or EtCN and we noticed the formation of a small amount of a yellow product but we failed to grow crystals suitable for X-Ray analysis of the major product. Using CuCl₂, surprisingly, a yellow material crystallizing as 3D polymer containing -Cl-Cu-Cl-Cu-Cl- chains assembled by five-membered 1,2-dithiolane ligands was isolated. Mechanistic details rationalizing this unexpected extrusion of a Ph-CH unit (most probably in form of benzaldehyde) and structure of this 3D network will be reported elsewhere.^{71, 72} Furthermore, the PXRD of the crude product obtained by reaction of CuCl₂ and **L5** matches perfectly with the one calculated from the single crystal of the CP containing 1,2 dithiolane ligand, confirming the formation of this compound as main product (Fig. S30).

*Treatment of 2-ferrocenyl-1,3-dithiane **L6** with CuI.* The construction of polynuclear assemblies and coordination polymers featuring an organometallo-ligand, especially the electrochemically active and thermally robust ferrocenyl group in the main chain or as a pendant side-fragment has stimulated much interest in material sciences.⁷³⁻⁸¹ Coordination polymers based upon ferrocenyltelluroethers or ferrocenylselenoethers are pre-catalysts promoting Ullmann C–N cross-coupling reactions in solution.⁸² Reaction of metal ions with ferrocenes functionalized with bis(thioether) substituents can give rise to the formation of discrete clusters.^{83, 84} Introduction of an additional donor site as in the case of 1,1-(4-dipyridinethio)ferrocene led to the formation of 1D CP when reacted with Cu(I) salts.^{85 86} Recently, we reported on the complexation of the related five-membered ferrocenyl-dithiolane Fc-C(H)S₂C₂H₄ on CuI and CuBr. A molecular heterometallic cluster [$\{\text{Cu}_4(\mu_2\text{-Br})_2(\mu_3\text{-Br})_2\}(\mu_2\text{-Fc-dithiolane})_2(\text{MeCN})_2$] was obtained with CuBr, whilst 1D polymeric [$\{\text{Cu}_2(\mu_4\text{-I})(\mu_2\text{-I})\}(\mu_2\text{-Fc-dithiolane})\}_n$] has been assembled with CuI. We were now intrigued to combine a ferrocenyl fragment with the 1,3-dithiane cycle to assemble coordination networks based on CuX salt to investigate their architecture and to compare the findings with our recent investigations using ferrocenyl-dithiolane.⁴⁹

The synthesis of the heterocyclic dithioacetal Fc-C(H)S₂C₃H₆ **L6** has been first reported by treatment of ferrocenecarbaldehyde with 1,3-propanedithiol in the presence of HCl as catalyst.⁸⁷ We have slightly modified the protocol using *p*-toluenesulfonic acid as catalyst. The crystal structure of this ferrocenyl-dithiane is shown in Figure S16, the crystallographic refinement

data are gathered in Table S7. The six-membered dithiane-heterocycle of **L6** adopts the chair conformation as encountered in 2-phenyl-1,3-dithiane.⁸⁸ Like the phenyl group in the latter thiaheterocycle, the ferrocenyl moiety occupies the equatorial position. The bond lengths and angles in **L6** are normal for this kind of molecules and deserve no further comments.

As shown in Scheme 7, the outcome of the complexation of **L6** on CuI in MeCN solution depends on the metal-to-ligand ratio and the order of reactant addition. A discrete molecular dinuclear species [$\{\text{Cu}(\mu_2\text{-I})_2\text{Cu}\}(\kappa_1\text{-L6})_2(\text{MeCN})_2$] **D1** is formed employing a 1:1 ratio. The crystal structure of this dimer depicted in Figure 17 shows a centrosymmetric Cu_2I_2 rhomboid in which the two Cu atoms are connected through a quite short Cu–Cu bond of only 2.6897(4) Å. The coordination sphere around each Cu center is completed by a datively bound MeCN ligand and one S atom of **L6**. Surprisingly, the bonding mode of **L6** is mono-hapto, with the second S atom prone for coordination of a second metal center. A bridging μ_2 -bonding of **L6** can be achieved by performing the reaction in a 2:1 CuI-to-ligand ratio. Indeed, when **L6** was added to 2 equivalent of CuI, PXRD analysis confirmed the formation of **D1**, whilst when adding 2 eq. of CuI to **L6**, an orange-colored crystalline solid [$\{\text{Cu}(\mu_3\text{-I})_2\text{Cu}\}(\mu\text{-L6})_n$] **CP19** was isolated. The unusual 1D-polymeric architecture of **CP19** is illustrated in Figure 18. The inorganic CuI ribbon of this material contains tetranuclear open Cu_4I_4 clusters as SBUs with a mean Cu–Cu distance of 2.7384 Å, below the sum of the Van der Waals radii of two Cu atoms. These tetranuclear units, capped by two μ_3 -type I2 atoms, are interconnected to adjacent ones through much looser $\text{Cu}2\cdots\text{Cu}2\#$ contacts of 3.224(8) Å and two μ_3 -bridging I atoms with Cu–I1 bond distances ranging from 2.6555(8)-2.6844(8) Å. **D1** exhibits in the IR spectrum two weak peaks at 2305 and 2275 cm^{-1} due to the $\nu(\text{C}\equiv\text{N})$ vibration (Figure S35). The structure of **CP19** differs from that encountered in the CP obtained by reaction of 2 eq. of CuI with the less flexible 2-ferrocenyl-1,3-dithiolane ligand.⁴⁹ In this latter case, the infinite ribbon was described as a meander-shaped array containing both μ_4 and $\mu_2\text{-I}$ ligands.



Scheme 7. Synthesis of **L6** and its complexation on CuI yielding **D1** and **CP19**.

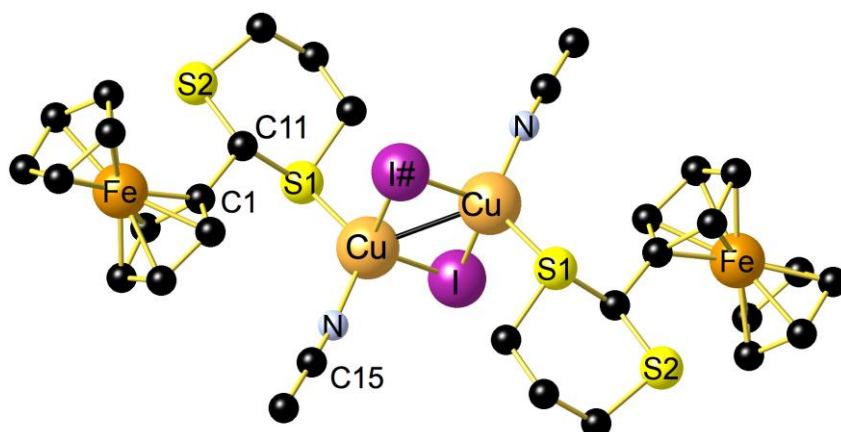


Figure 17. View of the molecular structure of $[\{\text{Cu}(\mu_2\text{-I})_2\text{Cu}\}(\kappa_1\text{-L6})_2(\text{MeCN})_2]$ (**D1**). Selected bond lengths (Å) and angles (°): Cu–Cu# 2.6897(4), Cu–I 2.6362(3), Cu–I# 2.7120(3), Cu–N 1.9770(16), Cu–S1 2.3010(5), C1–C11 1.493(2); N–Cu–S1 121.16(5), N–Cu–Cu# 123.71(5), N–Cu–I 111.95(5), I–Cu–I# 119.636(8), I–Cu–Cu# 61.214(9), S1–C11–S2 111.34(9). Symmetry transformations used to generate equivalent atoms: ¹1-X, 2-Y, 1-Z.

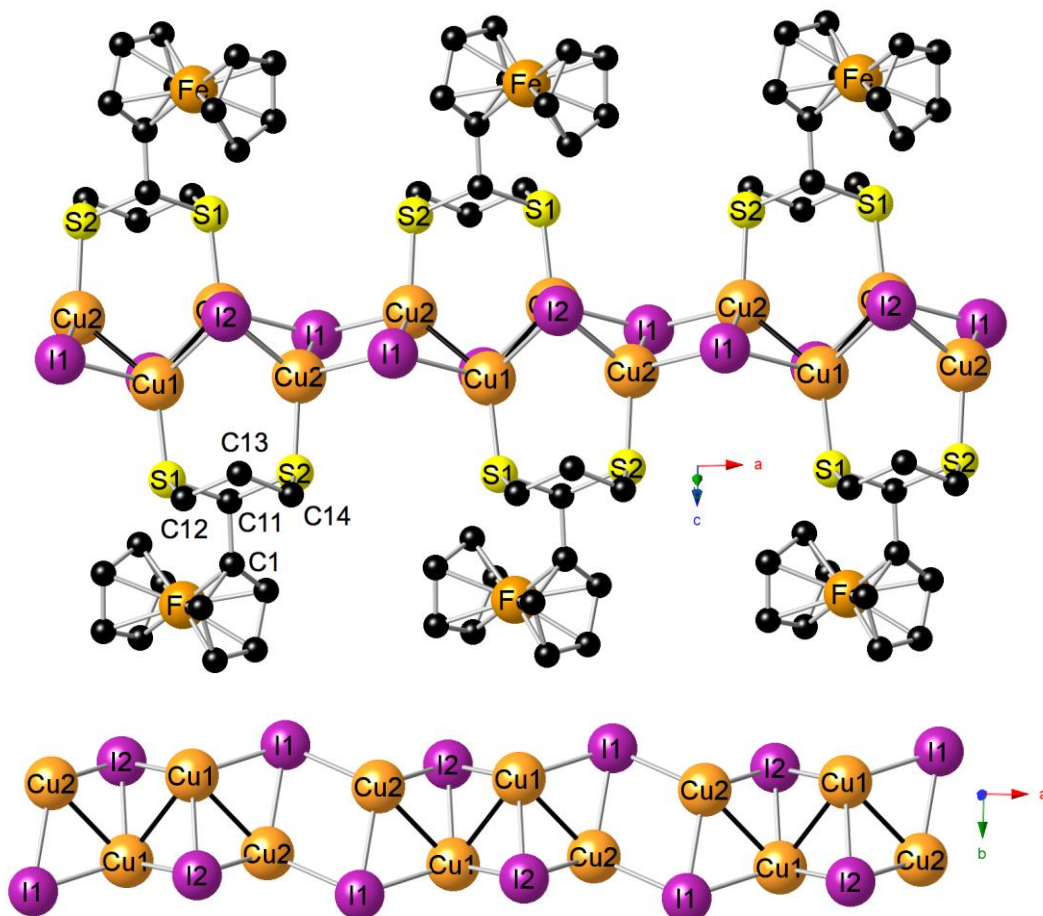


Figure 18. View of the 1D ribbon of $[\{\text{Cu}(\mu_3\text{-I})_2\text{Cu}\}(\mu_2\text{-L6})]_n$ **CP19** running along the *a* axis. Selected bond lengths (Å) and angles (°): Cu1–Cu1¹ 2.7215(9), Cu1–Cu2¹ 2.7469(7), Cu2–Cu1¹

2.7469(7), Cu1–I1 2.6555(8), Cu2¹–I1 2.6672(8), Cu2²–I1 2.6844(8), Cu1–I2 2.6272(10), Cu1¹–I2 2.6748(8), Cu2–I2 2.6729(9), Cu1–I2¹ 2.6748(8), Cu2–I1¹ 2.6672(8), Cu1–S1 2.3069(11), Cu2–S2 2.3047(11); Cu1–I1–Cu2¹ 62.138(11), Cu1–I1–Cu2² 115.81(3), Cu1–I2–Cu1¹ 61.763(16), Cu1–I2–Cu2 80.25(3), Cu2–I2–Cu1¹ 61.817(14), Cu1¹–Cu1–Cu2¹ 77.31(3), I1–Cu1–I2¹ 113.515(16), I1–Cu1–Cu1¹ 125.23(3), I2–Cu1–I1 101.03(3), I2–Cu1–I2¹ 118.237(16), I2¹–Cu1–Cu1¹ 58.25(2), I2–Cu1–Cu1¹ 59.982(19), S1–Cu1–I1 106.06(3), S1–Cu1–I2 119.75(3), S2–Cu2–I2 118.56(3), I1¹–Cu2–I2 113.195(13), I1¹–Cu2–Cu1¹ 58.722(19), I2–Cu2–I1³ 99.09(3), I2–Cu2–Cu1¹ 59.126(19). Symmetry transformations used to generate equivalent atoms: ¹1-X, 1-Y, 1-Z; ²-1+X, +Y, +Z; ³1+X, +Y, +Z.

Thermal properties

All compounds were found to be stable for several months under ambient atmosphere. The thermal properties of some selected CPs containing **L2** (**CP5**, **CP7**, **CP8**), **L3** (**CP10**, **CP11** and **CP12**) and Ferrocenyl **L6** ligands (**CP19**) were studied by TGA under air up to 850°C. The first derivative plots of the TGA traces are given in ESI (Figures S37-44) Temperatures of decomposition corresponding to a 5% loss of the total mass are given in Table 2. The thermogravimetric traces depicted in Figure 19 show that CPs containing **L2** and **L3** ligands present relatively identical thermal behavior. As already encountered for others thioether-based CPs, all thermal profiles of CPs containing bromide (**CP7** and **CP11**) or chlorine (**CP8**) atoms present three main losses while the thermal decomposition of **CP5** and **CP10** containing iodide presents only two well decomposition steps.⁸⁹ The first major weight loss can be attributed to the loss of ligands based on the comparison between the theoretical and experimental values (see Table 2). The final residual contents values are also close to those calculated based on the formation of CuO. Comparison of the traces between **CP7** and **CP8** within the **L2** series and between **CP11** and **CP12** within the **L3** series indicates that, independently to the dimensionality (1D or 2D), a higher stability is always obtained for CP containing Cu₂Br₂ SBUs than those containing Cu₂Cl₂ rhomboids. This observation is consistent with our previous studies.³⁷ It was however more difficult to obtain a tendency for CPs containing iodide. Compare to **CP7** and **CP8**, the 1D **CP5** that contains Cu₂I₂ rhomboids present a lower thermal stability. Oppositely, in the **L3** series, the thermal stability of **CP10** is higher than those of **CP11** and **CP12**. In this case, the highest stability might be due to the presence of a Cu₃I₃ core. Comparison of thermal degradation temperatures between **CP7** and **CP11** containing Cu₂Br₂ rhomboids and between **CP8** and **CP12** containing Cu₂Cl₂ rhomboids indicates that **L2** containing CPs (**CP7** and **CP8**) are more stable than **L3** containing materials (**CP11** and **CP12**). One explanation that has already been suggested for

this behavior is the difference in the boiling point value of the ligand. However, in our case, the boiling point of **L3** (250°C) is higher than that of **L2** (224°C). The dimer compound **D1** presents the lowest stability with a first degradation step from 60°C to 130°C attributed to the loss of coordinated acetonitrile (Table 2). After that initial decomposition step, the thermal degradation profiles of **D1** and **CP19** look alike. The final residues might include both FeO and CuO as evidenced by a comparison between theoretical and experimental values.

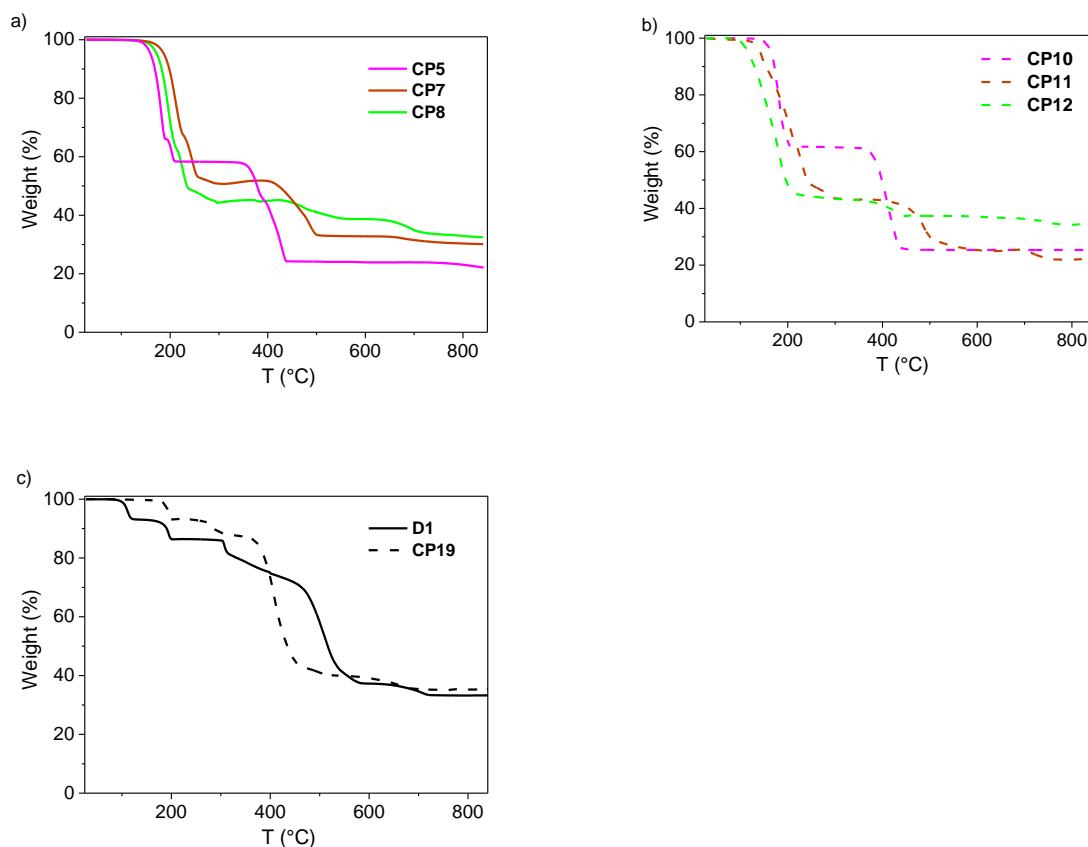


Figure 19. TGA traces of a) CP5, CP7, CP8 b) CP10, CP11, CP12 c) D1 and CP19 under air flow (rate: 10 °C.min⁻¹).

Table 2. TGA data for **CP5**, **CP7-CP8**, **CP10-CP12**, **D1** and **CP19**.

| CP | T _{Dec} (°C) | T (°C) | Mass loss (%wt) | | Residual mass (%wt) | |
|----------------------------------------------------------------------------------------|--------------------------|-----------|--------------------|-----|-----------------------------------|-----|
| | | | Theo | Exp | Theo. | Exp |
| CP5 [$\{\text{Cu}_2(\mu_2\text{-I})_2\}(\text{L2})_2\}_n$] | 160 | 100-210 | 41 ^a | 44 | 25 ^c | 23 |
| CP7 [$\{\text{Cu}_2(\mu_2\text{-Br})_2\}(\text{L2})_2\}_n$] | 187 | 100-350 | 48 ^a | 49 | 29 ^c | 30 |
| CP 8 [$\{\text{Cu}_2(\mu_2\text{-Cl})_2\}(\text{L2})_2\}_n$] | 173 | 100-350 | 57 ^a | 55 | 34 ^c | 32 |
| CP10 [$\{\text{Cu}_3(\mu_3\text{-I})(\mu_2\text{-I})_2(\text{L3})_2\}_n$] | 165 | 100-240 | 38 ^a | 38 | 25 ^c | 25 |
| CP 11 [$\{\text{Cu}_2(\mu_2\text{-Br})_2\}(\text{L3})_2\}_n$] | 142 | 100-350 | 54 ^a | 53 | 22 ^c | 25 |
| CP12 [$\{\text{Cu}_2(\mu_2\text{-Cl})_2\}(\text{L3})_2\}_n$] | 116 | 100-350 | 64 ^a | 57 | 29 ^c | 35 |
| D1 [$\{\text{Cu}_2(\mu_2\text{-I})_2\}(\kappa_1\text{-L6})_2(\text{MeCN})_2$] | 113 | 60-130 | 7.7 ^b | 7.0 | 15 ^c / 28 ^d | 33 |
| CP19 [$\{\text{Cu}_2(\mu_3\text{-I})_2\}(\text{L6})\}_n$] | 195 | | | | 23 ^c / 44 ^d | 35 |

^a values determined based on ligand loss^b value determined based on CH₃CN loss^c values determined based on the formation of CuO^d values determined based on the formation of CuO and FeO

Luminescence Properties

(CuI)_n-containing coordination polymers are known for they interesting luminescence properties.^{24, 46, 90-92} Here, **CP1**, **CP10**, **CP13** and **CP17** composed of different SBUs and networks were found to be only weakly emissive under an UV lamp at 366 nm. In these cases, the mean Cu····Cu separation lies above the sum of the Van der Waals radii of two copper atoms. However, taking into account that both **CP16** and **CP19** present relatively short Cu-Cu distances (2.6555Å and 2.7215Å respectively), we were intrigued to measure their luminescence spectra. **CP16** was found to be highly luminescent under UV irradiation. (Figure S47 ESI) The luminescence spectrum of **CP16** recorded at 298 K presents two emission bands at high energy (HE) and low energy (LE) with maxima at 435 nm and 554 nm (Figure 20 and Table 3). Other examples of CPs containing Cu₂I₂ rhomboids with

luminescence spectra exhibiting a band at high energy around 430 nm with a long tail spreading over 550 nm have been reported before. This includes rhomboids obtained by reaction of CuI with (i) 1,4-bis(cyclohexylthio)butane,⁹³ (ii) 1,5-bis(*p*-tolylthio)pentane or 1,5-bis(*p*-phenylthio)pentane³⁷ and (iii) trans-1,4-bis(*p*-phenylthio)-2-butene.⁸⁹ Our luminescence spectra, with two well separated emission bands looks much alike the one reported for a CP obtained by coordination of CuI with 1,2-dithiane ligand.²¹ At 77 K, only one emission band with maxima at 435 nm is observed and the intensity of this band is much higher than at room temperature (See Figure S45 ESI). The presence of a second band at low energy and the thermochromism phenomena observed was also described for cubane species such as Cu₄I₄(pyridine)₄⁹⁴ or other copper iodide clusters containing phosphine ligands.⁴⁷ Interestingly, we also found out that, as in the case of [Cu₄I₄(pyridine)₄], the LE and HE bands display different excitation spectra with reverse order: HE and LE missions correspond to the LE and HE excitation. We are not aware of any cubane CPs composed of thioether ligands showing disappearance of the low- energy band upon cooling. Thus, a plausible explanation that may come to mind is the contamination by another cubane species as reported in references 37 and 89. However, as stipulated before CP16 is highly luminescent under UV lamp and the crude powder can be considered as pure based on the comparison of experimental and simulated PXRD patterns (Fig S26) and elemental analysis results. We have shown above that CP16 undergoes a phase transition at around -50°C leading to a shortening of the Cu-Cu distance upon cooling. Currently, we are unable to conclude if this PT is responsible for the observed different luminescent properties at 298 and 77 K. Further computational studies, solid-state emission lifetimes are necessary to address this question to attribute the nature of the transitions involved.

The luminescence of CP19 presenting an unprecedented SBU is somehow different. The spectrum presents an intense band at HE, centered at 436 nm and a second broad band of lower intensity located at 536 nm. These two bands exhibit same excitation spectra. At 77 K, the luminescence profile remains the same even though the intensities of the two emission bands are stronger (Figure S46 in ESI). These spectra are thus more reminiscent to those reported for thioether-based CPs containing Cu₂I₂ rhomboids⁸⁹

Table 3. Photoluminescence data for CP16 and CP19 measured in the solid state at 298 K and 77 K

| Compound | T (K) | λ_{ex} (nm) | λ_{em} (nm) |
|-------------|-------|----------------------------|----------------------------|
| CP16 | 298 | 347 | 554 |
| | | 375 | 435, 554 |
| | 77 | 347 | 432 |
| | | 375 | 432 |
| CP19 | 298 | 377 | 436, 536 |
| | 77 | 360 | 436, 525 |

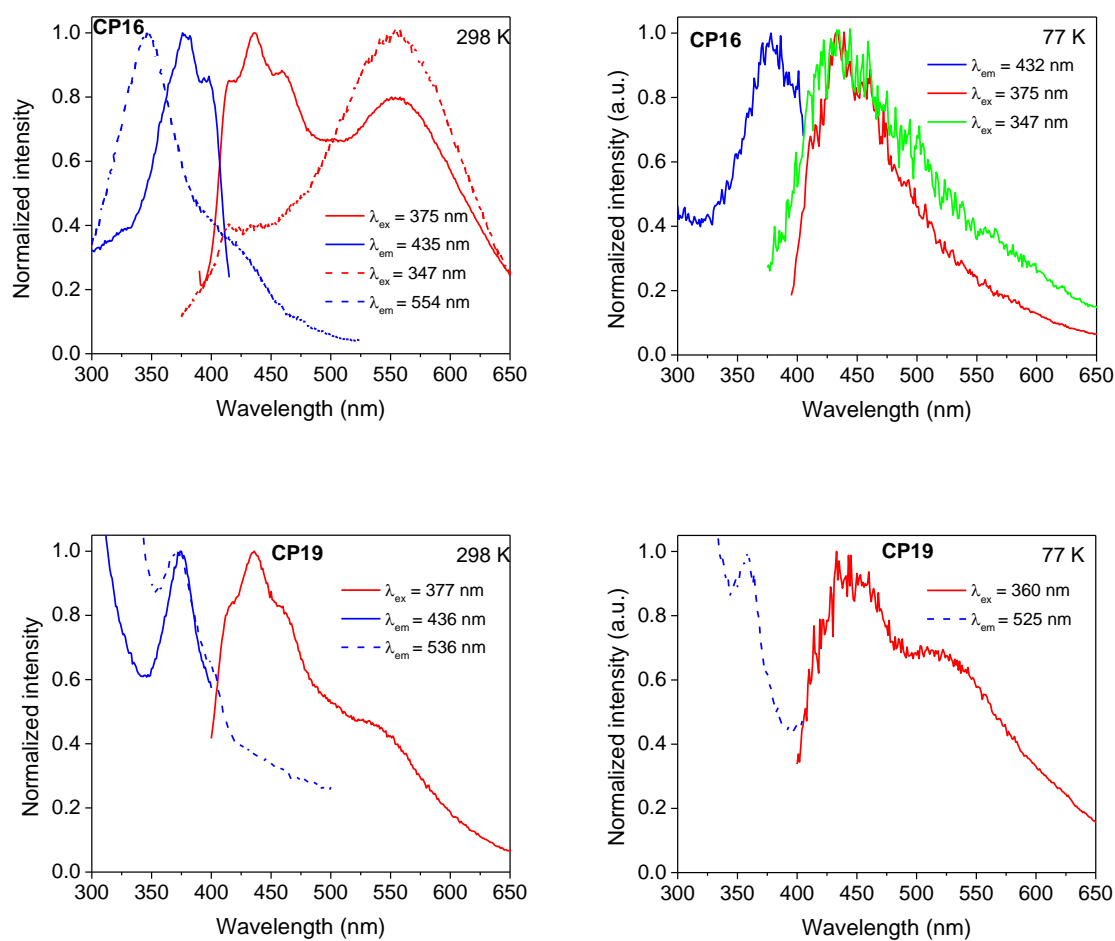


Figure 20. Solid-state excitation (blue lines) and emission spectra (red and green lines) of **CP16** and **CP19** recorded at room temperature (left) and 77 K (right)

CONCLUSION

In this project, we described a complete series of CPs obtained by reacting 2-substituted-1,3-dithiane with CuX salts, where X = I, Br and Cl. First, we have extended the work of Keller and Knaust on the coordination of 1,3-dithiane **L1** on [Cu(MeCN)₄]BF₄ covering the complete Cu(I) halide series and shown that in this latter case, the resulting CPs contain invariable Cu(μ₂-X)₂Cu rhomboids as SBUs instead of single Cu(I) center as in the former case. Another novel finding is the aptitude of **L1** to coordinate as μ₂-S,S 4-electron donor using the two non-bonding doublets of each S atom. The structural diversity of the architectures is further enriched when using dithiane derivatives that are monosubstituted at the 2-position of the thiaheterocycle. Even the “innocent” replacement of an H atom by a methyl group in **L2** allows in the case of CuI to modulate the dimensionality of the network from 1D to 3D and the nuclearity of the (CuI)_n SBUs as a function of the reaction conditions and of CuI-to-**L2** ratio. The crystallographic characterization of the isostructural series [$\{Cu(\mu_2-X)_2Cu\}(\mu_2-L2)_2\}_n$ **CP4**, **CP7** and **CP8** allowed also for the first time to correlate the Cu···Cu distances with the nature of the bridging halide. Although cyano groups in CuCN compounds may adopt a bridging μ₂-bonding mode via the C atom, no such C≡N bonding occurs in [$\{Cu(\mu_2-CN)_2Cu\}(\mu_2-L2)_2\}_n$ **CP9** but instead a linear Cu–CN–Cu linking is preferred.⁹⁵⁻⁹⁷ The use of the bulkier **L3** ligand bearing an *iso*-butyl group gives rise to a 2D material **CP10** featuring a hitherto unknown [$\{Cu_3(\mu_3-I)(\mu_2-I)_2\}S_4\]$ cluster architecture. Similarly, the use of **L5** bearing a phenyl group at the 2-position allows to generate 2D networks featuring similar unprecedented [$\{Cu_3(\mu_3-I)(\mu_2-I)_2\}S_4\]$ and [$\{Cu_3(\mu_3-Br)(\mu_2-Br)_2\}S_4\]$ cluster cores encountered in **CP17** and **CP18**. In the case of **L4** bearing a SiMe₃ function at the 2-position, independently to the halide nature, 1D ribbons featuring both μ₄-type and μ₂-type halide ligands were obtained.

The observation that in several examples the S atoms of **L1**, **L3** and **L5** may act both as 2-electron and 4-electron donors also contributes certainly to the structural richness of the numerous architectures presented in this exhaustive study. Although the luminescent closed-cubane cluster of type [Cu₄(μ₃-I)₄L₄] is a wide-spread motif often obtained by treatment of CuI with *N*, *P*, *As* and *Sb*-donor ligands and also results by coordination of simple sulfides such as Pr-S-Pr,^{23, 24, 98-104} cyclic thioethers such as tetrahydrothiophene and tetrahydrothiopyran,^{30, 31} as well as numerous dithioethers RS∩SR, it is surprising that this cubane motif is not encountered using 1,3-dithianes. However, the formation of the

octanuclear cluster SBU in $[\{\text{Cu}_8(\mu_3\text{-I})_8\}(\mu_2\text{-L2})_4]_n$ **CP6**⁴⁸ demonstrates that also in the case of dithianes, aggregation of CuX to clusters with a nuclearity > 3 can occur.

To conclude, despite the difficulty to anticipate the architecture generated by the self-assembly process between copper salts and dithianes, we have shown at least that: (i) using CuBr and CuCl, the resulting CPs show the same dimensionalities and SBUs (except in one case with **L1**); (ii) using CuI, functionalization of the dithiane ligand at the 2-position with a bulky group (Phenyl, isobutyl) affords 2D CPs incorporating Cu_3I_3 SBUs. The bulkier ferrocenyl-derivative **L6** also leads to the formation of a 1D CP with $\mu_3\text{-I}$ capped Cu centers. Independently of the nature of the halide, the $-\text{SiMe}_3$ bearing ligand **L4** led to the crystallogensis of 1D CPs containing a $[\text{Cu}_2(\mu_4\text{-X})(\mu_2\text{-X})]$ SBU. We have also shown that the dimensionality of all compounds is quite variable ranging from 0D in the molecular ferrocenyl compound $[\{\text{Cu}(\mu_2\text{-I})_2\text{Cu}\}(\kappa_1\text{-L6})_2(\text{MeCN})_2]$ **D1** to 3D in $[\{\text{Cu}_8(\mu_3\text{-I})_8\}(\mu_2\text{-L2})_4]_n$ **CP6**. We are convinced that further variation of the reaction conditions or substituent-pattern around the dithiane-framework may also permit to generate networks incorporating luminescent closed-cubane type $[\text{Cu}_4(\mu_3\text{-I})_4\text{dithiane}_4]$ SBUs. We are currently extending these investigations to other functionalized dithianes bearing chromophores such as anthracenyl groups for photophysical studies and intend to investigate more in depth the electrochemical properties of our ferrocenyl-dithiane based materials.

EXPERIMENTAL SECTION

Materials and methods. The CuX salts, **L1-L5**, 1,2-ethanedithiol and Ferrocenecarbaldehyde were commercial obtained from Acros, Alfa Aesar and Aldrich. The preparation of **CP4**, **CP5** and **CP6** has been recently described.⁴⁸ The ^1H and ^{13}C NMR spectra were obtained on a Bruker AVANCE 400 HD instrument. ^1H chemical shifts were referenced to the proton impurity of the NMR solvent and ^{13}C chemical shifts to the NMR solvent. The solid-state emission and excitation spectra were recorded at room temperature or 77K with a Jobin-Yvon Fluorolog-3 spectrometer using a cylindrical 5 mm diameter quartz capillary with a scan speed of 1 nm/s. Infrared spectra were recorded with a 2 cm^{-1} resolution on a Bruker vertex70 FTIR spectrometer using of a Platinum ATR accessory equipped with a diamond crystal. Thermogravimetric analysis (TGA) was carried out on a TA instruments Q600 in an alumina crucible under an air flow with a heating rate of $10^\circ\text{C min}^{-1}$ up to 850°C . Differential Scanning Calorimetry (DSC) measurements of phase-transition temperatures

were performed with a TA Instruments Q100. Samples of 5–10 mg were placed in a hermetically sealed aluminum pan; an empty pan was used as the reference. Pans were exposed to a N₂ flow atmosphere. The following measurement conditions were applied: (i) cooling from room temperature to -80 °C at a rate of 10 °C min⁻¹, (ii) heating to 25 °C at a rate of 10 °C min⁻¹.

X-ray Crystallography. X ray powder patterns were obtained at 295 K on a D8 Advance Bruker diffractometer using Ni-filtered K- α radiation. Single crystals of **CP1-CP19** and **D1** were mounted on a Bruker D8 Venture four-circle diffractometer equipped with a nitrogen jet stream low-temperature system (Oxford Cryosystems). The X-ray source was graphite monochromated Mo-K α radiation ($\lambda = 0.71073$ Å) from a microfocus sealed tube I μ S by Incoatec. In the case of **CP12**, the X-ray source was a microfocus sealed tube I μ S 3.0 by Incoatec. For **CP1**, **CP2**, **CP3**, **CP7**, **CP8**, **CP13**, **CP19** and **D1**, a Photon 100 CMOS detector by Bruker was used. Data collection for **CP9-CP12** and **CP14-CP18** was conducted with a Bruker Photon II CPAD detector. All data collections have been carried out at 100 K, in the case of **CP16** data were collected at five different temperatures: 100, 150, 200, 250 and 300 K, using the same crystal. The lattice parameters were obtained by least-squares fit to the optimized setting angles of the entire set of collected reflections. Intensity data were recorded as ϕ and ω scans with κ offsets. No significant intensity decay or temperature drift was observed during data collections. Data were reduced by using SAINT v8.37A (Bruker, 2015) software and absorption correction was carried out by SADABS-2016/2 (Bruker, 2016). The structure was solved using SHELXT (Sheldrick, 2015) with intrinsic phasing. Refinements were carried out by full-matrix least-squares on F² using SHELXL program (Sheldrick, 2015) on the complete set of reflections. All non-hydrogen atoms were refined with anisotropic thermal parameters, whereas the H atoms were treated in a riding mode. The crystal structure determination of **L6** was accomplished on an Oxford Xcalibur Sapphire3 diffractometer; data collection: CrysAlis CCD (Oxford Diffraction, 2006); cell refinement: CrysAlis RED (Oxford Diffraction, 2006); data reduction: CrysAlis RED; absorption correction: multi-scan (CrysAlis RED; Oxford Diffraction, 2006).

The crystal data, data collection and structure refinement of all compounds are presented in Tables S1–S7. Crystallographic data (excluding structure factors) have been deposited with the Cambridge Crystallographic Data Centre. The CIF files for the X-Ray structures presented in this publication have the following CCDC numbers: 1888353 for **CP1**, 1888455

for **CP2**, 1888456 for **CP3**, 1888460 for **CP7**, 1888477 for **CP8**, 1888478 for **CP9**, 1888479 for **CP10**, 1888480 for **CP11**, 1888481 for **CP12**, 1888483 for **CP13**, 1888487 for **CP14**, 1888489 for **CP15**, 1886853-1886857 for **CP16** at 100, 150, 200, 250 and 300 K, 1888490 for **CP17**, 1888497 for **CP18**, 1888515 for **CP19**, 1888524 for **D1**, and 1888541 for **L6**. These data may be obtained free of charge from the Cambridge Crystallographic Data Center through www.ccdc.cam.ac.uk/data_request/cif.

Synthesis

Synthesis of L6. A toluene solution of ferrocenecarbaldehyde (428 mg, 2 mmol) and 1,3-propanedithiol (260 mg, 2.4 mmol) was stirred at 60 °C with *p*-toluenesulfonic acid monohydrate (38 mg, 0.2 mmol) as a catalyst. After 24 h the solvent was evaporated and the residue was purified by column chromatography on silica gel eluting with a gradient of hexane/dichloromethane (100:0 to 80:20) to give **L6** as an orange solid (465 mg, 76%), mp. 115-116 °C. ¹H NMR (CDCl₃) δ (ppm): 1.79-1.86 (m, 1H), 2.05-2.09 (m, 1H), 2.75-5.80 (m, 2H), 2.91-2.98 (m, 2H), 4.08 (t, ³J = 2.0 Hz, 2H), 4.18 (s, 5H), 4.26 (t, ³J = 2.0 Hz, 2H), 4.90 (s, 1H). ¹³C{¹H} NMR (CDCl₃) δ (ppm): 25.7, 31.9, 47.3, 67.4, 68.0, 69.5, 86.9. IR (ATR): 3111 (w), 3092(w), 2931 (w), 2891 (w), 1410 (w), 1274 (w), 1238 (w), 1178 (w) , 1106 (m), 1038 (w), 1021 (w), 1001 (m), 929 (w), 904 (w), 874 (w), 815 (m), 775 (m), 725 (w), 679 (w), 654 (w), 620 (w), 493 (s), 483 (s), 418 (w) cm⁻¹. Anal. Calc for C₁₄H₁₆FeS₂ (304.25): C 55.27, H 5.30, S 21.08; found: C 55.63, H 5.36, S 21.12%.

Synthesis of CP1. To an EtCN solution of CuI (382 mg, 2.0 mmol) (40 mL) was added neat 1,3-dithiane (252 mg, 2.1 mmol). A white precipitate appeared within 2 min. The mixture was stirred for 3 h to complete the reaction and then heated to reflux for 5 min. After allowing to reach ambient temperature, the precipitate was filtered off, washed with 5 mL propionitrile and dried to give **CP1** as a white microcrystalline solid (566 mg, 91%). Conducting the reaction in MeCN using a 2:1 CuI-to-**L1** ratio afforded the same product. X-ray suitable crystals were grown by dissolution of a small amount of **CP1** in refluxing EtCN and subsequent slow cooling in an oil bath. mp 241 °C; IR (ATR): 2985 (w), 2952 (w), 2913 (w), 2902 (w), 1428 (m), 1417 (s), 1405 (m), 1389(w), 1366 (m), 1283 (w), 1242 (w), 1164 (m) , 1082 (m), 1012 (m), 923 (s), 914 (s), 891 (m), 889 (w), 817 (m), 746 (s), 738 (s), 664 (s), 637 (m), 476 (m) cm⁻¹. Anal. Calc for C₄H₈CuIS₂ (310.66): C 15.46, H 2.60, S 20.64; found: C 15.05, H 2.24, S 20.35%.

Synthesis of CP2. To a solution of 1,3-dithiane (252 mg, 2.1 mmol) in 20 mL of acetonitrile was added CuBr (286 mg, 2.0 mmol) in several portions. A white precipitate appeared within 5 min. The mixture was stirred for 3 h to complete the reaction, then heated to reflux for 3 min till almost entire dissolution of the solid. Upon cooling, the onset of progressive growth of colorless crystals occurred on the wall of the Schlenk tube. A further crop of crystal of **CP2** could be isolated after decanting the slight greenish mother liquor and storage at 5°C overnight in a fridge. Overall yield: (406 mg, 69%). mp 238 °C; IR (ATR): 2960 (m), 2934 (w), 2910 (w), 2896 (m), 1416 (m), 1365 (w), 1276 (w), 1234 (m), 1163 (m), 1090 (w), 1018 (m), 921 (s), 888 (m), 819 (m), 747 (m), 725 (m), 666 (m), 659 (m), 648 (m), 630 (m), 488 (m), 477 (m) cm^{-1} . Anal. Calc for $\text{C}_4\text{H}_8\text{BrCuS}_2$ (263.69): C 18.22, H 3.06, S 24.32; found: C 17.91, H 2.84, S 24.05 %.

Synthesis of CP3. To a solution of 1,3-dithiane (252 mg, 2.1 mmol) in 25 mL of acetonitrile containing 1 mL of MeOH was added CuCl (404 mg, 4.0 mmol) in several portions. A yellowish precipitate formed rapidly. The mixture was stirred for 3 h to complete the reaction, then heated to reflux for 3 min till almost entire dissolution of the solid. Upon cooling, the onset of progressive growth of yellowish crystals occurred on the wall of the Schlenk tube. A further crop of crystal of **CP3** could be isolated by decanting the greenish mother liquor and storage at 5°C overnight in a fridge. Overall yield: (540 mg, 85%). IR (ATR): mp 241 °C; IR (ATR): 2961 (m), 2897 (m), 1424 (m), 1275 (w), 1234 (m), 1164 (m), 1148 (m), 1103 (m), 1020 (m), 1001 (m), 920 (s), 889 (m), 821 (m), 775 (w), 729 (m), 652 (m), 634 (m), 490 (s), 419 (m) cm^{-1} . Anal. Calc. for $\text{C}_4\text{H}_8\text{Cl}_2\text{Cu}_2\text{S}_2$ (318.24): C 15.91, H 2.53, S 20.15; found: C 16.21, H 2.84, S 20.55 %.

Synthesis of CP7. This compound was prepared in a similar manner as detailed for **CP2**. Overall yield: 487 mg, 88%. mp. 225 °C; IR (ATR): 2956 (w), 2940 (w), 2912 (w), 28962 (w), 1453 (w), 1425 (s), 1408 (m), 1376 (m), 1231 (m), 1181 (m), 1164 (m), 1126 (m), 1078 (w), 1064 (m), 966 (s), 902 (m), 872 (m), 8112 (m), 710 (m), 664 (s) cm^{-1} . Anal. Calc for $\text{C}_5\text{H}_{10}\text{BrCuS}_2$ (277.72): C 28.77, H 3.63, S 23.09; found: C 28.31, H 3.34, S 22.75 %.

Synthesis of CP8. This compound was prepared in a similar manner as detailed for **CP3**. Overall yield: 373 mg, 79%. mp 198 °C; IR (ATR): 2959 (m), 2918 (w), 2863 (w), 2829 (w), 1456 (w), 1427 (s), 1410 (m), 1376 (m), 1233 (m), 1183 (w), 1165 (s), 1128 (m), 1080 (m), 902 (s), 872 (m), 810 (m), 712 (m), 665 (s), 444 (w) cm^{-1} . Anal. Calc for $\text{C}_5\text{H}_{10}\text{ClCuS}_2$ (233.26): C 25.75, H 4.32, S 27.49; found: C 25.31, H 3.94, S 27.05 %.

Synthesis of CP9. This compound was prepared by refluxing a suspension of CuCN (179 mg, 2.0 mmol) during 3h in MeCN in the presence of an excess of **L2**. Overall yield: 348 mg, 78%. IR (ATR): 2957 (m), 2911(w), 2859 (w), 2810 (w), 2121 (s), 1442 (w), 1420 (w), 1407 (m), 1378 (w), 1272 (w), 1230 (w), 1180 (w), 1166 (m), 1119 (w), 1076 (w), 1057 (m), 1046 (w), 999 (w), 973 (w), 902 (m), 866 (w), 818 (w), 708 (m), 666 (m), 520 (w), 485 (w), 442 (w) cm^{-1} . No satisfactory elemental analysis could be obtained for **CP9**.

Synthesis of CP10. **L3** (0.3 mL, 1.7 mmol) was dissolved in 5 mL of acetonitrile and an MeCN solution (25 mL) of CuI (226 mg, 1.2 mmol) was added dropwise. A white precipitate was observed within 5 minutes. The mixture was then stirred for 3 h to complete the reaction. The precipitate was filtered, washed with 2×10 mL acetonitrile and dried. **CP10** was isolated as a white solid (173 mg, 46%). A small amount of this CP (20 mg) was dissolved in hot MeCN (10 mL). Overnight standing of the solution at 5°C provided single-crystals suitable for X-ray crystallography. IR (ATR): 3100 (s), 2907 (m), 2863 (w), 1464 (m), 1416 (s), 1387(w), 1367 (w), 1269 (w), 1237 (w), 1192 (s), 1167 (w), 1131 (w), 1104 (w), 1056 (w), 1028 (w), 1005 (w), 946 (w), 907 (s), 881 (w), 819 (w), 744 (m), 655 (m), 623 (w), 501 (w), 467 (w), 421(w) cm^{-1} . Anal. Calc for $\text{C}_{16}\text{H}_{32}\text{Cu}_3\text{I}_3\text{S}_4$ (924.04): C 20.80, H 3.49, S 13.88; found: C 20.45, H 3.24, S 13.47%.

Synthesis of CP11. This material was prepared by following the same protocol by mixing **L3** (0.3 mL, 1.7 mmol) and CuBr (175 mg, 1.2 mmol) providing **CP11** as a white solid (103 mg, 27%). mp 152 °C; IR (ATR): 2955 (s), 2899 (m), 2868 (w), 1464 (m), 1416 (s), 1384 (w), 1366 (w), 1271 (w), 1236 (w), 1187(s), 1169 (w), 1131 (w), 1109 (w), 1038 (w), 1005 (w), 947 (w), 908 (s), 889 (w), 871 (w), 828 (w), 817 (w), 764 (m), 677 (m), 661 (w), 637 (w), 463 (m) cm^{-1} . Anal. Calc for $\text{C}_{16}\text{H}_{32}\text{Cu}_2\text{Br}_2\text{S}_4$ (639.59): C 30.05, H 5.04, S 20.05; found: C 30.15, H 4.84, S 19.47%.

Synthesis of CP12. This material was prepared by addition of CuCl (200 mg, 2.0 mmol) to a MeCN solution of 1.2 equiv. of **L3** providing **CP12** as a pale yellow solid (369 mg, 67%). IR (ATR): 2956 (w), 2922 (w), 2899 (w), 2868 (w), 1489 (w), 1414 (m), 1253 (m), 1167(m), 1129 (w), 1083 (w), 1037 (w), 999 (w), 905 (m), 880 (m), 841 (s), 758 (m), 731 (m), 639 (w), 474 (w) cm^{-1} . Anal. Calc for $\text{C}_{16}\text{H}_{32}\text{Cu}_2\text{Cl}_2\text{S}_4$ (550.69): C 34.90, H 5.86, S 23.29; found: C 32.90, H 5.60, S 21.91%.

Synthesis of CP13. This CP was prepared by addition of neat **L4** (2.0 mmol) to a MeCN solution of CuI (382 mg, 2.0 mmol), affording a white solid (458 mg, 80%). mp 221 °C IR (ATR): 2953 (w), 2933 (w), 2909 (w), 2894 (w), 2854 (w), 1414 (w), 1251 (m), 1175 (w), 1089 (w), 999 (w), 902 (m), 881 (w), 843 (s), 759 (m), 728 (m), 638 (w) cm⁻¹. Anal. Calc for C₇H₁₆Cu₂I₂S₂Si (573.32): C 14.66, H 2.81, S 11.19; found: C 14.75, H 2.54, S 10.97%.

Synthesis of CP14. This CP was prepared in a similar manner as white solid (393 mg, 82%). mp 224 °C IR (ATR): 2942 (w), 2913 (w), 2862 (w), 1413 (w), 1249 (m), 1170 (w), 1084 (w), 998 (w), 902 (m), 880 (m), 840 (s), 756 (m), 730 (m), 637 (m), 570 (w), 473(w) cm⁻¹. Anal. Calc for C₇H₁₆Cu₂Br₂S₂Si (479.32): C 17.54, H 3.36, S 13.38; found: C 17.25, H 2.99, S 12.98%.

Synthesis of CP15. This CP was obtained in a similar manner as a pale yellow solid (393 mg, 62%). IR (ATR): 2948 (w), 2921 (w), 2894 (w), 2857 (w), 1414 (w), 1253 (m), 1167 (w), 1083 (w), 998 (w), 904 (m), 881 (m), 840 (s), 757 (m), 731 (m), 639 (m), 574 (w), 474(w) cm⁻¹. Anal. Calc for C₇H₁₆Cu₂Cl₂S₂Si (390.42): C 21.53, H 4.13, S 16.43; found: C 21.25, H 3.98, S 16.06%.

Synthesis of CP16. This CP was obtained **by** dissolving CuI (191 mg, 1.0 mmol) in MeCN and subsequent addition of 1 equiv of neat **L5** **providing CP16** as a white solid (393 mg, 64%). IR (ATR): 2965 (w), 2915 (w), 2309 (w), 2275 (w), 1495 (w), 1453 (w), 1420 (m), 1366(w), 1272 (w), 1224 (w), 1171 (w) , 1072 (w), 1027 (w), 904 (w), 879 (w), 738 (m), 696 (s), 669 (m), 6451 (w), 589 (w), 497 (w) cm⁻¹. Anal. Calc for C₁₄H₁₈Cu₂I₂N₂S₂ (659.34): C 25.50, H 2.75, N 4.25, S 9.73; found: C 25.17, H 2.25, N 3.99, S 10.10 %.

Synthesis of CP17. This CP was obtained **by** dissolving CuI (382 mg, 2.0 mmol) in warm EtCN **followed by** addition of neat **L5** (196 mg, 1 mmol) and subsequent refluxing the white precipitate. (520 mg, 90%). mp 237 °C; IR (ATR): 3055 (w), 3030 (w), 2967 (w), 2932 (w), 2902 (w), 1584 (w), 1494 (w), 1453 (w), 1407 (w), 1272 (w), 1222 (w), 1174 (w), 1157 (w), 1072 (w), 1030 (w), 1008 (w), 904 (w), 889 (w), 876 (w), 827 (w), 778 (w), 721 (m), 689 (s), 666 (w), 644 (m), 591 (w), 489 (w), 423 (w) cm⁻¹. Anal. Calc for C₂₀H₂₄Cu₃I₃S₄ (964.03): C 24.92, H 2.50, S 13.30; found: C 25.12, H 2.27, S 12.98 %.

Synthesis of CP18. This CP was obtained dissolving CuBr (286 mg, 2.0 mmol) in MeCN and subsequent addition of neat **L5** (196 mg, 1 mmol), affording a white precipitate. (400 mg, 83%). mp 186 °C; IR (ATR): 3057 (w), 3031 (w), 2988 (w), 2949 (w), 2904 (w), 2818 (w),

1584 (w), 1494 (w), 1452 (w), 1418 (m), 1273 (w), 1221 (w), 1158 (w), 1072 (w), 1032 (w), 1009 (w), 905 (w), 877 (w), 837 (w), 780 (w), 727 (m), 690 (s), 667 (w), 645 (w), 490 (w) cm⁻¹. Anal. Calc for C₂₀H₂₄Cu₃Br₃S₄ (823.02): C 29.19, H 2.93, S 15.58; found: C 28.82, H 2.67, S 15.18 %.

Synthesis of CP19. To a solution of **L6** (30 mg, 0.1 mmol) in CH₂Cl₂ (5 mL) was added a MeCN solution of CuI (38 mg, 0.2 mmol). After stirring for 2h, a yellow precipitate was obtained, which was dissolved by heating. The solution was cooled to room temperature and then kept at 5°C. Overnight standing gave orange crystals, which were filtered off and air-dried to give **CP19**. (45 mg, 66 % yield). mp 197 °C IR (ATR): 2955 (w), 2922 (w), 2900 (w), 2858 (w), 1468 (w), 1414 (m), 1270 (w), 1253 (m), 1167 (m), 1083 (w), 1042 (w), 999, 905 (m), 881 (m), 840 (s), 758 (m), 731 (w), 701 (w), 639 (w), 483 (w) cm⁻¹ Anal. Calc for C₁₄H₁₆FeCu₂I₂S₂ (685.16): C 24.54, H 2.35, S 9.36; found: C 24.97, H 2.50, S 9.79 %.

Synthesis of D1. To a solution of **L6** (30 mg, 0.1 mmol) in CH₂Cl₂ (5 mL) was added acetonitrile solution of CuI (38 mg, 0.2 mmol). After stirring for 2h, yellow precipitate was obtained. The precipitate was re-dissolved by heating. The solution was cooled to room temperature and then kept at 5°C. Overnight standing gave orange crystals, which were filtered off and air-dried to give **D1**. (50 mg, 70 % yield). mp 192 °C IR (ATR): 3092(w), 3080 (w), 2894 (w), 2305 (w), 2275 (w), 1421 (w), 1413 (w), 1364 (w), 1268 (w), 1229 (w), 1163 (w), 1105 (m), 1036 (w), 1021 (w), 998 (m), 936 (w), 905 (w), 874 (w), 817 (m), 776 (m), 722 (w), 618 (w), 501 (s), 485 (s) cm⁻¹ Anal. Calc for C₃₂H₃₈Fe₂Cu₂I₂N₂S₄ (1071.52): C 35.87, H 3.57, N 2.61, S 11.97; found: C 35.47, H 3.50, N 2.41, S 12.10 %.

ASSOCIATED CONTENT

Supporting Information. Crystallographic data in CIF file, summary of X-ray data collection and refinement for all structures studied, structure views of **CP1**, **CP2**, **CP7-CP18**, **L6**, Powder X-Ray Patterns of **CP1**, **CP2**, **CP7**, **CP8**, **CP10-CP14**, **CP17-CP19**, **D1**, ATR-IR spectra of **CP9**, **CP16**, **D1**, DSC traces of **CP16** and TGA traces of **CP5**, **CP7**, **CP8**, **CP10-CP12** and **D1**. The following files are available free of charge on the ACS publication website at [hppt://pubs.acs.org](http://pubs.acs.org).

AUTHOR INFORMATION

*E-mail: Michael.Knorr@univ-fcomte.fr

* E-mail: lydie.viau@univ-fcomte.fr

* E-mail: carsten.strohmann@tu-dortmund.de

ACKNOWLEDGEMENTS

We are grateful to the *CNRS* and the *Ministère de la Recherche et Technologie* for financial support and the region of Franche-Comté for funding a Post-doc fellowship for A. R. (grant RECH-MOB15-000017). We are also thankful to Marie-Laure Léonard from ESIREM Dijon, France for obtaining the TGA results reported herein and to Dr. Jean-Baptiste Sanchez for his help with DSC measurements.

REFERENCES

1. De Groot, B.; Giesbrecht, G. R.; Loeb, S. J.; Shimizu, G. K. H. Copper(I) and silver(I) complexes of the crown thioether ligand 2,5,8-trithia[9]-o-benzenophane (TT[9]OB). Structures of [Cu(PPh₂Me)(TT[9]OB)][ClO₄] and [Ag(PPh₃)(TT[9]OB)][ClO₄]. *Inorg. Chem.* **1991**, *30*, 177-182.
2. Blake, A. J.; Reid, G.; Schröder, M. Thioether macrocyclic chemistry: Synthesis of [RhCl([15]aneS₅)]²⁺ and [Ru(PPh₃)([15]aneS₅)]²⁺. The single crystal X-ray structure of [Ru(PPh₃)([15]aneS₅)](BPh₄)₂ ([15]aneS₅ = 1,4,7,10,13-pentathiacyclopentadecane). *Polyhedron* **1992**, *11*, 2501-2506.
3. Shen, J.; Pickardt, J. (Dichloro)-μ-(1,3,5-trithiane)copper(II), [CuCl₂.C₃H₆S₃]_n, and (dichloro)(1,4,7-trithiacyclononane)copper(II), [CuCl₂.C₆H₁₂S₃]. *Z. Naturforsch., B: Chem. Sci.* **1992**, *47*, 1736-40.
4. Blake, A. J.; Gould, R. O.; Radek, C.; Schröder, M. The synthesis and single-crystal X-ray structure of the tetranuclear silver(I) complex {[Ag₂([18]aneS₂O₄)₂}(PF₆)₄([18]aneS₂O₄ = 1,4,7, 10-tetraoxa-13, 16-dithiacyclooctadecane). *J. Chem. Soc., Chem. Commun.* **1994**, 985 - 986.
5. Brooks, N. R.; Blake, A. J.; Champness, N. R.; Cooke, P. A.; Hubberstey, P.; Proserpio, D. M.; Wilson, C.; Schröder, M. Discrete molecular and extended polymeric copper(I) halide complexes of tetradentate thioether macrocycles. *J. Chem. Soc., Dalton Trans.* **2001**, 456 - 465.
6. Levason, W.; Matthews, M. L.; Patel, R.; Reid, G.; Webster, M. Unusual structural variations within a family of thioether macrocyclic complexes. Tin(IV) halide adducts of [12]-, [14]- and [16]-aneS₄. *New J. Chem.* **2003**, *27*, 1784-1788.
7. Lee, J. Y.; Lee, S. Y.; Sim, W.; Park, K.-M.; Kim, J.; Lee, S. S. Temperature-Dependent 3-D CuI Coordination Polymers of Calix[4]-bis-dithiacrown: Crystal-to-Crystal Transformation and Photoluminescence Change on Coordinated Solvent Removal. *J. Am. Chem. Soc.* **2008**, *130*, 6902-6903.

8. Bi, Y.; Liao, W.; Wang, X.; Deng, R.; Zhang, H. Self-Assembly from Two-Dimensional Layered Networks to Tetranuclear Structures: Syntheses, Structures, and Properties of Four Copper–Thiacalix[4]arene Compounds. *Eur. J. Inorg. Chem.* **2009**, 2009, 4989–4994.
9. Jin, Y.; Kim, H. J.; Lee, J. Y.; Lee, S. Y.; Shim, W. J.; Hong, S. H.; Lee, S. S. Hard/Soft Heterometallic Network Complex of a Macrocyclic with Endo/Exocyclic Coordination. *Inorg. Chem.* **2010**, 49, 10241–10243.
10. Chang, Y.-P.; Levason, W.; Reid, G. Developments in the chemistry of the hard early metals (Groups 1–6) with thioether, selenoether and telluroether ligands. *Dalton Trans.* **2016**, 45, 18393–18416.
11. Van Rooyen, P. H.; Dillen, J. L. M.; Lotz, S.; Schindehutte, M. π -Arene complexes: I. The crystal and molecular structures of π -benzenedicarbonyl-1,3-dithianechromium(0) and π -methylbenzoatedicarbonyl-1,3-dithianechromium(0). *J. Organomet. Chem.* **1984**, 273, 61–68.
12. Cotton, F. A.; Kolb, J. R.; Stults, B. R. Reactivity of diiron nonacarbonyl in tetrahydrofuran. : IV. The synthesis and crystal and molecular structure of 1,3-dithianeiron tetracarbonyl, (cyclo-1,3- $\text{C}_4\text{H}_8\text{S}_2$) $\text{Fe}(\text{CO})_4$. *Inorg. Chim. Acta* **1975**, 15, 239–244.
13. Green, M.; Draganjac, M.; Jiang, Y.; Nave, P. M.; Cordes, A. W.; Bryan, C. D.; Dixon, J. K.; Folkert, S. L.; Yu, C. H. Reaction of $\text{CpRu}(\text{PPh}_3)_2\text{Cl}$ with six-member cyclothioethers. Structures of the $[\text{CpRu}(\text{PPh}_3)_x\text{L}]\text{Y}$ complexes ($\text{L} = \text{pentamethylene sulfide}$, $x = 2$, $\text{Y} = \text{BF}_4^-$; $\text{L} = 1,3\text{-dithiane}$; $1,3,5\text{-trithiane}$, $x = 2$, $\text{Y} = \text{CF}_3\text{SO}_3^-$; $\text{L} = 1,4\text{-dithiane}$, $x = 1$, $\text{Y} = \text{BF}_4^-$). *J. Chem. Crystallogr.* **2003**, 33, 473–479.
14. Yamamoto, Y.; Sakamoto, S.; Ohki, Y.; Usuzawa, A.; Fujita, M.; Mochida, T. Preparation and characterization of rhodium(III), iridium(III) and ruthenium(II) bearing 1,3- or 1,4-dithianes. *Dalton Trans.* **2003**, 3534–3540.
15. Rossi, S.; Kallinen, K.; Pursiainen, J.; Pakkanen, T. T.; Pakkanen, T. A. Reactions of cyclic thioethers with $\text{Ru}_3(\text{CO})_{12}$. Synthesis, reactivity and crystal structures of $\text{HRu}_3(\text{CO})_9$ ($\mu_3\text{-}\eta_3(\text{C,S,S})\text{-}1,3\text{-dithiacyclohexane}$), $\text{Ru}_3(\text{CO})_9(\mu_3\text{-}\eta_3\text{-}1,3,5\text{-trithiacyclohexane})$ and $\text{Ru}_3(\text{CO})_9(\mu_2\text{-}\eta_3\text{-}1,4,7\text{-trithiaheptane})$. *J. Organomet. Chem.* **1992**, 440, 367–387.
16. Räsänen, T. M.; Jaaskelainen, S.; Pakkanen, T. A. Heteroligand substitution in clusters of ruthenium and cobalt. *J. Organomet. Chem.* **1998**, 553, 453–461.
17. Leung, K. S.-Y.; Wong, W.-T. Synthesis, structural characterization and reactivities of hexaosmium carbonyl clusters with six-membered cyclic thioether and thioxane ligands. *J. Chem. Soc., Dalton Trans.* **1999**, 2077–2086.
18. Brodersen, K.; Liehr, G.; Rölz, W. Stabile Quecksilber(I)-Schwefel-Verbindungen. II. Die Kristallstruktur des 1,3-Dithian-diquecksilber(I)-dinitrats. *Z. Anorg. Allg. Chem.* **1977**, 428, 166–172.

19. Brammer, L.; Rodger, C. S.; Blake, A. J.; Brooks, N. R.; Champness, N. R.; Cunningham, J. W.; Hubberstey, P.; Teat, S. J.; Wilson, C.; Schroeder, M. Bridging mode flexibility of 1,3-dithiacyclohexane in silver(I) co-ordination polymers. *J. Chem. Soc., Dalton Trans.* **2002**, 4134-4142.
20. Knaust, J. M.; Keller, S. W. Supramolecular coordination isomers: synthesis and crystal structures of four new one-dimensional copper(I) coordination polymers with 1,3-dithiane. *CrystEngComm* **2003**, 5, 459-465.
21. Knorr, M.; Guyon, F.; Khatyr, A.; Allain, M.; Aly, S. M.; Lapprand, A.; Fortin, D.; Harvey, P. D. Unexpected Formation of a Doubly Bridged Cyclo-1,2-dithian 1D Coordination Cu₂I₂-Containing Luminescent Polymer. *J. Inorg. Organomet. Polym. Mater.* **2010**, 20, 534-543.
22. San Filippo, J., Jr.; Zyontz, L. E.; Potenza, J. Synthesis and characterization of some halocopper(I)-alkyl sulfide complexes including the crystal structure of μ -(diethyl sulfide)-bis(diethyl sulfide)tetra- μ -iodo-tetracopper(I), [(C₂H₅)₂S]₃[CuI]₄. *Inorg. Chem.* **1975**, 14, 1667-1671.
23. Zhou, J.; Bian, G.-Q.; Dai, J.; Zhang, Y.; Zhu, Q.-Y.; Lu, W. Luminescent 2-D Double-layered Polymer, [(CuI)₄(CH₃SCH₃)₃], Containing Helical Chains Constructed by Flower-Basket-Shaped Cu₄I₄ Clusters. *Inorg. Chem.* **2006**, 45, 8486 -8488.
24. Kim, T. H.; Shin, Y. W.; Kim, J. S.; Lee, S. S.; Kim, J. Luminescent staircase copper(I) coordination polymer based on planar Cu₃I₃. *Inorg. Chem. Commun.* **2007**, 10, 717-719.
25. Li, J.-R.; Bu, X.-H. Structural Diversity and Modulation of Coordination Architectures with Flexible Dithioether or Disulfoxide Ligands. *Eur. J. Inorg. Chem.* **2008**, 27 - 40.
26. Peng, R.; Li, M.; Li, D. Copper(I) halides: A versatile family in coordination chemistry and crystal engineering *Coord. Chem. Rev.* **2010**, 254, 1-18
27. Knorr, M.; Guyon, F.; Kubicki, M. M.; Rousselin, Y.; Aly, S. M.; Harvey, P. D. Effect of t-BuS vs. n-BuS on the topology, Cu...Cu distances and luminescence properties of 2D Cu₄I₄/RS(CH₂)₄SR metal-organic frameworks. *New J. Chem.* **2011**, 35, 1184-1188.
28. Lapprand, A.; Bonnot, A.; Knorr, M.; Rousselin, Y.; Kubicki, M. M.; Fortin, D.; Harvey, P. D. Formation of an Unprecedented (CuBr)₅ Cluster and Zeolite-type 2D-Coordination Polymer; a Surprising Halide Effect. *Chem. Commun.* **2013**, 49, 8848-8850.
29. Henline, K. M.; Wang, C.; Pike, R. D.; Ahern, J. C.; Sousa, B.; Patterson, H. H.; Kerr, A. T.; Cahill, C. L. Structure, Dynamics, and Photophysics in the Copper(I) Iodide-Tetrahydrothiophene System. *Cryst. Growth Des.* **2014**, 14, 1449-1458.
30. Chiang, H.; Moon, C. J.; Kwon, E.; Park, H.; Im, H.; Choi, M. Y.; Kim, T. H.; Kim, J. Copper(I) Complexes Based on Pentamethylene Sulfide: Luminescence Thermochromism of Cu₄I₄(C₅H₁₀S)₄. *Bull. Korean Chem. Soc.* **2018**, 39, 1139-1143.
31. Kim, T. H.; Lee, K. Y.; Shin, Y. W.; Moon, S.-T.; Park, K.-M.; Kim, J. S.; Kang, Y.; Lee, S. S.; Kim, J. New crystalline framework formed from a podal ligand with S₂O₂ donor and CuI: non-

- interpenetrating square-grid with cubane-like Cu_4I_4 cluster nodes. *Inorg. Chem. Commun.* **2005**, 8, 27-30.
32. Peindy, H. N.; Guyon, F.; Khatyr, A.; Knorr, M.; Strohmann, C. Construction of 1D and 2D copper(I) coordination polymers assembled by $\text{PhS}(\text{CH}_2)_n\text{SPh}$ ($n = 1, 2$) dithioether Ligands: surprising effect of the spacer length on the dimensionality, cluster nuclearity and the fluorescence properties of the metal-organic framework. *Eur. J. Inorg. Chem.* **2007**, 1823-1828.
33. Knorr, M.; Guyon, F.; Khatyr, A.; Daeschlein, C.; Strohmann, C.; Aly, S. M.; Abd-El-Aziz, A. S.; Fortin, D.; Harvey, P. D. Rigidity effect of the dithioether spacer on the size of the luminescent cluster $(\text{Cu}_2\text{I}_2)_n$ ($n = 2, 3$) in their coordination polymers. *Dalton Trans.* **2009**, 948-955.
34. Xie, C.; Zhou, L.; Feng, W.; Wang, J.; Chen, W. Varying the frameworks of coordination polymers with $(\text{CuI})_4$ cubane cluster by altering terminal groups of thioether ligands. *J. Mol. Struct.* **2009**, 921, 132-136.
35. Martinez-Alanis, P. R.; Ugalde-Saldivar, V. M.; Castillo, I. Electrochemical and Structural Characterization of Tri- and Dithioether Copper Complexes. *Eur. J. Inorg. Chem.* **2011**, 212-220.
36. Zhang, J.; Xue, Y.-S.; Li, Y.-Z.; Du, H.-B.; You, X.-Z. Cuprous iodide coordination polymers $(\text{CuI})_x(\text{L})_y \cdot z(\text{solvent})$ built on linear thioether linkers. *CrystEngComm* **2011**, 13, 2578-2585.
37. Knorr, M.; Guyon, F.; Khatyr, A.; Strohmann, C.; Allain, M.; Aly, S. M.; Lapprand, A.; Fortin, D.; Harvey, P. D. Construction of $(\text{CuX})_{2n}$ Cluster-Containing ($\text{X} = \text{Br}, \text{I}; n = 1, 2$) Coordination Polymers Assembled by Dithioethers $\text{ArS}(\text{CH}_2)_m\text{SAr}$ ($\text{Ar} = \text{Ph}, p\text{-Tol}; m = 3, 5$): Effect of the Spacer Length, Aryl Group, and Metal-to-Ligand Ratio on the Dimensionality, Cluster Nuclearity, and the Luminescence Properties of the Metal-Organic Frameworks. *Inorg. Chem.* **2012**, 51, 9917-9934.
38. Yang, X.-J.; Li, H.-X.; Xu, Z.-L.; Li, H.-Y.; Ren, Z.-G.; Lang, J.-P. Spacer length-controlled assembly of $[\text{Cu}_n\text{I}_n]$ -based coordination polymers from CuI and bis(4-phenylpyrimidine-2-thio)alkane ligands. *CrystEngComm* **2012**, 14, 1641-1652.
39. Aly, S. M.; Pam, A.; Khatyr, A.; Knorr, M.; Rousselin, Y.; Kubicki, M. M.; Bauer, J. O.; Strohmann, C.; Harvey, P. D. Cluster-Containing Coordination Polymers Built Upon $(\text{Cu}_2\text{I}_2\text{S}_2)_m$ Units ($m = 2, 3$) and $\text{ArSCH}_2\text{C}\equiv\text{CCH}_2\text{SAr}$ Ligands: Is the Cluster Size Dependent Upon Steric Hindrance or Ligand Rigidity? *J. Inorg. Organomet. Polym. Mater.* **2014**, 24, 190-200.
40. Knorr, M.; Khatyr, A.; Dini Aleo, A.; El Yaagoubi, A.; Strohmann, C.; Kubicki, M. M.; Rousselin, Y.; Aly, S. M.; Fortin, D.; Lapprand, A.; Harvey, P. D. Copper(I) Halides ($\text{X} = \text{Br}, \text{I}$) Coordinated to Bis(arylthio)methane Ligands: Aryl Substitution and Halide Effects on the Dimensionality, Cluster Size, and Luminescence Properties of the Coordination Polymers. *Cryst. Growth Des.* **2014**, 14, 5373-5387.

41. Harvey, P. D.; Bonnot, A.; Lapprand, A.; Strohmann, C.; Knorr, M. Coordination $\text{RC}_6\text{H}_4\text{S}(\text{CH}_2)_8\text{SC}_6\text{H}_4\text{R}/(\text{CuI})_n$ Polymers (R (n) = H (4); Me (8)): An Innocent Methyl Group that Makes the Difference. *Macromol. Rapid Commun.* **2015**, *36*, 654–659.
42. Bonnot, A.; Juvenal, F.; Lapprand, A.; Fortin, D.; Knorr, M.; Harvey, P. D. Can a highly flexible copper(I) cluster-containing 1D and 2D coordination polymers exhibit MOF-like properties? *Dalton Trans.* **2016**, *45*, 11413–11421.
43. Chaabéne, M.; Khatyr, A.; Knorr, M.; Askri, M.; Rousselin, Y.; Kubicki, M. M. Bis{(4-methylthio)phenylthio}methane as assembling ligand for the construction of Cu(I) and Hg(II) coordination polymers. Crystal structures and topological (AIM) analysis of the bonding. *Inorg. Chim. Acta* **2016**, *451*, 177–186.
44. Harvey, P. D.; Bonnot, A.; Karsenti, P.-L.; Juvenal, F.; Golz, C.; Strohm, C.; Fortin, D.; Knorr, M. The 3D $[(\text{Cu}_2\text{Br}_2)\{\mu\text{-EtS}(\text{CH}_2)_4\text{SEt}\}]_n$ Material: A Rare Example of a Coordination Polymer Exhibiting Triplet-Triplet Annihilation. *Phys. Chem. Chem. Phys.* **2016**, *18*, 24845–24849.
45. Saha, S.; Biswas, K.; Basu, B. 1-D copper(I) coordination polymer based on bidentate 1,3-dithioether ligand: Novel catalyst for azide-alkyne-cycloaddition (AAC) reaction. *Tetrahedron Lett.* **2018**, *59*, 2541–2545.
46. Cariati, E.; Lucenti, E.; Botta, C.; Giovanella, U.; Marinotto, D.; Righetto, S. Cu(I) hybrid inorganic-organic materials with intriguing stimuli responsive and optoelectronic properties. *Coord. Chem. Rev.* **2016**, *306*, 566–614.
47. Perruchas, S.; Tard, C.; Le Goff, X. F.; Fargues, A.; Garcia, A.; Kahlal, S.; Saillard, J.-Y.; Gacoin, T.; Boilot, J.-P. Thermochromic Luminescence of Copper Iodide Clusters: The Case of Phosphine Ligands. *Inorg. Chem.* **2011**, *50*, 10682–10692.
48. Schlachter, A.; Viau, L.; Fortin, D.; Knauer, L.; Strohmann, C.; Knorr, M.; Harvey, P. D. Control of Structures and Emission Properties of $(\text{CuI})_n$ 2-Methyldithiane Coordination Polymers. *Inorg. Chem.* **2018**, *57*, 13564–13576.
49. Raghuvanshi, A.; Dargallay, N. J.; Knorr, M.; Viau, L.; Knauer, L.; Strohmann, C. 1,3-Dithiolane and 1,3-Ferrocenyl-dithiolane as Assembling Ligands for the Construction of Cu(I) Clusters and Coordination Polymers. *J. Inorg. Organomet. Polym. Mater.* **2017**, *27*, 1501–1513.
50. Brooks, N. R.; Blake, A. J.; Champness, N. R.; Cooke, P. A.; Hubberstey, P.; Proserpio, D. M.; Wilson, C.; Schröder, M. Discrete molecular and extended polymeric copper(I) halide complexes of tetradentate thioether macrocycles. *Journal of the Chemical Society, Dalton Transactions: Inorganic Chemistry* **2001**, 456 – 465.
51. Yim, H. W.; Rabinovich, D.; Lam, K. C.; Golen, J. A.; Rheingold, A. L. Di- μ -iodo-bis{[methyltris(methylthiomethyl)silane- $\kappa^2\text{S,S}'$]copper(I)}. *Acta Crystallogr., Sect. E* **2003**, *E59*, m556–m558.

52. Tan, S. F.; Ang, K. P. Copper, gold, and platinum complexes of 1,3-dithiane. *J. Singapore Natl. Acad. Sci.* **1987**, *16*, 111-14.
53. Guy, J. T.; Cooper, J. C.; Gilardi, R. D.; Flippenanderson, J. L.; George, C. F. Transition-metal-promoted oxidation of organic sulfides - synthesis, characterization, and structure of (μ_4 -oxo)hexakis(μ_2 -chloro)tetrakis(dialkyl sufoxide)tetracopper(II). *Inorg. Chem.* **1988**, *27*, 635-638.
54. Ainscough, E. W.; Brodie, A. M.; Husbands, J. M.; Gainsford, G. J.; Gabe, E. J.; Curtis, N. F. Sulfur ligand metal-complexes. Part 16. Copper-complexes of thioethers and the single-crystal X-Ray structure of the polymeric mixed-valence complex, penta- μ -chloro-tris- μ -tetrahydrothiophene-tetracopper(I,II). *J. Chem. Soc., Dalton Trans.* **1985**, 151-158.
55. Abel, E. W.; King, G. D.; Orrell, K. G.; Pring, G. M.; Sik, V.; Cameron, T. S. A dynamic nuclear magnetic resonance study of 1,3-intramolecular shifts in pentacarbonylchromium(0) and -tungsten(0) complexes of β -2,4,6-trimethyl-1,3,5-trithiane, 1,3,5-trithiane, 1,3-dithiane and 2-methyl-1,3-dithiane: the x-ray crystal structure of $[\text{W}(\text{CO})_5\{\text{SCH}(\text{Me})\text{SCH}(\text{Me})\text{SCH}(\text{Me})\}]$. *Polyhedron* **1983**, *2*, 1117-1124.
56. Cane, D. J.; Graham, W. A. G.; Vancea, L. Synthesis and nuclear magnetic resonance study of the compounds (2-X-1,3-dithiane) (X = H, Me, SiMe₃, GeMe₃, SnMe₃, PbMe₃) and their tetracarbonyliron complexes. *Can. J. Chem.* **1978**, *56*, 1538-44.
57. Bonnot, A.; Knorr, M.; Strohmam, C.; Golz, C.; Fortin, D.; Harvey, P. CuX (X = Cl, Br, I) Containing Coordination Polymers Built Upon Isomeric RSCH₂C \equiv CCH₂SR (R = *p*-Tolyl, Benzyl) Dithioether Ligands: First Example of a Luminescent (CuCl)_n/Dithioether Network. *J. Inorg. Organomet. Polym. Mat.* **2015**, *25*, 480-494.
58. Bowmaker, G. A.; Hanna, J. V.; Hart, R. D.; Healy, P. C.; White, A. H. Structural and solid-state ³¹P nuclear magnetic resonance studies on 1:1:1 mixed nitrogen and phosphine base complexes with copper(I) halides. *J. Chem. Soc., Dalton Trans.* **1994**, 2621-9.
59. Naito, T.; Nishibe, K.; Inabe, T. New Binuclear Copper Complexes [(9S3)Cu(CN)Cu(9S3)]X_n (X=BF₄, n=1; X=TCNQ, n=2) (9S3 = 1, 4, 7-trithiacyclononane): Syntheses, Crystal Structures and Magnetic Properties. *Z. Anorg. Allg. Chem.* **2004**, *630*, 2725-2730.
60. Dembo, M. D.; Dunaway, L. E.; Jones, J. S.; Lepekhina, E. A.; McCullough, S. M.; Ming, J. L.; Li, X.; Baril-Robert, F.; Patterson, H. H.; Bayse, C. A.; Pike, R. D. Structure and luminescence of copper(I) cyanide-amine and -sulfide networks. *Inorg. Chim. Acta* **2010**, *364*, 102-114.
61. Bowmaker, G. A.; Lim, K. C.; Skelton, B. W.; White, A. H. Syntheses, structures and vibrational spectroscopy of some adducts of copper(I) cyanide with pyridine bases. *Z. Naturforsch., B: Chem. Sci.* **2004**, *59*, 1264-1276.
62. Cheng, J.-K.; Yao, J.-G.; Zhang, J.; Zhao-Ji Li; Cai, Z.-W.; Zhang, X.-Y.; Chen, Z.-N.; Chen, Y.-B.; Kang, Y.; Qin, Y.-Y.; Wen, Y.-H. A Simultaneous Redox, Alkylation, Self-Assembly Reaction

under Solvothermal Conditions Afforded a Luminescent Copper(I) Chain Polymer Constructed of Cu_3I_4 - and $\text{EtS-4-C}_5\text{H}_4\text{N}^+\text{Et}$ Components ($\text{Et} = \text{CH}_3\text{CH}_2$). *J. Am. Chem. Soc.* **2004**, *126*, 7796-7797.

63. Ryu, H.; Park, K.-M.; Ikeda, M.; Habata, Y.; Lee, S. S. A Ditopic O_4S_2 Macrocyclic and Its Hard, Soft, and Hard/Soft Metal Complexes Exhibiting Endo-, Exo-, or Endo/Exocyclic Coordination: Synthesis, Crystal Structures, NMR Titration, and Physical Properties. *Inorg. Chem.* **2014**, *53*, 4029-4038.

64. Nardin, G.; Randaccio, L.; Zangrando, E. Stereochemistry of copper(I) complexes. Part II. The molecular structure of the 3 : 2 reaction product between copper iodide and bis(diphenylphosphino)methane: di- μ -[bis(diphenylphosphino)methane]- μ -iodo-di- μ_3 -iodo-triangulo-tricopper(I)-0.5 dichloromethane *J. Chem. Soc., Dalton Trans.* **1975**, *23*, 2566-2569.

65. Gschwind, F.; Sereda, O.; Fromm, K. M. Multitopic Ligand Design: A Concept for Single-Source Precursors. *Inorg. Chem.* **2009**, *48*, 10535-10547.

66. Paulsson, H.; Berggrund, M.; Fischer, A.; Kloo, L. Novel Layered Structures Formed by Iodocuprate Clusters Stabilized by Dialkylsulphide Ligands. *Z. Anorg. Allg. Chem.* **2004**, *630*, 413 - 416.

67. Rim, C.; Zhang, H.; Son, D. Y. Silyl-Substituted Thioether Ligands and Their Ag(I) Complexes. *Inorg. Chem.* **2008**, *47*, 11993-12003.

68. Kim, T. H.; Yang, H.; Park, G.; Lee, K. Y.; Kim, J. γ -CuI Nanocrystals from Self-Assembled Coordination Polymers. *Chem. Asian J.* **2010**, *5*, 252-255.

69. Zeng, G.; Xing, S.; Han, X.; Xin, B.; Yang, Y.; Wang, X.; Li, G.; Shi, Z.; Feng, S. Reversible photoluminescence switching behavior and luminescence thermochromism of copper(I) halide cluster coordination polymers. *RSC Adv.* **2015**, *5*, 40792-40797.

70. Oliinik, V. V.; Goreshnik, E. A.; Zhonchinska, Z.; Glovyak, T. The π -complex of copper(I) bromide with diallyl sulfide $5\text{CuBr}\cdot 2\text{DAS}$: synthesis and crystal structure. *Russ. J. Coord. Chem.* **1997**, *23*, 595-598.

71. Mathew, L.; Sankararaman, S. Mild and efficient photochemical and thermal deprotection of thioacetals and ketals using DDQ. *J. Org. Chem.* **1993**, *58*, 7576-7577.

72. Roth, H. D.; Shen, K.; Lakkaraju, P. S.; Fernandez, L. Oxidative ring contraction of 2-phenyl-1,3-dithiane in ZSM-5: restricted mobility of 1,2-dithiolane radical cations in zeolite channels. *Chem. Commun.* **1998**, 2447-2448.

73. Neumann, B.; Siemeling, U.; Stammeler, H.-G.; Vorfeld, U.; Delis, J. G. P.; van Leeuwen, P. W. N. M.; Vrieze, K.; Fraanje, J.; Goubitz, K.; Fabrizi de Biani, F.; Zanello, P. Co-ordination chemistry of octamethyl-5,5'-di(2-pyridyl)ferrocene. *Dalton Trans.* **1997**, 4705-4712.

74. Siemeling, U.; Vor der Brueggen, J.; Vorfeld, U.; Neumann, B.; Stammeler, A.; Stammeler, H.-G.; Brockhinke, A.; Plessow, R.; Zanello, P.; Laschi, F.; Fabrizi de Biani, F.; Fontani, M.; Steenken, S.; Stapper, M.; Gurzadyan, G. Ferrocenyl-functionalised terpyridines and their transition-metal

complexes: Syntheses, structures and spectroscopic and electrochemical properties. *Chem. Eur. J.* **2003**, *9*, 2819-2833.

75. Nguyen, P.; Gomez-Elipe, P.; Manners, I. Organometallic Polymers with Transition Metals in the Main Chain. *Chem. Rev.* **1999**, *99*, 1515-1548.

76. Zhang, H. F.; Li, Z. F.; Li, G.; Wang, L. P.; Li, J. B.; Mei, G. J. Novel Zn(II) ladder-like coordination polymer constructed from designed ferrocenyl ligand. *Chin. Chem. Lett.* **2008**, *19*, 1499-1503.

77. Schindler, A.; Zabel, M.; Nixon, J. F.; Scheer, M. Hexaphosphaferrocene [Fe(η_5 -P₃C₂tBu₂)₂] as a connecting moiety in oligomeric and polymeric compounds. *Z. Naturforsch., B: Chem. Sci.* **2009**, *64*, 1429-1437.

78. Chandrasekhar, V.; Thirumoorthi, R. Coordination polymers containing ferrocene backbone. Synthesis, structure and electrochemistry. *Dalton Trans.* **2010**, *39*, 2684-2691.

79. Zhong, H.; Wang, G.; Song, Z.; Li, X.; Tang, H.; Zhou, Y.; Zhan, H. Organometallic polymer material for energy storage. *Chem. Commun.* **2014**, *50*, 6768-6770.

80. Pietschnig, R. Polymers with pendant ferrocenes. *Chem. Soc. Rev.* **2016**, *45*, 5216-5231.

81. Moussa, J.; Guyard-Duhayon, C.; Boubekeur, K.; Amouri, H.; Yip, S. K.; Yam, V. W. W. Self-assembly of one- and two-dimensional coordination polymers with quinonoid backbones featuring coinage metals as nodes. *Cryst. Growth Des.* **2007**, *7*, 962-965.

82. Ji, W.; Qu, J.; Jing, S.; Zhu, D.; Huang, W. Copper(I) halide clusters based upon ferrocenylchalcogenoether ligands: donors, halides and semi-rigidity effects on the geometry and catalytic activity. *Dalton Trans.* **2016**, *45*, 1016-1024.

83. Canales, S.; Crespo, O.; Fortea, A.; Gimeno, M. C.; Jones, P. G.; Laguna, A. Gold and silver complexes with the ligands Fc(SPh)₂ and Fc(SePh)₂ (Fc = (η_5 -C₅H₄)₂Fe). *J. Chem. Soc., Dalton Trans.* **2002**, 2250-2255.

84. Clement, S.; Guyard, L.; Knorr, M.; Villafane, F.; Strohmman, C.; Kubicki, M. M. (2,2-Dibromovinyl)ferrocene as a building block for the assembly of heterodinuclear complexes - preparation of an s-alkenylpalladium complex and dimetallic dithioether complexes. *Eur. J. Inorg. Chem.* **2007**, 5052-5061.

85. Horikoshi, R.; Mochida, T.; Torigoe, R.; Yamamoto, Y. Preparation and Electrochemical Properties of Polynuclear Organometallic Complexes Derived from Ferrocene-Containing Bidentate Ligands. *Eur. J. Inorg. Chem.* **2002**, 3197-3203.

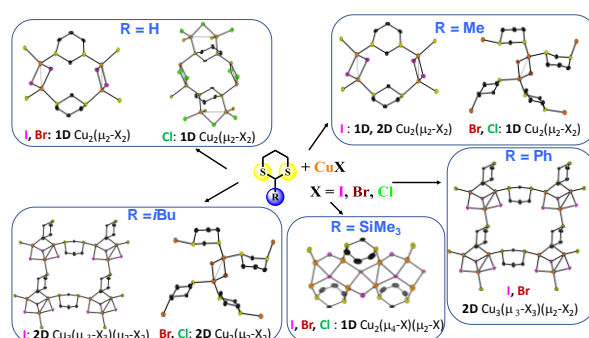
86. Horikoshi, R.; Mochida, T. Ferrocene-Containing Coordination Polymers: Ligand Design and Assembled Structures. *Eur. J. Inorg. Chem.* **2010**, *2010*, 5355-5371.

87. Reuter, M. J.; Damrauer, R. Preparation and basicity measurements of ferrocenyl trimethylsilyl ketone. *J. Organomet. Chem.* **1974**, *82*, 201-208.

88. Kalff, H. T.; Romers, C. The conformation of non-aromatic ring compounds. XXI. The crystal and molecular structure of 2-phenyl-1,3-dithiane. *Acta Crysta.* **1966**, *20*, 490-496.
89. Bonnot, A.; Knorr, M.; Guyon, F.; Kubicki, M. M.; Rousselin, Y.; Strohmman, C.; Fortin, D.; Harvey, P. D. 1,4-Bis(arylthio)but-2-enes as Assembling Ligands for $(\text{Cu}_2\text{X}_2)_n$ ($\text{X} = \text{I}, \text{Br}; n = 1, 2$) Coordination Polymers: Aryl Substitution, Olefin Configuration, and Halide Effects on the Dimensionality, Cluster Size, and Luminescence Properties. *Cryst. Growth Des.* **2016**, *16*, 774–788.
90. Ford, P. C.; Cariati, E.; Bourassa, J. Photoluminescence properties of multinuclear copper(I) compounds. *Chem. Rev.* **1999**, *99*, 3625-3647.
91. Harvey, P. D.; Knorr, M. Luminescent Coordination Polymers Built Upon Cu_4X_4 ($\text{X} = \text{Br}, \text{I}$) Clusters and Mono- and Dithioethers. *Macromol. Rapid Commun.* **2010**, *31*, 808-826.
92. Harvey, P. D.; Knorr, M. Stabilization of $(\text{CuX})_n$ Clusters ($\text{X} = \text{Cl}, \text{Br}, \text{I}; n=2, 4, 5, 6, 8$) in Mono- and Dithioether-Containing Layered Coordination Polymers. *J. Cluster Sci.* **2015**, *26*, 411-459.
93. Bonnot, A.; Strohmman, C.; Knorr, M.; Harvey, P. D. Metal-to-Ligand Ratio Effect on the Size of Copper Iodide and Copper Bromide Clusters in 1,4-Bis(cyclohexylthio)butane-Spanned Coordination Polymers. *J. Cluster Sci.* **2014**, *25*, 261-275.
94. Angelis, F. D.; Fantacci, S.; Sgamellotti, A.; Elena Cariati; Ugo, R.; Ford, P. C. Electronic Transitions Involved in the Absorption Spectrum and Dual Luminescence of Tetranuclear Cubane $[\text{Cu}_4\text{I}_4(\text{pyridine})_4]$ Cluster: a Density Functional Theory/Time-Dependent Density Functional Theory Investigation. *Inorg. Chem.* **2006**, *45*, 10576 -10584.
95. Tronic, T. A.; dekrafft, K. E.; Lim, M. J.; Ley, A. N.; Pike, R. D. Copper(I) cyanide networks: Synthesis, luminescence behavior and thermal analysis. Part 1. Diimine ligands. *Inorg. Chem.* **2007**, *46*, 8897-8912.
96. Hou, L.; Shi, W.-J.; Wang, Y.-Y.; Liu, B.; Huang, W.-H.; Shi, Q.-Z. Two new coordination polymers with multiform helical features based on flexible dithioether ligands and CuCN : from self-penetrating to 3-fold interpenetrating structures. *CrystEngComm* **2010**, *12*, 4365-4371.
97. Jian, W.-Y.; Li, W.; Lv, Q.-Y.; Min, X.; Liu, Y.-Y.; Zhan, S.-Z. Isolation and Properties of a Chain of Cyano-Bridged Complex $\{\text{LCu}^{\text{II}}(\mu\text{-CN})\}_n$ With Triazenido Ligand and a Cyano-Bridged Mixed-Valence Complex $\{\text{Cu}^{\text{II}}\text{CuI}(\mu\text{-CN})_3\}_n$. *Synth. React. Inorg. Met.-Org. Chem.* **2012**, *42*, 1375-1380.
98. Knorr, M.; Bonnot, A.; Lapprand, A.; Khatyr, A.; Strohmman, C.; Kubicki, M. M.; Rousselin, Y.; Harvey, P. D. Reactivity of CuI and CuBr toward Dialkyl Sulfides RSR: From Discrete Molecular $\text{Cu}_4\text{I}_4\text{S}_4$ and $\text{Cu}_8\text{I}_8\text{S}_6$ Clusters to Luminescent Copper(I) Coordination Polymers. *Inorg. Chem.* **2015**, *54*, 4076-4093.
99. Schramm, V.; Fischer, K. F. Crystal structure of morpholine copper(I) iodide ($\text{CuI.C}_4\text{H}_9\text{NO}$). *Naturwissenschaften* **1974**, *61*, 500-501.

100. Hardt, H. D.; Stoll, H. J. The fluorescence thermochromism of acetonitrilo copper iodide with dibenzo-18-crown-6. *Z. Anorg. Allg. Chem.* **1978**, 442, 221-224.
101. Jasinski, J. P.; Rath, N. P.; Holt, E. M. Structural comparison of $(\text{CuICH}_3\text{CN}_4\text{dibenzo-18-crown-6})_x$ (I) and $(\text{CuICH}_3\text{CN})_x$ (II) fluorescent copper(I) materials. *Inorg. Chim. Acta* **1985**, 97, 91-97.
102. Rath, N. P.; Holt, E. M.; Tanimura, K. Fluorescent copper(I) complexes: structural and spectroscopic characterization of bis(p-toluidine)bis(acetonitrile)tetraiodotetracopper and bis[(p-chloroaniline)(acetonitrile)diiododicopper] tetrameric complexes of mixed-ligand character. *Inorg. Chem.* **1985**, 24, 3934-3938.
103. Taylor, W. V.; Soto, U. H.; Lynch, V. M.; Rose, M. J. Antimony-Supported Cu_4I_4 Cuboid with Short Cu-Cu Bonds: Structural Premise for Near-Infrared Thermoluminescence. *Inorg. Chem.* **2016**, 55, 3206-3208.
104. Huitorel, B.; El Moll, H.; Utrera-Melero, R.; Cordier, M.; Fargues, A.; Garcia, A.; Massuyeau, F.; Martineau-Corcos, C.; Fayon, F.; Rakhmatullin, A.; Kahlal, S.; Saillard, J.-Y.; Gacoin, T.; Perruchas, S. Evaluation of Ligands Effect on the Photophysical Properties of Copper Iodide Clusters. *Inorg. Chem.* **2018**, 57, 4328-4339.

For Table of Contents Only



A complete series of Cu(I) coordination polymers with varying dimensionalities and incorporating $(\text{CuX})_n$ cluster as SBUs was prepared from 2-substituted 1,3-dithianes